Hybrid Polymer and Peptide-Based Nanostructures for Stimuli-Responsive Drug Delivery

by

Daniel Bacinello

A thesis
presented to the University of Waterloo
in fulfillment of the
thesis requirement for the degree of
Doctor of Philosophy
in
Chemical Engineering - Nanotechnology

Waterloo, Ontario, Canada, 2014

Author's Declaration

I hereby declare that I am the sole author of this thesis. This is a true copy of the thesis, including any required final revisions, as accepted by my examiners. I understand that my thesis may be made electronically available to the public.

Abstract

Targeting of human tissues by nanomedicines can occur both passively, benefiting from the enhanced permeation and retention (EPR) effect, and actively, through design elements which exploit the unique microenvironment (pH, redox environment, enzymatic expression etc...) of specific tissues. In this study novel drug delivery systems (DDS) are designed to exploit the enzymatic and pH environments of human tissues. Specifically, the enzymes matrix metalloproteinase (MMP) 2 and 9 are known to be associated strongly with aggressively invasive cancer and are expressed in very high levels in tumour tissues. These highly studied enzymes have been shown to selectively cleave the peptide sequence PVGLIG. In addition, the pH in different organs and cells in the human body can vary significantly creating opportunity to trigger pH-sensitive systems.

The peptide PVGLIG, which is known to be selectively cleaved by the tumor-associated enzyme matrix metalloproteinase-2 (MMP-2), was conjugated to α-alkene poly(trimethylene carbonate) (PTMC) blocks of varying sizes *via* UV-initiated thiol-ene "click" chemistry. The PTMC precursor was synthesized by metal-free ring-opening polymerization using allyl alcohol as an initiator and an *N*-heterocyclic carbene as an organic catalyst. The unprecedented PVGLIG-*b*-$PTMC_n$ hybrids were self-assembled in aqueous solution and various sub-micron sized morphologies obtained by a nanoprecipitation process. Characterization of particle morphology was carried out by multi-angle dynamic light scattering (DLS) and static light scattering (SLS) evidencing spherical nanoparticles with different morphologies and narrow size distributions. Microstructure details were also observed on transmission electron micrographs and were in good agreement with light scattering measurements showing the assembly of core-

shell, large compound micelles and vesicle morphologies, the particle morphology varying with the hydrophilic weight fractions (f) of the hybrids. These nanostructures displayed selective degradation in the presence of the cancer-associated enzyme MMP-2, as probed by the morphological change both by TEM and DLS. All these results demonstrated that PVGLIG-*b*-PTMC hybrids were suitable to target the tumor microenvironment.

The synthetic strategy developed for production of $PTMC_n$-*b*-PVGLIG diblock systems was then expanded for the synthesis of multi-functional a triblock copolymer. The synthetic semi-crystalline polymer $PTMC_{50}$ was conjugated to the synthetic poly(amino acid) poly(glutamic acid) (PGA) using the peptide PVGLIG as a linker by a combination of UV-initiated thiol-ene coupling and ROP. Stable, monodispersed, sub-micron sized polymersomes were subsequently obtained by self-assembly and characterized by dynamic and static light scattering (DLS and SLS) and TEM. These vesicles showed selective degradation in the presence of MMP-2 as probed by DLS. The model drug imipramine hydrochloride was loaded at 35 % encapsulation efficiency by co-precipitation and displayed a controlled drug-behaviour.. Drug release rates from these vesicles showed several fold increases when exposed to pH, temperature and most significantly, the tumor-associated enzyme MMP-2. Such structures may hold promise as future specific and controlled drug-delivery systems.

Control of membrane integrity is a key factor in producing stable particles for drug delivery. $PTMC_{50}$-*b*-PVGLIG-*b*-PGA_{15} nano-vesicles were subjected to multiple rounds of heating and cooling in order to probe the effect of membrane melting on the structure and stability of the vesicles. Vesicles are observed to undergo a chain-melting transition resulting in significant size and morphology changes when heated above the melting temperature of the PTMC block for extended periods. This morphology change is linked to increases in the

structure melting temperature and molar melting enthalpy towards that of the bulk material. This increase is suggestive of a higher degree of crystallinity attained in larger vesicles..

Towards a better understanding of how the drug-carrier relationship impacts encapsulation and release, isothermal titration calorimetry (ITC) was used to probe the chemical interactions between two model drugs and a polymersome carrier. The amphiphilic copolymer $PTMC_{30}$-*b*-PGA_{13} was synthesized using a chemical platform previously established based on a combination of organo-catalyzed ring-opening polymerization (ROP) and UV-initiated thiol-ene coupling. The copolymer was self-assembled using a nanoprecipitation technique to form stable polymersomes with low PDI. Procaine hydrochloride (PrHy) or imipramine hydrochloride (IMI) was loaded into the vesicles as model drugs by co-precipitation. The loading of these drugs and release from the vesicles was monitored used drug-selective electrodes at pH 7.4 and 4.5. The significant differences in the loading and release of the two drugs from the vesicle carrier correlates well with the drug-carrier interactions probed by ITC. High intensity interaction was clearly linked with a higher drug loading capacity and a slower drug release rate. The drug-carrier interaction was monitored by ITC at pH 9.5, 7.4 and 4.5 and was in good agreement with the observed loading and release rates.

Acknowledgements

Throughout my PhD I have been very fortunate to be surrounded with countless wonderful people, who have made this time a success.

Firstly, I'd like to express my sincere gratitude to my supervisors, Sébastien Lecommandoux, Michael Tam and Daniel Taton for all of their guidance, support and patience throughout this project. The direction and encouragement I have received from these three has been invaluable from day one. I appreciate being given the opportunity to be a part of their research groups.

I would like to acknowledge all of the friendly and talented colleagues at the LCPO and at the University of Waterloo whom I have had the privilege to work with over the years. My friends, my coworkers and my fellow students at both institutions have made this experience truly memorable. I have been fortunate to be a part of the IDS FunMat program, which has given me the chance to interact with an incredible group of students from around the world. The times I have spent with these students have left me with countless fond memories for which I am very grateful.

I would like to thank the Conseil Régional d'Aquitaine, the Waterloo Institute for Nanotechnology and the IDS FunMat program for their generous financial support of this work.

I would like to thank my family and friends in Canada and around the world that have been a constant source of support and encouragement throughout this work. Finally, for his support, encouragement, sacrifice and seemingly unending patience I would like to thank my wonderful partner and fiancé Cameron Macdonald.

Table of Contents

List of Figures

List of Tables

List of Schemes

Chapter 1 Introduction

Hybrid materials based on conjugation between biocompatible polymers and biologically relevant peptide sequences have recently emerged as a new and exciting class of soft matter materials[1–3]. The recent developments in synthetic methods allowed the design of sophisticated hybrid materials which take advantage of the chemical, physical and stimuli-responsive properties of both polymers and peptides, in a significant step towards biomimetic materials. Through advances in our understanding of the self-assembly phenomenon, these hybrid materials can be assembled into a variety of architectures, incorporating biologically relevant peptide sequences as structural elements in nanoparticles[3–7]. Such hybrid materials can be engineered to address major challenges in targeted cancer therapy and drug delivery. The design of multifunctional drug-delivery systems, combining ability to load a large amount of therapeutic molecules, possibility to release its content in a spatial and temporal controlled manner, and serving as a contrast agent for magnetic resonance imaging or other imaging methods is the major challenge facing nanomedicine today[8–10].

The main challenge of the coming decade is to move from the current use of hybrid materials in a "passive" way to an "active" one, where the material itself will have a functional role, mimicking the activity of molecules and substrates in biological systems. In this context, our project aims at developing new nano-carriers for drug delivery applications based on biologically relevant peptides and biocompatible polymers.

Targeting of cancer tissue by nanomedicines can occur both passively, benefiting from the enhanced permeation and retention (EPR) effect, and actively, through design elements that exploit the unique microenvironment (pH, redox environment, enzymatic expression etc...) of tumour tissue. Active targeting relies on stimuli-responsive elements in the drug delivery system (DDS) to target unique characteristics of disease tissues. DDSs with responsive elements rely on these unique microenvironmental conditions to trigger and/or control drug release at the target site, either by enhancing the permeability of the DDS or by completely destabilizing the DDS. Active targeting can also include targeting by tissue-specific antibodies or receptor-specific ligands conjugated to the DDS. In this study a novel DDSs are designed to exploit the enzymatic environment of invasive tumour tissues. Specifically, the enzymes matrix metalloproteinase (MMP) 2 and 9 are known to be associated strongly with aggressively invasive cancer and are highly expressed in tumour tissues. These widely studied enzymes have been shown to selectively cleave the peptide sequence PVGLIG.

This project will focuses on the design of nanostructures from polymer-peptide hybrid materials. We seek to incorporate the biologically-relevant peptide PVGLIG into nanoparticles to act as a structural element. In this way structures can be disrupted in the presence of the tumor-associated enzymes MMP-2 and 9. It is believed that this peptide would be able to act as a trigger for the structural degradation of drug-loaded nanoparticles when in contact with MMP-2,9, resulting in an enhanced drug release. One of the primary goals of this project is to use the PVGLIG peptide as a linker between two larger polymer blocks for the self-assembly and eventual disruption of polymersomes.

A primary component of the systems used in this study will be poly(trimethylene carbonate) (PTMC), a well-known semi-crystalline polymer. The crystallinity of PTMC has previously been shown to play a significant role in self-assembly, resulting in highly stable structures. The influence of this polymer in the development of polymer-peptide hybrids is addressed at length in this work. In addition, the poly(amino acid) poly(glutamic acid) PGA will be incorporated in order to give assembled nanostructures surface charge and pH-sensitivity.

The project will also aim to modify traditional synthetic methods for the chosen polymers in order to synthesize them in less stringent conditions. The synthesis of the di and triblock systems is done using a combination of organocatalyzed ring-opening polymerization (ROP) and macromolecular thiol-ene click chemistry. Vesicles and other structures will be formed through a nanoprecipitation technique and drugs encapsulated during self-assembly. Following synthesis and self-assembly, considerable effort will focus in the characterization of the produced nanostructures, with particular attention paid to understanding the relationship between particle morphology and copolymer characteristics.

Within liposomes, and analogous polymersomes, membrane integrity and permeability can be largely influenced by the presence of crystallinity. Polymer and phospholipid chains are known to undergo a gel to liquid-crystal transition across the chain melting temperature (T_m), resulting in the occurrence of fusion and/or fission events and subsequent structural changes in the vesicles. These events are probed with the polymer-peptide hybrid vesicles assembled in this work by heating and cooling the structures across their T_m. This study aims to gain a better

understanding of the influence of the molecular subunits and crystallinity on vesicle membrane integrity and stability.

In addition to the design and investigation of polymer-peptide hybrid materials for assembly of drug delivery systems, special attention will be given to understanding the relationship between drug-carrier interactions and their influence on drug loading and release. In simple systems drug release from a carrier occurs through simple diffusion across a membrane (acting as a physical barrier), however, in more complex systems other factors such as interaction forces, chemical affinity and membrane permeability can play significant roles in the release rate.

This project is part of the International Doctoral School in Functional Materials and is a joint venture between the University of Bordeaux I and the University of Waterloo as well as an industrial partner; Vive Crop Protection Inc.

Outline of Report

This report is divided into 7 main chapters. **Chapter 2** is a **literature review** on the subject of polymer vesicles. It broadly covers key structural characteristics of polymersomes as well as common self-assembly techniques. The literature review focuses largely on the use of polymersomes in drug delivery applications, with special attention given to stimuli-responsive vesicles, hybrid materials and active targeting of polymersomes. This provides the broad knowledge base from which the current project was designed.

Chapter 3 focuses on the synthesis of diblock polymer-peptide hybrids and their subsequent self-assembly. The morphologies are characterized and discussed in detail in relation to the composition of the molecular subunits. The degradation of these structures in the presence of active enzymes is presented and the applications of these structures as drug delivery systems is discussed.

Chapter 4 covers the synthesis of a triblock system in which an enzyme substrate is used as a linker between two polymer blocks. The assembly of vesicles is observed and drug loading and release studies are presented. Drug release under varying temperature, pH and in the presence of active enzymes is presented.

The study outlined in **Chapter 5** focuses on the effects of temperature and crystallinity on membrane integrity and the structure of hybrid vesicles. The observed changes in melting temperature, heat capacity and structure morphology are discussed at length with particular focus on vesicle fusion and fission events in relation to the chain-melting transition.

The final research chapter of this report, **Chapter 6**, is an investigation of the effect of drug-carrier interaction on the loading and release of drugs from polymer vesicles. Two model drugs are investigated, and their interactions with polymer vesicles observed by isothermal titration calorimetry (ITC). The relevance of this work towards development of tailored drug-carrier combinations is discussed.

Chapter 7 outlines the relevant contributions of the work to the body of scientific knowledge. This chapter summarizes the conclusions of all research performed and the recommendations for continuation of this work. The next steps and potential applications of the major findings are presented.

Chapter 2 Literature Review

Introduction to Polymer Vesicles

Amphiphilic block copolymers are capable of self-assembly into a variety of nanostructure morphologies, with a broad range of applications[11–13]. Amphiphiles designed from di-block and tri-block copolymers as well as dendritic and graft copolymers have been used for nano-structure self assembly producing a broad range of particle morphology[3,14–16]. Structures as varied as micelles, lamellar, rod-like and a variety of unique architectures have been designed, exploiting a range of synthetic polymers. For application in biomedicine, however, polymersomes (or polymer vesicles) hold the greatest potential for development into clinically relevant drug delivery systems[17–19]. Key characteristics of polymer vesicles, such as long-circulations times, stability and capacity to encapsulate both hydrophilic and hydrophobic payloads make these structures particularly appealing. Broadly speaking polymer vesicles are spherical particles analogous to liposomes with an aqueous internal cavity surrounded by a bi-layer membrane with a hydrophobic interior[20]. However, compared to liposomes, polymer vesicles have significantly higher performance with thicker and more robust membranes, higher stability and longer circulation times[17,21,22]. The membrane is hydrophilic at both the interior and exterior surfaces acting as a physical barrier separating the aqueous core from the outside medium (Figure 1). Polymersomes have been assembled with sizes varying from < 100 nm to well above 1 μm. Due to the presence of both a hydrophilic compartment (aqueous cavity) and a hydrophobic compartment (membrane interior) polymer vesicle can be used for loading of a diverse range of payloads, including drugs, dyes and biologically relevant macromolecules[23–26].

The possibility to load both hydrophilic and hydrophobic drugs into polymer vesicles is of particular interest for applications in drug delivery.

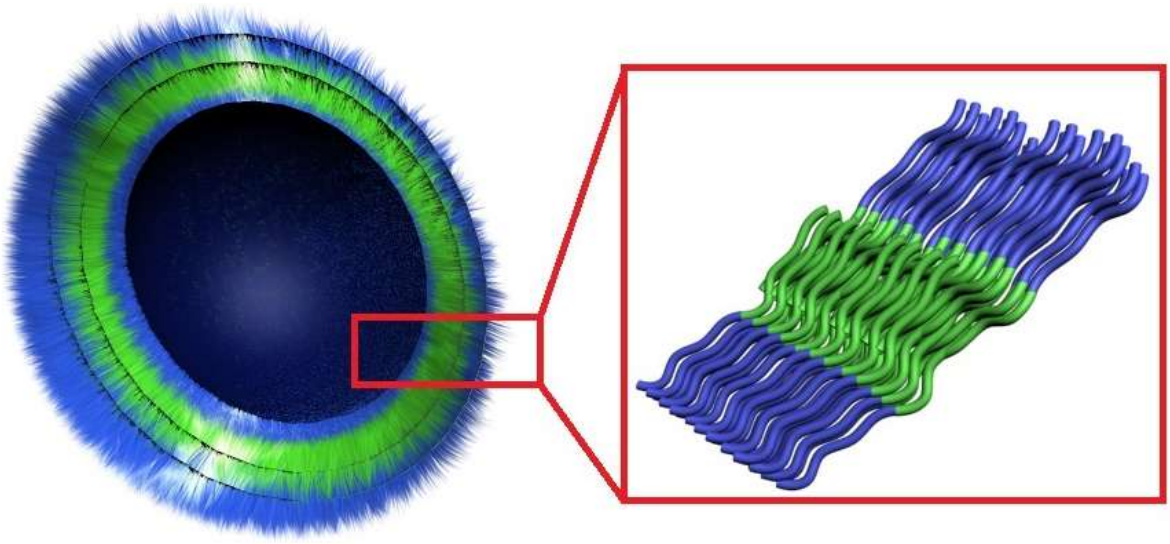

Figure 1 Schematic illustration of a 3D cross-section of a polymer vesicle from a diblock system

Polymer vesicles are generally comprised of a combination of synthetic block copolymers and/or poly(amino acid)s and can be developed to include biologically relevant macromolecules such as peptide or protein fragments[27–31]. The amphiphiles are comprised of one or more blocks covalently linked, in this manner, macrophase separation is avoided and self-assembly on the nanoscale can occur[32]. With particular applications in biomedicine, polymer vesicles have been shown to be highly stable in vitro as well as having long circulation times in vivo. The appeal of such polymer vesicles is the versatility with which they can be prepared due to the diversity of possible amphiphiles available. Variations in block composition and molecular weight can result in vesicles of different sizes and membrane permeability[32–34]. Additionally,

stimuli-responsive blocks, capable of rapid changes in microstructure in response to stimuli, incorporated into the vesicle structure can give the structures a wide range of sensitivities and properties[35–37]. Synthetic polymers may also be combined with additional blocks such as poly(amino acid)s or enzymatic substrates to further vary the vesicle responsiveness and characteristics[3,27]. Such materials can increase the interaction of nanostructures with a biological environment. The variety of synthetic techniques available for production of polymeric amphiphiles has allowed for the introductions of a range of functionalities or chemically and biologically active monomers. The stable and thick membranes (2-50 nm) of polymer vesicles have most often been achieved with amphiphiles of relatively high molecular weight, though smaller chain length polymers (< 20 repeating units) have more recently been exploited in such structures[38,39]. Biocompatibility and extended circulation times have been achieved by use of polymers with "stealth" properties such as poly(ethylene glycol) (PEG) and poly(oxazolines) (POZ). Additionally, such biocompatible, biodegradable and hydrophobic polymers have been used such as poly(trimethylene carbonate) (PTMC), poly(lactic acid) (PLA) and poly(ε-caprolactone) (PCL) [3,40,41]. Vesicles formed with PEG surface layers have been shown to have great "stealth" potential and have been exploited in a number of studies.

In recent years polymer vesicles have gained special attention for their application as drug delivery systems (Figure 2)[17,41,42]. Their multi-compartment properties (hydrophilic cavity and hydrophobic core) for encapsulation of both hydrophilic and hydrophobic payloads makes them particularly attractive compared to other single-compartment structures such as micelles or nanogels. Additionally, their increased stability and circulation times have set them apart from analogues such as liposomes[43]. Research has largely focused on incorporation of stimuli-

responsive materials into the structure of polymer vesicles in order to control in both a special and temporal fashion the release of drugs from the vesicles. Block copolymers that are responsive to pH[9,20,44], temperature[45–47], redox conditions[48,49], light[50–52], magnetic field[53,54], ionic strength[49] and concentration of glucose[55] among other stimuli have been synthesized and used to prepare biodegradable and/or stimuli-responsive polymer vesicles. For applications as guided therapeutics and site-targeted payload delivery efforts have been made to enhance the nanostructure interaction with cellular features and biological sites. This can be achieved by introducing targeting moieties, for example, antibodies, antibody fragments, or peptides and proteins on the surface of the polymer vesicles[56]. Polymer vesicles with these features can be directed to specific biological sites and can respond to local stimuli at a desired site. Targeted drug delivery systems have the potential to enhance therapeutic effects of drugs and reduce unwanted side-effects by minimizing damage to surrounding healthy tissues. Design of polymer vesicles requires an understanding of vesicle self-assembly, requirements for successful assembly as well as knowledge of characterization.

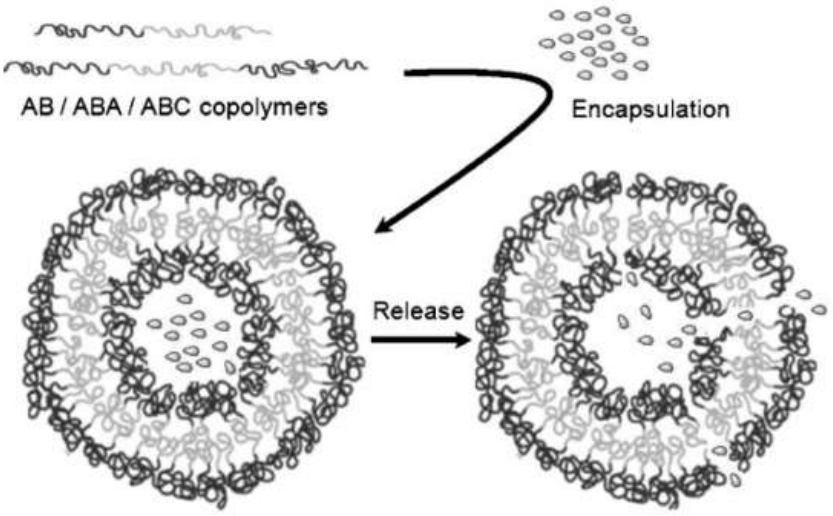

Figure 2 Schematic representation of vesicle self-assembly, payload encapsulation and release.[57]

Additionally, research focus has shifted to design of biologically active vesicles that incorporate relevant peptide sequences as structural elements[3,4]. Such polymer-peptide hybrid structures are unique in that they have the potential to interact directly with cellular systems, either with enzymes in local environments or with cell receptors to encourage internalization[6]. Such hybrid vesicles represent the next step towards biomimetic nanostructures.

Self-Assembly of Polymer Vesicles

Generally speaking the structure of polymer vesicles is defined by a single bi-layer membrane enclosing an aqueous cavity, however it is worth noting that a broad range of other

vesicle conformations have been observed. Figure 3 shows representative microphraphs of more exotic vesicle morphologies that have been observed. This review will focus on the more traditional single bi-layer vesicles and the methods of preparation involved with those.

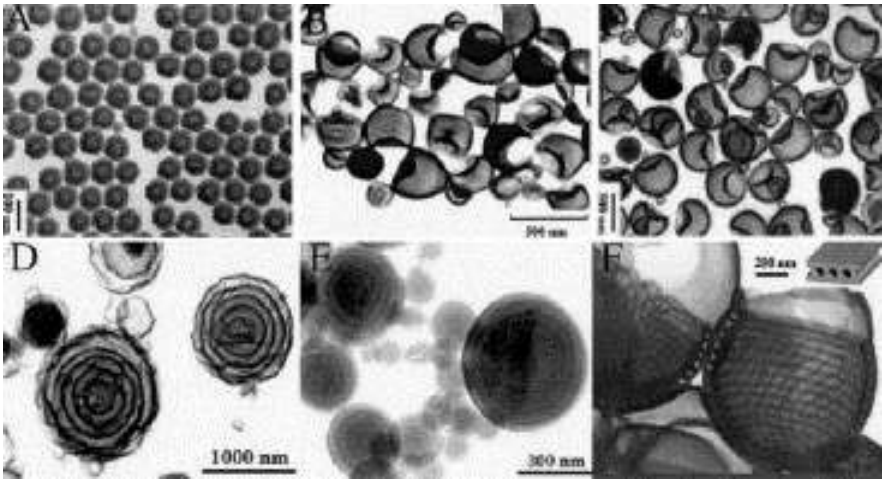

Figure 3 Micrographs of the diversity of vesicle morphology observed. A) Small vesicles (PS_{410}-*b*-PAA_{13}), B) Large polydisperse vesicles (PS_{100}-*b*-PEO_{30}), C) entrapped vesicles (PS_{200}-*b*-PAA_{20}), D) hallow concentric vesicles (PS_{132}-*b*-PAA_{20}), E) onions (PS_{260}-*b*-$P4VPDI_{70}$), F) Tube-walled vesicles (PS_{100}-*b*-PEO_{30})[58]

Polymer vesicles are prepared by self-assembly of amphiphilic block copolymers and can be achieved by a number of different techniques. Most commonly polymer vesicles are prepared by either solvent-displacement[56,58–60] (which includes rapid nanoprecipitation), also known as phase-inversion, and film or polymer rehydration[58]. Techniques involving extrusion or microfluidics[61] can also be used for narrowing of vesicle size distributions or for assembly of multi-layer vesicles. In both solvent-displacement and film hydration, self-assembly relies on hydration of either a dried or dissolved block copolymer into vesicle structure. In the case of solvent-displacement the block copolymers must first be well-dissolved in a solvent appropriate

for both hydrophilic and hydrophobic components of the amphiphile. The solution is then hydrated with aqueous solution. The hydration process renders the hydrophobic blocks of the amphiphile insoluble, triggering the self-assembly process. By varying the solvents used as well as the rate of hydration, the vesicle size and characteristics can be adjusted[61].

The second technique commonly used for vesicle assembly is film rehydration. This technique relies on hydration of a deposited copolymer film in order to induce the assembly of vesicles. As with solvent-displacement, polymers are first dissolved well in an organic phase appropriate for all blocks. A film is produced by deposition and evaporation of the organic phase. Finally, the film is rehydrated with an aqueous solution. The aqueous solution can permeate the polymer layer through defects, causing bulging and finally separation of the polymer from the surface and vesicle formation. Compared to solvent-displacement methods, film hydration produces vesicles with much larger size distributions. Distributions have been reduced by following the self-assembly by extrusion or by application of an electrical field during the self-assembly. The electrical current can help to control the rate of hydration of the polymer layer.

By the processes described above amphiphilic block copolymers can assemble into a wide range of morphologies and are not limited to vesicles. Such morphologies include spherical or cylindrical micelles, core-shell or vesicles. The achieved morphology is dependent on a number of factors, including chemical properties of homopolymers, chain length and interaction forces, but is most closely correlated to the mass or volume ratio between the hydrophilic and hydrophobic components of the amphiphile. Vesicle morphology is generally

thermodynamically favoured for copolymers with a hydrophilic weight fraction (*f*) between 10 – 40 %. As the hydrophilic weight fraction is increased, traditionally, cylindrical micelles (45-55%) or spherical micelles (55-70 %) are favoured[62,63]. The various morphologies achievable result in differing packing parameters (p) of the polymer chains; a numerical description of the chain stacking. Classically, for surfactants and surfactant-like polymers, the packing parameter is characterized by the hydrophobic-hydrophilic interface based on the mean curvature (*H*) and its Gaussian curvature (*K*). These parameters are related by the equations below, in which *v* is the volume of the hydrophobic part of the polymer, *a* is the interfacial area per molecule and *l* the chain length of the hydrophobic part of the polymer[64,65].

$$\frac{v}{al} = l + Hl + \frac{Kl^2}{3}, p = v/(al)$$

In addition to the hydrophilic weight fraction, varying particle morphologies can also be predicted by calculating the copolymer packing parameter. Different morphologies correspond to different values of *p*. In general, p < 1/3 results in a spherical morphology, 1/3 < p < 1/2 a cylindrical one and ½ < p < 1 is characteristic of a vesicle morphology[17]. All the scaling laws, some being purely empirical generally consider the system at thermodynamic equilibrium, in cases of fluid systems. Out of equilibrium conditions can also influence particle morphology and the formation of vesicles, particularly by altering the method and conditions of preparation, the materials used as well as experimental conditions such as solvent, polymer concentration and solvent-water volume ratio[64].

Membrane Integrity and Crystallinity

One of the key features of polymer vesicles is the enhanced stability of the membrane relative to liposomes. This stability has made these structures promising candidates for drug delivery vehicles. Within this context several attempts at varying the permeability and stability of vesicle membranes have been made. Modification of membrane stability has been demonstrated by Discher *et al* with a PEO-*b*-PBD and PGA-*b*-PBD vesicle system.[66] The vesicles formed showed very high stability capable of hydration and dehydration without damage to the membrane. Stable, defect-free membranes were demonstrated with high micron-scale surface areas. The unique strength of the vesicle developed is attributed to the crystalline nature of the polymer blocks.

Changes in membrane permeability are most commonly achieved by use of stimuli-responsive materials. This strategy will be discussed further later in this review. Membrane permeability can also be enhanced by incorporation of biological structures and macromolecules into the vesicle membrane. This strategy is more analogous to the presence of intergral membrane proteins observed in biological systems. Biological membranes are significantly more complex than polymer or lipid vesicles produced in vitro, and are comprised of not only lipids, but also glycolipids, membrane proteins, small molecules and glycoproteins. With synthetic vesicles, incorporation of membrane proteins into the vesicle membrane has given rise to specific and reversible molecule exchange across the membrane. Such strategies have given rise to systems with enhanced permeability to fluid molecules, as well as delivery of DNA or exchange of ions for biomineralization.

In liposomal systems, membrane stability can be attributed in part to the ability for the saturated alkyl chains of phospholipids to crystallize within the membrane[14]. This crystallinity can give rise to a temperature-sensitivity due to the chain-transition temperature (also called the gel-liquid-crystal transition). Across this critical temperature, crystalline liposomes (and polymer vesicles) exhibit a change from a gel state to a liquid-crystal state, resulting in changes in the permeability of the membrane to diffusion[67]. This transition has been exploited in drug delivery systems as release kinetics are highest above the chain transition. By varying the molecular weights and composition of vesicle subunits this critical temperature can be tuned to give a temperature-sensitive membrane permeability[68].

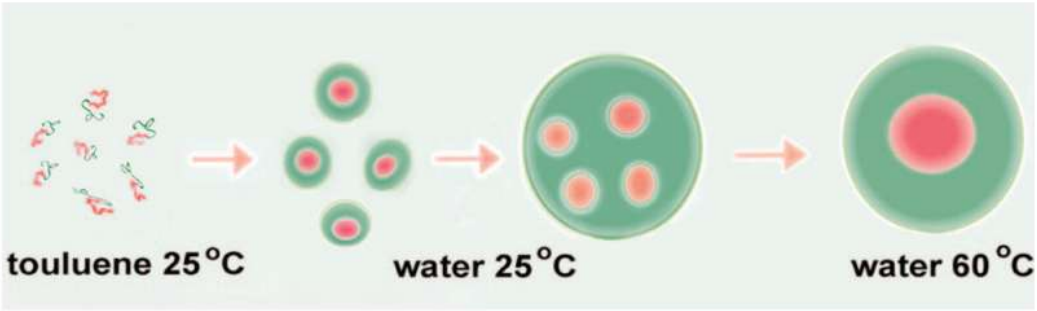

Figure 4 Schematic representation of temperature induced morphology changes from PE-*b*-PEO copolymer. Temperature increases the hydrophobic character of the PE block inducing greater levels of self-assembly.[69]

Although more common in liposomes, vesicles comprised of synthetic polymers have also been made using crystalline polymers[40,45,69–71]. Significant research has been done to exploit crystallinity in polymer structures to induce changes in membrane permeability and structure morphology. Most commonly, PEO has been used as a crystalline polymer in self-assembled

structures. Diblock copolymers comprised of PE-*b*-PEO have been shown to form compound micelles with crystalline character observed in the PEO cores within the structure[69]. The character of the crystalline regions in these structures differed significantly from that of the bulk material due to the confinement of the PEO chains within the structure. Specifically, a large change in the chain-transition temperature was observed. In this system heating above the chain-transition temperature was shown to induce rearrangement of the crystalline regions and a morphology change in the structures. The observed progression from copolymer to structure is shown schematically in Figure 4. In other examples, semi-crystalline copolymers were shown to form lamellar structures, spherical micelles as well as cylindrical micelles[69]. Crystallization was evidenced to be the main driving force in the formation of these structures.

Co-polymers for Nanostructure and Vesicle Formation

The basic structural element of polymer vesicles is the amphiphilic block copolymer, comprised of one or more homopolymer blocks[17]. As such, the polymers chosen have a great influence on the final properties and therefore potential applications of the self assembled structures produced. The structural and chemical properties of polymer vesicles can be altered by using block copolymers of varying molecular weights, compositions, and structural characteristics. For polymer vesicles and indeed all self-assembled structures, assembly relies on the presence of both a hydrophobic component and a hydrophilic component. The increased size of the amphiphiles relative to those of liposomes results in a lower membrane permeability. In addition the diversity of amphiphiles allows for greater functionalization a range of

characteristics of polymer vesicles. A broad range of both hydrophilic and hydrophobic polymers have been studied with success and will be discussed broadly.

Some of the most common hydrophobic blocks used include such non-biodegradable polymers as poly(styrene) (PS), poly(butadiene) (PBD)[32,54,72,73], poly(dimethylsiloxane) (PDMS)[74,75] and poly(ethyl ethylene) (PEE)[32]. In the context of drug delivery systems often bio-degradable systems are desired and hydrophobic block such as poly(lactide) (PLA)[46], poly(caprolactone) (PCL)[56] and poly(trimethylene carbonate) (PTMC)[3,40,56] have been used due to their ability to undergo hydrolytic and/or enzymatic cleavage. Such cleavage can be controlled by varying the block molecular weight, pH and can be enhanced in the presence of specific enzymes. As with hydrophobic blocks, a broad range of hydrophilic polymers have been exploited in self-assembly. Most commonly, poly(acrylic acid) (PAA)[76,77] and the poly(amino acid) poly(L-glutamic acid) (PGA)[54,73] as well as poly(ethylene glycol) (PEG)[21,78,79].

Often, spatial and temporal control of drug release from delivery systems has relied on exploiting specific environmental conditions through the incorporation of stimuli-responsive materials into the vesicle structure[36,80]. With such materials, self-assembly can be achieved by simple alteration of environmental conditions. The most commonly used thermo-sensitive polymer is poly(N-isopropylacrylamide) (PNIPAAm) which has been extensively studied as a hydrophobic component in vesicle systems[46,81–83]. PNIPAAm is unique in that it has a sharp and tunable thermal transition within biologically relevant ranges (30 – 50 °C). This lower critical solution temperature (LCST) is characterized by a phase transition of the polymer form coil to globule and from hydrophilic to hydrophobic[84,85]. This phase transition has allowed for the

assembly of nanostructures from PNIPAAm-containing conjugates by altering the environmental temperature. Polymer vesicles containing PNIPAAm were first reported by Feijen *et al* with the PEG-*b*-PNIPAAm system[86]. Subsequently, a number of other thermo-sensitive systems have been produced using PNIPAAm as well as other thermo-sensitive polymers.

In addition to thermo-sensitive polymers, significant attention has been paid to pH-responsive systems[20,87–89]. In general, such polymers are characterized by the presence of a titratable group which can be either protonated or deprotonated by changing of the environmental pH[90,91]. This protonation can result in changes in surface charge or cleavage and can be used to self-assemble vesicles or change the arrangement or morphology of nanoparticles. A prime example is the spontaneous assembly of vesicles from poly(2-methacryloyloxyethylphosphorylcholine)-*b*-poly(2-(diisopropylamino) ethyl methacrylate) (PMPC-*b*-PDPA) observed upon undergoing a pH change from 2 to 6. The presence of tertiary amine groups on the PDPA group renders the system pH-sensitive. Deprotonation of the amine group renders the block insoluble and drives the self-assembly.

Among pH-sensitive polymers, the poly(amino acid) PGA has been of particular interest, due to its biocompatible nature and success in forming highly stable structures. PBD-*b*-PGA[92] was shown to self-assemble at low pH conditions, once again, due to the titratable carboxyl pendant function. Vesicles showed a pH-tunable size between 100 and 150 nm. In this case the change in pH results in a coil-helix transition which drives the vesicle size change. This transition has been exploited with particularly impressive effect by Chécot *et al* by combining PGA with a second pH-sensitive poly(amino acid) poly(L-lysine) (PLys). Vesicles formed from

PLys-*b*-PGA have been termed "schizophrenic" due to their invertible membrane, as shown in Figure 5. At low pH PGA is hydrophobic and forms the membrane core, however as the pH is raised the membrane is inverted with the now hydrophobic PLys forming the membrane core.

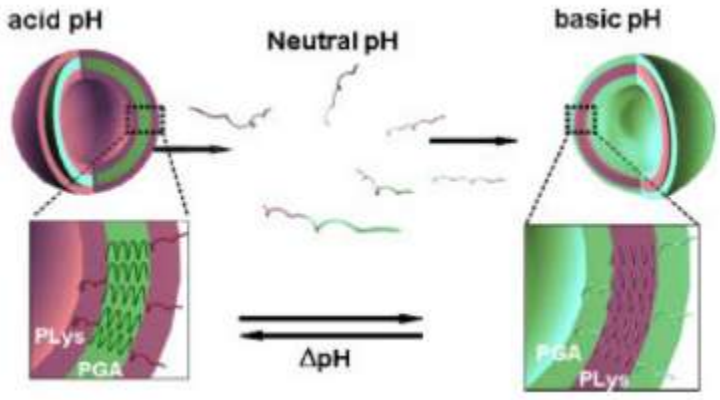

Figure 5 Self-assembly of "schizophrenic vesicles" from the di-block copolymer PLys-PGA. The hydrophobic and hydrophilic character of the two blocks are reversed by protonation and deprotonation of the copolymers with changes in pH.[92]

It is clear that there exists a great diversity of relevant stimuli-responsive materials that have been developed into nano-structured drug carriers. Table 1 below presents many of the recent systems that have been developed with particular emphasis on common copolymer systems and polymer-peptide hybrid materials. As well attention is given to systems with demonstrated sensitivities for control of degradation and/or payload release.

Table 1 Polymer vesicles from polymer-peptide and polymer-poly(amino acid)s

Polymer	Formation Method	Sensitivity/Target/Release Mechanism	Reference
PEG-*b*-PLA	Solvent Displacement	Enzymatic Degradation	[93]
PEG-*b*-PCL	Solvent Displacement	Enzymatic Degradation	[80]
PEG-*b*-PTMBPEC	Solvent Displacement	pH-triggered hydrolysis	[20]
PBLG-*b*-HYA	Solvent Displacement	CD44 receptor	[94]
PB-*b*-PGA	Dissolution (Water)	pH, Magnetic field, ionic strength	[73]
PTMC-*b*-PGA	Solvent Displacement	Magnetic field, pH	[40]
PGA-*b*-PBD	Hydration (High pH)	pH (Size Change)	[18]
PEG-*b*-(PG2MA-IND)	Hydration (pH 2.0 – 3.5)	pH (Hydrolysis)	[90]
PEG-*b*-P2VP	Solvent Displacement	pH (deformation)	[95]
PLys-*b*-PLE	Solvent Displacement	pH (deformation)	[96]
PLLys-*b*-PLTyr	Dissolution (Water)	Lactobionolactone, cross-linking	[97]
PLArg-*b*-PLLeu	Solvent Displacement	Cell-penetrating	[97]
PMPC-*b*-PDPA	Hydration (pH 2.0 – 6.0)	pH < 6	[98]
PEG-b-PS-*b*-PDEAMA	Solvent Displacement	pH (membrane permeability)	[99]
PLys-*b*-PGA	Hydration (pH <4 or >10)	pH (membrane inversion)	[100]
PAMPA-*b*-PNIPAAm	Dissolution, Heating	Temperature	[101]
PCEMA-*b*-PNIPAAm	Dissolution, Heating	Temperature	[46]
PEG-*b*-PNIPAAm	Dissolution, Heating	Temperature	[83]
PHA-*b*-PLLeu	THF/Water processing	Cell-penetrating	[102]
mPEG-*b*-P(Asp)	Dissolution (Tris-HCL, pH 7.4)	PICsome	[103]
PLGA-*b*-PPO-*b*-PLGA	Dissolution (0.1 M KOH)	pH and Temperature	[104]
PLA-*b*-PNIPAAm	Hydration	Temperature	[105]

PEG-*b*-PPS-*b*-PEG	Solvent Displacement	Oxidation	[55]
PEG-SS-PPS	Film Rehydration	Reduction	[106]
PAA-*b*-PAzoMA	Solvent Displacement	UV light (deformation)	[107]
PGA-*b*-PBD	Fe_20_3 in Water	Magnetic field	[54]
PEG-*b*-PI	Fe_20_3, magnetic field	Megnetic Field	[14]
PLL-*b*-PGly	Film Rehydration	pH	[108]
PNIPAAm-*b*-PZLys	Solvent Displacement	pH and Temperature	[109]
PBLG-*b*-K/E	Hydration	Enhanced immunogenicity	[110]

The comprehensive summary given in table 1 provides an overview of current materials used in stimuli-responsive drug-delivery systems. Several of these systems will be described in detail in the sections to follow.

Techniques for Characterization of Polymer Nanostructures

A key component of the study of nanostructures in general (and vesicles in particular) is the ability to well-characterize and well-define the structure morphology. To this end, a number of techniques have been utilized, the most common of which are dynamic and static light scattering (DLS and SLS respectively). Light scattering techniques are used primarily for determination of size and polydispersity of dispersed nanostructures, providing both the hydrodynamic radius (R_H) and the radius of gyration (R_G)[111]. The comparison of these values gives the R_G/R_H ratio, a valuable indicator of structure morphology. Data produced from these measurements can also provide estimates of the mean molecular weight, aggregation number and the 2nd viral coefficient (a measure of the chain-solvent interactions).

For dilute solutions, the scattered light measured from a polymer solution consists of the light scattered by the small solvent molecules plus the scattering from the large polymeric

species. If the scattering of the pure solvent is measured separately it can be subtracted from the solution scattering and the scattering due to the polymer molecules alone can be isolated. The data can be analyzed via a Zimm Plot in which the KC/R_θ values are plotted on the y-axis versus (sin ($\theta/2$) + kc) on the x-axis, where k is an arbitrary constant.

Samples measured at constant concentration with varying angle of incident light can be extrapolated to a "zero-angle" point (with an x-coordinate equal to kc). Likewise, samples measured at constant angle with varying concentration can be extrapolated to a "zero-concentration" point (with an x-coordinate equal to ($\sin 2(\theta/2)$). Each of the extrapolated "zero angle" points can be extrapolated to zero-concentration (x value equal to 0). Similarly the extrapolated "zero-concentration" points can be extrapolated to zero-angle (x value equal to 0) and these two lines ideally intersect on the y-axis, the inverse of the molecular weight. The second viral coefficient is obtained from the initial slope of the zero-angle line and the radius of gyration is abstracted from the initial slope of the zero-concentration line.

A variation of the Zimm Plot used for analyzing high molecular weight samples. Was proposed by Berry, is to plot $(KC/R_\theta)^{1/2}$ values. The intercept then yields the inverse of the molecular weight and the viral coefficient and radius of gyration can be determined similarly to the Zimm plot. The larger the difference in scattered intensity between the solvent and solution, the greater the precision of the parameters determined from the light scattering experiment. The increase in scattering intensity of the polymer solution over that of the pure solvent (at constant measuring angle) depends on four factors: the polymer molecular weight, the concentration of the polymer solution, the difference in the refractive index between the solvent and the polymer solution, and the wavelength of the laser. The polymer molecular weight is obviously fixed but the other parameters can be adjusted to increase the scattering intensity for a poor scattering

sample. Increasing the solution concentration (being careful to remain in the dilute solution region, changing the solvent to one with a larger dn/dc value for the particular polymer, and decreasing the wavelength of the laser, all increase the scattering intensity.

Additionally, light scattering has been used to monitor vesicle stability under degradation conditions or under changing pH or temperature conditions. Zeta potential measurements by DLS can also give information about the electrophoretic mobility of nanostructures, depending on the surface charge of vesicles. This can be of particular interest for pH-sensitive structures. By measuring the light scattered from the particles, a number of properties can be extrapolated, however, for direct visualization of nanostructures, one must turn to microscopy.

Microscopy provides direct visualization of nanoparticles for examination of size, morphology and uniformity. In general, optical microscopy is not suited for examination of nano vesicles due to its intrinsically limited resolution, and so electron microscopy is most commonly used. For high resolution images, both scanning and transmission electron microscopy (SEM and TEM) are used[62,63] for visualization of nano-sized structures. In general, sample preparation can be quite simple, though depending on the polymers used, additional staining may be required. Sample preparation requires drying of the suspended vesicles onto a substrate, a process that can distort the structures. As a result, cryogenic-TEM is sometimes utilized. By this technique, vesicles are rapidly frozen in order to visualize more accurately[62].

With the aim of visualizing the specific localization of certain blocks within a vesicle structure, fluorophores can be used as labels and fluorescence microscopy used[112]. By this method, again limited by intrinsic resolution, specific regions of vesicle structures can be

accurately and clearly seen, giving information about their internal structure. Confocal laser scanning microscopy (CLSM) is another popular tool for visualization of polymer vesicles[113,114]. Optical slices of polymer vesicles in the z-direction can be obtained by using CLSM and in principle the slices can be combined providing a 3D stacked vesicular image. One of the interesting possibilities of fluorescence techniques is to study the dynamics such as diffusion and rotational mobility of nanostructures by time-resolved measurements.

Nanostructures from Polymer-Peptide Hybrids

In recent years, research has moved past the use of simple synthetic polymer and poly(amino acid)s for nano-structure design and effort has been made to create structures that contain biologically relevant peptide sequences. Such sequences have a greater potential for interaction with biological environments and have begun to show some success. Synthesis of peptides and polypeptides for this purpose can be achieved by a variety of methods.

With the aim of developing a method for producing well-defined, high-purity polypeptides, Solid-Phased Peptide Synthesis (SPPS) was first developed by Merrifield and coworkers[115]. The process involves using an N-protected amino acid, covalently linked to a solid support resin for the step-wise growth of the larger polypeptide. Deprotection of the supported amino acid yields the reactive N-terminal which can be used for coupling of the next sequential amino acid. SPPS thus involves repeated rounds of coupling and deprotection with purification (washing) after each cycle to produce carefully tailored polypeptides. Attachment of the polypeptide to the solid support during the synthetic process allows the desired product to be

retained during the washing cycles permitting high purity to be achieved. The final polypeptide product is obtained by removal of the solid resin. A number of amino acid protecting groups are commonly used including 9-fluorenylmethyloxycarbonyl (FMOC) and t-butyloxycarbonyl (BOC), each requiring different chemistries for deprotection. Due to the efficiency of its cleavage relative to the BOC, FMOC is known to give both higher purity and higher yield.

Although this method can be laborious recent advanced in technology mean it can be automated with a microwave-based peptide synthsizer. Additionally this method allows for production of high purity peptides resulting from the wash cycles performed after each amino acid addition. Unlike production of peptides by other methods, SPPS allows for total control over the peptide sequence and can be used for production of compound that may be difficult to produce by other means.

Although this method is widely used for production of smaller (< 50 amino acids) peptides, larger peptide sequences are not generally possible. As the peptide length increases the coupling efficiency decreases, meaning complex polypeptides cannot be prepared. Additionally, purity and solubility become increasingly challenging at higher molecular weights and can limit the length of the polypeptide prepared in this fashion. Finally, in all steps of this process it is necessary to utilize an excess of amino acid for the coupling resulting in increased usage of materials. Consequently, SPPS is generally only used for production of smaller polypeptide sequences[115].

For production of much larger polypeptide sequences or protein fragments, smaller segments are often synthesized separately and linked together by means of native chemical ligation[116]. This method allows for creation of large complex protein fragments by means of a chemoselective reaction between two unprotected peptide fragments. The reaction avoids the use of traditional peptide bonds by reacting a peptide-thioester with an unprotected cysteint residue on an adjacent peptide. This reaction produces a thioester intermediate product which is unstable, which rearranges to the stable amide bond (in place to the classical peptide bond).[116]

Native chemical ligation does not utilize large BOC or FMOC protecting groups and so many of the solubility and stability issues associated with SPPS are avoided allowing for larger polypeptides to be produced. Additionally, due to the chemoselective nature of the reaction, minimal byproducts are procuded. Apart from linking smaller peptide segments to produce larger ones, this method is also often employed to include unique functional groups in polypeptides that may not generally be available with traditional amino acids[117].

The main advantages of this method are the possibility to produce very large polypeptides, the avoidance of protecting groups and typical solubility issues as well as the avoidance of unwanted by-products. In generally, this is a very simple reaction compared to production of peptides by SPPS, however as it is used for linking of smaller peptide fragments, this fragments must still be synthesized by other means[118].

Production of large (milligram) quantities of well-defined poly peptides has been a significant challenge with the previously discussed synthetic techniques. More commonly, for

large scale production synthesis can be performed by the ring-opening polymerization of a *N*-carboxyanhydride functionalized amino acid. This technique is commonly used for production of poly(amino acids) and block copolymers based on polypeptides. ROP produced less well-defined macromolecules compared to SPPS or NCL, but can produce larger quantities more readily and enables the production of more unique molecular archetectures. In addition, for application in drug deliveray and nanostructure self-assembly ROP of a NCA is most commonly utilized[119]. This method has been used with success for production of a broad range of polypeptides and block copolymers from both natural and synthetic amino acids and analogues.

The ROP of NCA generally proceeds through one of two mechanisms; the activated monomer mechanism or more commonly the amine mechanism.[119] The primary difference between the two mechanisms is in their initiation, the former proceeding *via* a deprotonation and the later by nucleophilic substitution. ROP of NCA can proceed via two mechanisms: the normal amine mechanism (NAM, induced by nucleophilic substitution) and the activated monomer mechanism (AMM, induced by deprotonation). In both cases a relatively broad size-distribution is common resulting from the polymer propagation and chain growth. Narrow distributions are particularly difficult to achieve when high degrees of polymerization is required or when branched or complex architectures are designed, due to unwanted side reaction s which can also be initiated by amine groups or deprotonation.

In recent years ROPs of NCAs have been attempted with a number of other mechanisms each with its own problematic drawbacks.[120] Use of heavy metal catalysts results in a final product requiring intense purification to remove the metallic products, which can be time

consuming and difficult. Certain amine salts have been used such as hexamethyldisilazane (HMDS) amines, however they are highly sensitive to degradation and require stringent conditions for use. The most promising progress in this area has been the use of a BF4 primary amine as an initiator, as used by Coneios-Sanchez and coworkers.[121] The use of this salt has allowed for production of large quantities of well-defined polypeptides resulting from the non-neucleophilic character of the initiator salt. This method offers a great degree of control over the molecular weight, functionality and polydispersity.

The opportunity to use functional non-natural polymers in combination with the scalable synthesis makes the ROP of NCA a great choice to reach well-defined polypeptides. Besides their multiple functionalities, adjustable *M*ws (1–1000 KDa) and structural homogeneity favor self-assembly into defined nanostructures with potential biomedical and pharmaceutical applications. One of the trends in the development of polymeric based nanomedicines is the building of well-defined, reproducible and homogenous architectures. Thus, the synthesis of narrowly distributed polypeptides for their potential use in biomedicine is a desirable goal.

Several nano-scale systems based on polymer-peptide hybrid materials have recently been developed that use biologically relevant peptides within their nanostructures in order to interact with biological systems. To this end Jabbari et al produced nano-vesicles from the polymer-peptide hybrid V6K2-poly(lactic acid) (PLA)[7]. The V6K2 peptide is derived from intracellular proteins and incorporated into the polymer conjugate with the expectation of improving cellular uptake of the assembled particles. Nanoparticles assembled from these conjugates showed enhanced cellular uptake over a 24 hour period compared to that of analogous

PEG-*b*-PLA particles. Fluorescence imaging to the incubated cells is shown in Figure 6, where the drug loaded particle can be seen in green, localized in the cellular matrix.

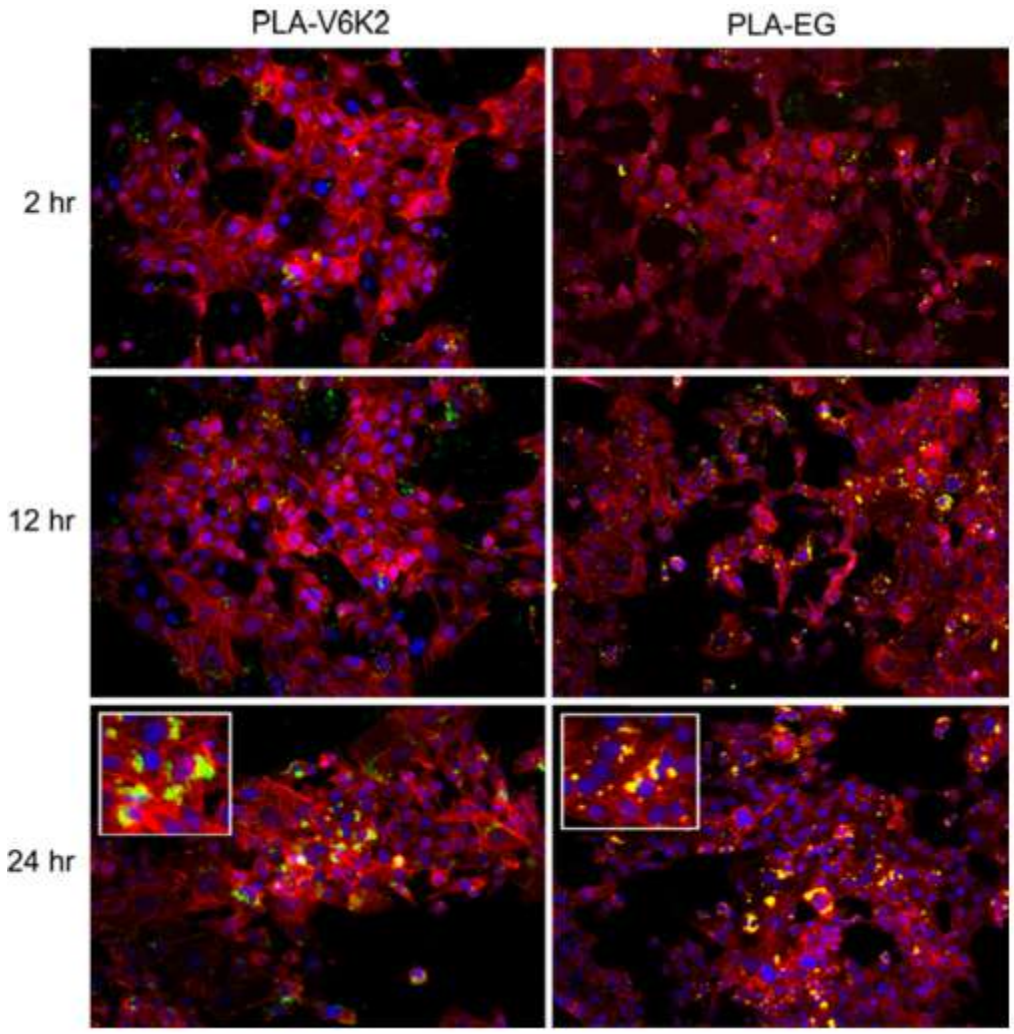

Figure 6 Fluorescence time lapsed micrographs of cellular localization of polymer-peptide hybrid particles[7]

With similar goals, Drappier *et al* were able to form nanoparticle from the HIV-associated peptide sequence TAT, conjugated to the semi-crystalline polymer PTMC[4,128]. This sequence has been shown to enhance cellular uptake and was shown to form stable well defined nanoparticles. Such peptide-polymer hybrids show potential not only to increase interaction with biological systems, but also increase "stealth" capabilities, and potential to successfully cross the blood-brain barrier; a significant challenge in drug delivery systems[129]. Mathews et al successfully designed two conjugates RGDPAYQGRFL-*b*-poly(ε-caprolactone) (PCL)-*b*-poly(ethylene glycol) (PEO) and WXEAAYQRFL-*b*-PCL-*b*-PEO polymer-peptide hybrids, which showed extremely higher affinity for cancer cell lines than previously known tumor homing proteins, such as RDG-mimicking proteins[5]. Anti-cancer drugs could be directly conjugated to these structures or alternatively these structures could be used as encapsulating structures for storage and delivery of active ingredients. By this strategy, polymer-peptide hybrids can be exploited for enhanced targeting of nanostructures.

Peptides are the natural substrates for biological enzymes and as such have been used with particular efficacy for development of enzyme-responsive nanostructures with potential applications in biomedicine. The peptide sequence AYL was coupled to a branched PEG polymer for production of a hydrogel. In the presence of the enzymes plasmin and trypsin the hydrogel was shown to selectively degrade.[130] Conceptually, this idea can be extended for production of structures sensitive to a broad range of biological enzymes.

The ability of certain peptides to form stable secondary structures has recently been exploited, to produce a micelle system capable of being cleaved by the biological enzyme

chymotrypsin. In this case the enzymatic substrate AAKLVFF, known to form stable β-sheets was coupled to a high molecular weight PEG to produce micelles. The peptide can be cleaved by chymotripsin for release of the peptide which can proceed to influence gene expression.

As previously discussed the attachment of PEG provides a stealth feature to nanoparticles, improving the circulation time of PEGylated structures and reducing biological clearance. Extended circulation lifetimes result from reduced recognition by the host response system (reduced immunogenicity) and reduced enzymatic degradation. This concept has been widely employed in the development of therapeutic materials.

The group of Kataoka conjugated P(asp) to PEG for production of polyionic micelles, having a highly charged character. Due to the charged nature of the micelle, oppositely charged drugs and payloads were shown to have a high affinity for the carrier through electrostatic interactions with the charged peptide block. Additionally, in aqueous solutions the charged enzyme lysozyme could become trapped in the micelles leading to the degradation of the structure. This affinity was further enhanced by addition of aromatic groups to the copolymer structure. In the case of this PEG-b-PAsp structure the presence of the charged peptide and the level of interaction between the peptide and the payload and enzyme were key to the structure function.

Indeed the use of charged nanostructures based on polypeptides has been widely used for stabilization and enhanced affinity with specific enzymes and drugs. This technique has been utilized for enhancement of solubility of insoluble compounds and/or insoluble hydrophobic

molecules. PEG-SS-PAsp has been developed to not only enhance the solubility of the anticancer drug adriamycin,[131] but additionally to provide a redox-sensitive release mechanism. Within the cytoplasmic environment the disulfide bridge linking the polymer and peptide could be selectively reduced by glutathione. Adriamycine showing strong interaction with the PAsp block through the electrostatics between the carboxyl unit of the peptide and the amine group of the drug. Such drug-carrier interactions are here greatly exploited for the benefit of the delivery system. In a similar redox-sensitive system, PEG-b-PLys and PEG-b-PAsp were complexed to form micelles and showed a reversible cross-linking in the presence of either reductive or oxidative conditions.[103]

Likely, the most commonly used polypeptide is PGA, which has been widely used as a pH-sensitive block for polymer-peptide conjugates. Similar to poly(aspartic acid) diblocks, conjugates of PEG with poly-(glutamic acid) have been used for the delivery of the anticancer drug doxorubicin[65]. Following a similar concept, a hydrazone unit has been used as an acid-sensitive linker to release adriamycin from PEG−p(Asp) conjugates in endosomes or lysosomes. Complexation of PEG−b-PGA−cholesterol conjugate with a platinum-containing anticancer agent leads to the formation of metal-containing polymersomes.

For application in DNA therapy several polypeptide-based systems have been developed which take advantage of the high cationic charge of the well-known PLys. When conjugated to PEG this system has been shown to form micelles with long-circulation times, capable of binding (through electrostatic complexation) with plasmin DNA in vitro. PLL−PEG diblock copolymers have been used as micellar drug delivery systems for DNA, showing an increased

resistance to nucleases of plasmid DNA encapsulated in the core because of electrostatic interaction with PLL. A similar system based on Plys-b-PEG-b-Plys allowed for the stable and slow release of the drug paclitaxel from the formed charged micelles.[103]

For applications in x-ray imaging nanoparticles assembled from PLL−b-PEG diblocks were shown to have extended circulation times. Photodynamic therapy has been proposed as a means to treat disease, such as cancer. The concept is based on first localizing nanoparticles at the site of diseased tissued and subsequently inducing toxicity via a light-triggered mechanism. PEG−b-PLL diblocks form charged ionic micelles upon complexation with oppositely charged porphyrins. Porphyrins provide the structures with a high level of photodynamic efficiency which can be exploited intracellularly as a therapeutic structure. Micelle forming PEG−peptides incorporating synthetic peptides such as PBLG or PBLA have similarly been used to encapsulate a variety of poorly water-soluble drugs.[132] PEG−b-PBLG diblocks have been observed to self-assemble in aqueous solution, and the core of the micelles can be loaded with the benzodiazepine drug clonazepam. The release rate decreases with increasing PBLG chain length. A PEG−b-PBLA diblock has been used to solubilize indomethacin, a nonsteroidal anti-inflammatory drug[133]. The release rate was found to increase with pH in the range 1.2−7.4.

Drug Delivery Systems from Polymeric Nanostructures

Two main factors make polymer vesicles particularly attractive as drug delivery vehicles. The first is their stability, which relative to analogous structures such as liposomes is comparatively long-term. Secondly, is the structure itself, comprised of two main regions; the

aqueous cavity and the hydrophobic membrane interior. As a result of this multi-compartment systems, polymer vesicles, similar to biological cells, can be used as carriers for hydrophobic, hydrophilic and amphiphilic molecules. Hydrophobic and amphiphilic molecules can be encapsulated within the hydrophobic region of the membrane with water-soluble molecules encapsulated in the aqueous cavity. Recent studies have seen a wide range of payloads loaded into the membranes of polymer vesicles, including dyes and quantum dots as well as molecules more relevant to drug delivery such as anticancer drugs and membrane proteins[20,21,60,134]. Such proteins and drugs have been shown to maintain their functionality regardless of encapsulation[60].

Encapsulation of drugs and other payloads can be localized within the aqueous cavity or membrane interior of polymer vesicles by a number of strategies. By incorporating the molecules into the organic phase along with the copolymer prior to vesicle formation, drugs can be encapsulated during the self-assembly process. This method can be used for encapsulation of both hydrophilic molecules in the aqueous cavity as well as hydrophobic molecules in the membrane interior. This method has been used successfully for encapsulation of drugs such as paclitaxel (PTX) and doxorubicin (DOX)[20,89]. In many cases polymer vesicles show comparable drug loading capacity to liposomes and in some cases have far exceeded traditional loading capacities[89]. In addition to high loading capacity, polymer vesicles were shown to be much more stable than comparable liposome formulations. In addition to this coprecipitation technique, drugs can also be loaded into pre-formed vesicles by application of pH or salt gradient which drives the diffusion of drug molecules into the vesicle[135,136].

The vesicle membrane acts as a physical (and in cases a chemical) barrier holding payloads within the structure. Drugs are released from the vesicle by a diffusive mechanism with the drugs crossing the vesicle membrane, driven by a concentration gradient with the external medium. In the simplest of cases, drug release from polymer vesicles is governed by diffusion, but can be strongly influenced by chemical interactions between the drug and copolymers used as well as by the localization of the drug within the vesicle structure[137,138]. Drug release has been shown to also be somewhat influenced by the size and distribution of the vesicle population. Spatial and temporal control of drug release can be controlled by selection of specific copolymers or changes to the environmental conditions of release.

As discussed earlier, much research has focused on the use of stimuli-responsive materials for the production of "smart" polymer vesicles capable of controlled and/or triggered drug release[56,139]. To this end, vesicles with responses tunable to changing external environments have been developed. Most commonly, polymers have been used that are responsive to changes in local conditions such as temperature, pH, redox environment and glucose concentration as well as external conditions such as light, magnetic field or ionic strength. In general, strategies involving stimuli-responsive materials are used in order to trigger or enhance membrane permeability, disrupt the vesicle structure or alter the hydrophobic/hydrophilic characteristics of the copolymer structure in order to induce drug release. By exploiting stimuli-responsive vesicles, drugs can be stably encapsulated within the carrier and triggered to release only at a target site. This technology holds potential for site-specific drug delivery for reduction of therapeutic side-effects and enhancement of efficacy.

In drug delivery systems for biomedical applications, one of the most relevant stimuli is pH, due to the changing pH conditions throughout the body and in various cellular compartments. Particularly relevant for drug delivery systems are the acidic environments of cancerous tissues (pH 6.5-7.2) , endosomes (pH 5.0-6.5) and lysosomes (pH 4.5-5.0) which have been utilized for anticancer drug delivery and intracellular drug delivery[140,141]. pH-responsive systems are generally designed to encapsulate and remain stable at physiologically neutral pH (7.4) and to be triggered to release in the more acidic organs or organelles of the body[142]. Sensitivity to pH of a polymer is dependent on the presence of a titratable group (usually a carboxyl or amine function) along the polymer side-chains or within the polymer backbone. Changes in pH can protonate or deprotonate these functionalities triggering release of the payload. The critical pH of the copolymer is dependent on the pKa of the functional groups. Most commonly, a change in pH of the system will result in a disruption of the hydrophilic/hydrophobic balance of the copolymer, which is critical to the assembly of the system, resulting in structural disruption and triggered release. For example, PEG-*b*-poly(2-vinylpyridine) (PEG-P2VP) vesicles can be completely solubilized at a pH below 5[95]. P2VP is insoluble in water under neutral and basic conditions, but soluble at acidic conditions. Similarly, PLys-*b*-poly(leucine) (PLys-*b*-PLE) vesicles showed a pH-dependent solubility and eventually a pH-triggered release[96]. Upon lowering the pH, PLys becomes protonated, leading to the solubilization of the membrane and the release of the encapsulated payload.

In addition to disruption of the hydrophilic/hydrophobic balance, changes in pH can also induce cleavage of covalent bonds within the copolymer structure or cause alterations in the permeability of the vesicle membrane. These changes can be used to create a ‘burst’ release or to

modulate the release rate of encapsulated drugs. This strategy has been used to particular effect by Chen *et al* in creation of their DOX and PTX-loaded vesicles from PEG-*b*-poly(2,4,6-trimethoxybenzylidenepentaerythritol carbonate) (PTMBPEC)[20]. The drug release could be modulated and enhanced by changing pH to affect the rate of degradation of the polymer backbone. Faster degradation occurred under low pH conditions resulting in a more rapid drug release. Reported "breathing" polymer vesicles based on a tri-block copolymer of PEG-*b*-PS-*b*-(poly(2-diethylaminoethyl methacrylate), PDEAMA) showed pH-sensitive membrane properties[99]. In this case, the permeability and thickness of the membrane could be modulated under changing pH conditions due to increasing and decreasing electrostatic interactions between the titratable copolymer chains. Due to the presence of a rigid PS layer at the membrane interior no disassembly was observed, however, significant changes in the membrane thickness could be observed. Micrographs of this effect can be seen in Figure 7, showing the change in vesicle size between pH 10.4 and 3.4[99].

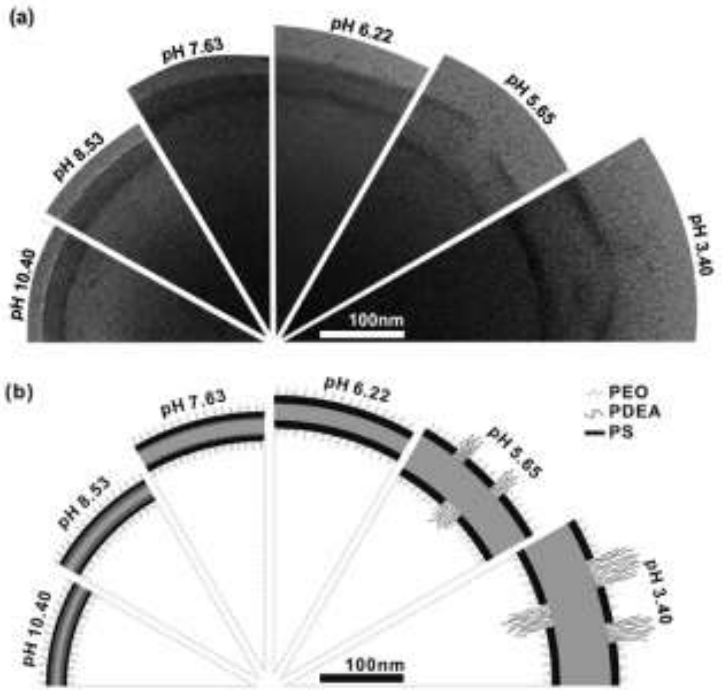

Figure 7 (a) Cryo-TEM images of the vesicle wall at several pH values. (b) Membrane structure at corresponding pH values[99]

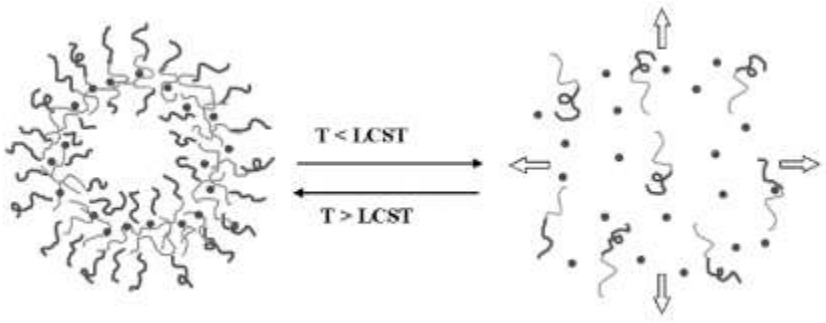

Figure 8 Schematic illustration of vesicles from PEG-*b*-PNIPAAm copolymer at 37 ºC and 25 ºC, respectively[143]

Temperature as a stimulus is also of particular relevance in drug delivery due to the stable well-defined body temperature. Most commonly, thermo-responsive drug delivery systems have included the well known polymer PNIPAAm, which has been frequently used for production of stable polymer vesicles. As discussed earlier, the sharp phase transition temperature (LCST) of PNIPAAm close to human body temperature induces a coil to globule conformation change in the polymer resulting in a hydrophilic/hydrophobic transition. This property was exploited with particular effect by Qin *et al*[143], who prepared stable vesicles by dispersing the full hydrophilic PEG-*b*-PNIPAAm copolymer in water and raising the system temperature above the LCST to induce assembly. This process was completely reversible with vesicle disassembly occurring when the temperature was once again reduced below the LCST. This process is shown schematically in Figure 8.

In addition to pH and temperature, there are large changes in the redox environments of different cellular systems. Within extracellular environments, conditions are generally oxidative, however in inflamed tissues or within cancerous and intracellular compartments, reductive

conditions exist. This difference in microenvironment can be exploited by using redox-sensitive polymers for the design of drug delivery vesicles. Hubbell and co-workers developed oxidation responsive polymer vesicles based on PEG-*b*-poly(propylene sulfide)-*b*-PEG (PEG-*b*-PPS-*b*-PEG)[106]. Over a two hour period, under oxidative conditions, the PPS layer was shown to destabilize due to oxidation, resulting in disruption of the nanostructure. This disruption could also be observed within cellular endosomes.

In addition to systems that respond to specific stimuli, much research has been directed to systems that can respond to biological enzymes. Of particular interest are the cancer-associated enzymes matrix metalloproteinase (MMP) 2 and 9 which are known to be strongly associated with aggressive solid tumours[144,145]. These enzymes are found highly expressed in tumour tissues but in only low levels in healthy adult tissues. They thus represent an ideal target for a DDS. Additionally, MMP-2, 9 are known to selectively cleave the peptide proline-valine-glycine-leucine-isoleucine-glycine (PVGLIG) between the gylcine and leucine residues[146].

Chau *et al*. used conjugates containing the PVGLIG peptide to demonstrate selective release of PTX in the presence of MMP-2, relative to conjugates containing a nonsense peptide or none at all[147,148]. The same conjugates were then able to preferentially localize PTX within tumor tissues in vivo. It is evident that the design of potential drug carriers and nanostructures which can incorporate PVGLIG offers a unique opportunity for drug targeting of the tumor microenvironment.

It is clear that for clinical applications of drug delivery systems it is desirable to use biocompatible and biodegradable polymers for vesicle formation. Approaches in triggered release have begun to exploit the biodegradable nature of some polymers in order to control the release rate of drugs. Biodegradation most commonly occurs via hydrolysis of the polymer, however the rate of hydrolysis is greatly dependant on the nature of the specific polymers chosen. By selecting specific biodegradable polymers, the rate of biodegradation can be controlled, in the presence of water or biological enzymes. The most common biodegradable polymers used for this purpose are PLAs[129], PCLs[149], PTMC[40] and PEG[56], each showing unique hydrolysis rates under biologically relevant conditions.

Passive and Active Targeting of Drug Delivery Systems

Current chemotherapies suffer from a number of drawbacks which limit the efficacy and versatility of the treatment. The most significant disadvantage of these kinds of therapies is a lack of specificity. Traditional chemotherapeutic agents are administered to a patient intravenously, circulate throughout the body and interact with both cancerous and healthy tissues. Since the healthy tissues as well as cancerous tissues are exposed to the active agents (drugs), chemotherapy often results in significant and severe unwanted side effects for the patient, due to the damage caused to surrounding healthy tissues. The damage caused to healthy tissues limits the treatments in two significant ways. Firstly, due to the adverse effects of the drugs on the patient, treatment often needs to be stopped prematurely to avoid permanent damage to other healthy tissues. Secondly, the achievable drug dose in a tumour, for example, is limited by the damage being done to surrounding tissues. The drug dose at the target site may be

well below the dose required to successfully treat the cancer effectively. Current cancer therapies are thus greatly limited not by the drugs being used but by their lack of specificity. There is thus a need for targeting cancer therapy using a drug delivery system (DDS).

Targeting drug delivery systems to tumour tissues can be broadly divided into two categories; passive targeting and active targeting. Passive targeting results from a size-based accumulation of particles in tumour tissues caused by the enhanced permeation and retention (EPR) effect[150–152]. This effect is a result of the unique physiology of cancer tissues compared to healthy adult tissues. The physiological difference is shown schematically in Figure 9 below. As cancerous tissues expand and grow very rapidly, their biological structures are comparatively underdeveloped. In healthy tissues, tight junctions within the walls of blood vessels prevent diffusion of everything but the smallest molecules into the surrounding tissues. Within rapidly expanding tumor tissues, however, the vessels are more leaky allowing for the diffusion of not only small molecules, but also large macromolecules and small structures. In addition, the lack of proper lymphatic vessels for drainage means that these particles cannot be removed effectively. As a result, there is a selective-accumulation of large molecules and small particles in tumor tissues. The EPR effect is seen in nearly all types of cancers which produce solid tumors, and can affect particles between approximately 20 and 200 nm[150]. This type of passive targeting allows DDSs to be concentrated in diseased tissues over time. The dose of the encapsulated drug is effectively enhanced in the immediate environment of the diseased cells, while simultaneously being reduced in the surrounding healthy tissues. While DDSs benefit from the EPR effect, it is only effective in limited types of diseased tissues (such as solid tumours). Consequently, additional targeting mechanisms must necessarily be investigated.

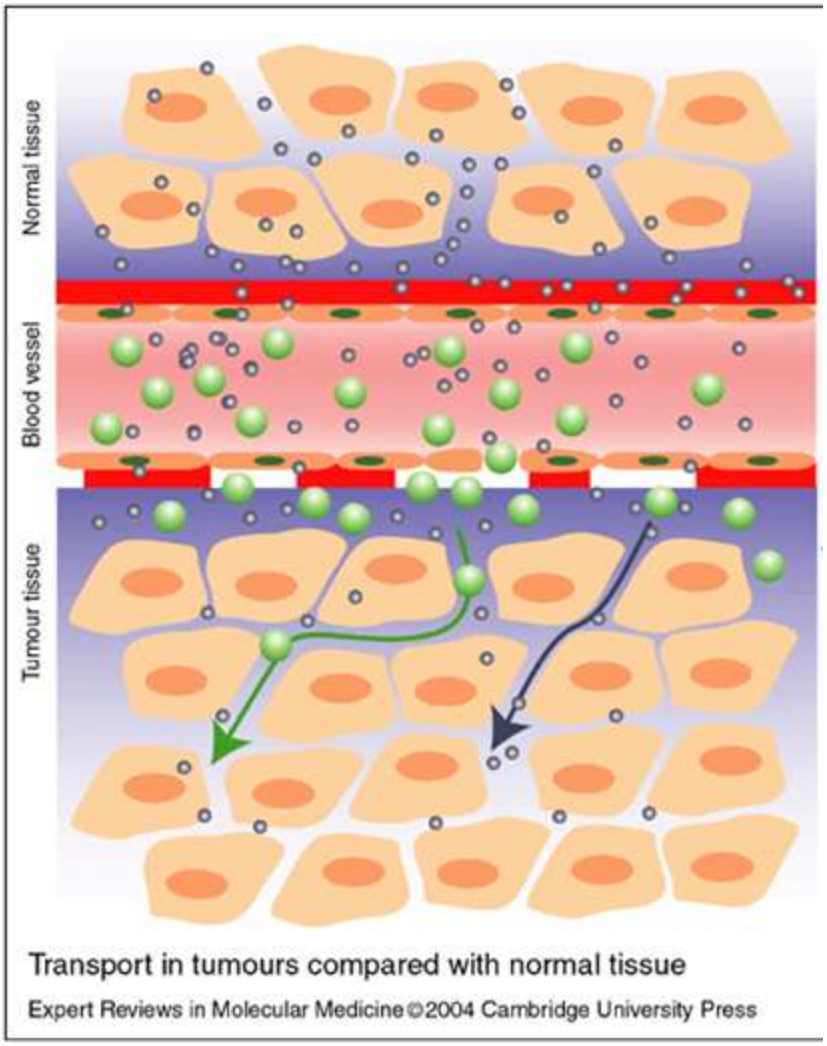

Figure 9 Schematic representation comparing transport in healthy tissues to the EPR effect seen in cancerous tissues.[150]

Within the application of drug delivery systems, one of the primary concerns for development of stable, long-circulating carriers is the clearance of nanocarriers by the body's immune system. Rapid clearance of nanocarriers will negate any designed therapeutic benefit. As

such, vesicles with "stealth" properties have been developed in order to avoid the body's natural clearance mechanisms[78,153,154]. These mechanisms begin with adsorption of biological proteins called opsonins during a process called opsonisation. These proteins can then bind to receptors on the primary immune cells, mononuclear phagocytes (MPSs)[155]. The carrier can then be internalized and broken down by these immune cells. It is clear that strategies for creating long-circulating vesicles must focus on avoiding of opsonisation.

To this end, several delivery systems have been developed to reduce the capacity of proteins to adsorb on the carrier surface[154]. Strategies to achieve this have focused on introducing surface layers on the vesicle comprised of various hydrophilic polymers that are not contusive to protein adsorption. Such polymers include polysaccharides, poly(amino acid)s (and their derivatives), poly(hydroxyethyl methacrylate) (PHMA) and most commonly PEG[156–158]. Such polymers have been extensively studied for use in drug carriers due to the remarkable stealth properties they can impart on nano-vesicles. Structures produced with "stealth" polymers have been shown to minimize interaction with blood components such as opsonins. The effect of these polymers on protein interaction is however, dependent on several factors, including molecular weight, concentration and the conformation of the polymer block. A comprehensive study of protein adsorption and PEG molecular weight was performed and showed that increase molecular weight was correlated with decrease protein adsorption, and therefore longer circulation times *in vivo*[21]. While it is clear that "stealth" materials have an important role to play, other factors such as particle morphology and surface charge may also have significant roles.

Interestingly, while the presence of PEG and other "stealth" polymers have been shown to increase circulation times *in vivo*, evidence has suggested that they may also limit the uptake of nanoparticles by all biological cells, due to reduced structure-cell interaction. Therefore the challenge moving forward is to design stable polymer vesicles with long-circulation times, without decreasing their ability to be internalized by target cells[21]. With this goal, several studies have focused on conjugation of actively targeted moieties to the surface of PEG-containing vesicles. Such molecules have included antibodies or antibody fragments or peptides recognized by internalization mechanisms of the target cells.

By using a combination of the targeting strategies mentioned, Li *et al* designed polymer vesicles with both "stealth" capabilities based on the presence of a PEG brush, but also cell penetrating character by presentation of a biologically relevant peptide sequence[6]. Nano-vesicles assembled from PEG-*b*-PAsp, in which the PAsp is modified in order to complex with DNA fragments, with the tumor-associated peptide sequence GPLGVRG linking the two polymer blocks were shown to have long-circulation times. In the presence of MMP-2 active enzyme, were shown to shed their PEG brush and become internalized by cancer cell lines. The strategy used by Li *et al* is shown below in Figure 10. Such systems can circulate freely in biological systems and can be directed to release active payloads within cells upon internalization. In the context of drug delivery systems, such hybrid systems able to combine the characteristics of both synthetic polymers and naturally occurring, biologically relevant peptides offer the greatest potential for future clinical applications.

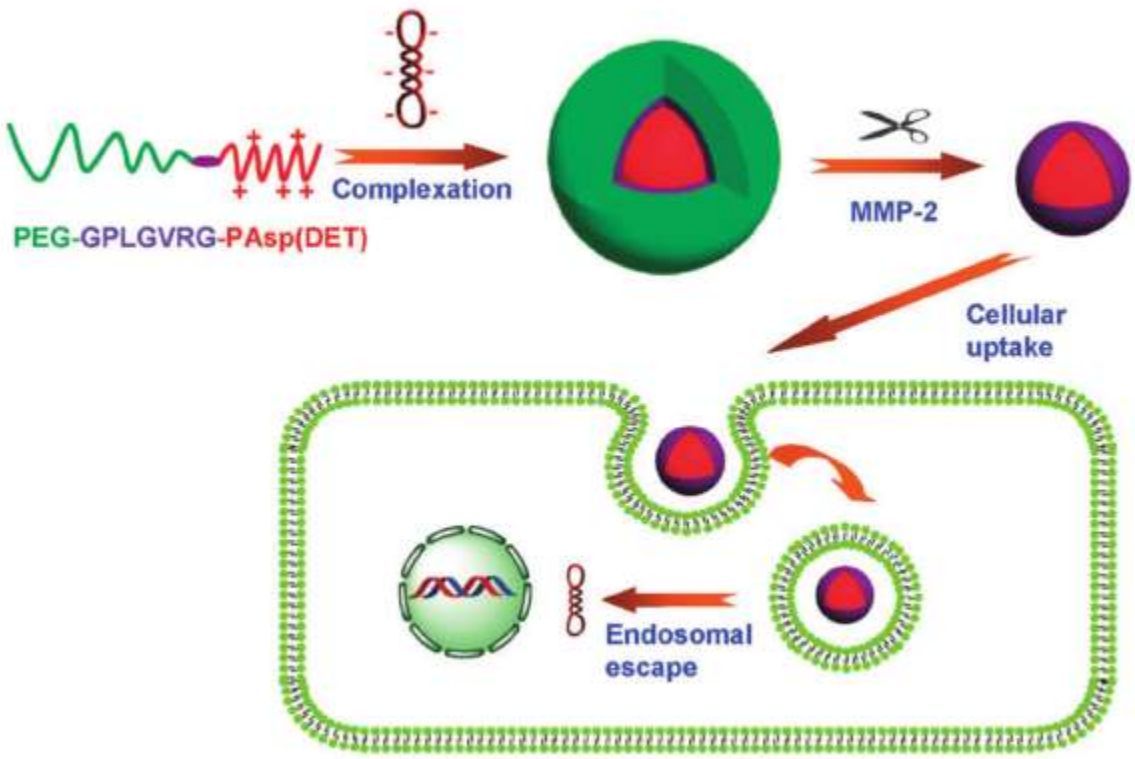

Figure 10 Strategy for exploitation of "stealth" characteristics and cellular internalization of polymer vesicles[6]

Chapter 3 Enzyme-Degradable Self-Assembled Nanostructures From Polymer-Peptide Hybrids

Introduction

In recent decades, amphiphilic block copolymers have garnered considerable interest for their ability to generate a broad range of self-assembled nanoscale structures[11–13,159]. With applications abound, considerable attention has been given to their use as drug delivery systems (DDS)[18,19]. The challenge in drug delivery has now become to move from polymers as "passive" materials to "active" ones where the material itself plays a functional role in the drug delivery process, *via* triggered release or imbuing environment-responsive attributes on the system[37]. To this end, poly(amino acids) have attracted significant interest due to their biocompatibility, stability and controlled secondary conformations[27]. These materials have been explored extensively in nanostructure formation to produce stable and responsive structures for controlled and triggered drug release[28]. Despite extensive research into poly(amino acid)-based systems, few self-assembled systems have been developed that incorporate biologically relevant peptides as both a structural and functional element[29,30]. Specific peptides that can act as cleavage substrates for highly selective enzymes offer an opportunity for the development of delivery vehicles with exceedingly specific degradation environments.

Hybrid materials based on the conjugation between synthetic polymers and biologically relevant peptides have recently emerged as a new class of soft nanomaterials[28]. These hybrid materials are capable of combining characteristics and functionalities of both polymers and

peptides allowing for unique chemistry, properties, functionality, self-assembly and applications[160–169]. These materials are of particular relevance in biomedical applications such as biological scaffolding and drug delivery, due to the often inherent biocompatibility of biologically relevant peptides and poly(amino acids)[170–172]. By combining characteristics and functionalities of both peptides and synthetic polymers, these hybrid systems provide a path towards new biomimetic materials.

Several actively targeted DDSs have previously been developed that respond to certain stimuli in the disease microenvironment such as temperature, pH, redox conditions and enzymatic complement[6,35,36]. Recently, systems incorporating biologically relevant peptide sequences have been engineered with some success, such as V6K2-poly(lactic acid) (PLA) by Jabbari et al.[7], Tat-*b*-PTMC by Drappier et al.[4,128] and RGDPAYQGRFL-*b*-Poly(caprolactone)(PCL)-*b*-poly(ethylene glycol) (PEO) and WXEAAYQRFL-*b*-PCL-*b*-PEO conjugates by Mathews et al.[5] Of particular interest in targeted cancer therapy is the well-known tumor-associated enzymes matrix metalloproteinase 2 and 9 (MMP-2, MMP-9), known to selectively cleave the peptide sequence PVGLIG[146,148,173]. These enzymes are part of the collagenase family associated with the degradation of the extracellular matrix and tissue remodeling[144]. In healthy tissues they are normally found in high levels during embryonic development and reproduction. In adults, these enzymes are expressed in extremely low levels in healthy tissues, however they are present in relatively high concentrations in aggressive tumors, that degrade the extracellular matrix to allow for tumor expansion[144]. This offers an ideal target for DDS design, where the nanoparticle can be concentrated and selectively degraded in the tumor microenvironment.

Chau et al. have previously demonstrated the cleavability of PVGLIG in the presence of MMP-2, -9 as well as the selective tumor accumulation of conjugates containing PVGLIG[147,148]. It is evident that the design of potential drug carriers and nanostructures which can incorporate PVGLIG offers a unique opportunity for drug targeting of the tumor microenvironment.

In this study, we demonstrate a versatile coupling of the MMP-sensitive, hydrophilic peptide PVGLIG to a hydrophobic and biodegradable polymer, namely, poly(trimethylene carbonate) (PTMC). We have utilized fast and easy UV-initiated thiol-ene chemistry to "click" ene-functionalized PTMCs of varying size to a thiol-containing version of PVGLIG. The subsequent hybrids were then self-assembled into nanostructures of differing morphology (vesicles, compound micelles and core-shell) depending on the polymer block-size. In addition, selective degradation of the nanostructures by MMP-2 is demonstrated. Such physiologically stable, self-assembled structures prepared from the biologically relevant peptide PVGLIG hold potential as both passively and actively tumor targeting drug delivery systems and offers an insight into the self-assembly properties of complex polymer-peptide hybrids.

Experimental

Materials

Trimethylene carbonate (1,3-dioxane-2-one: TMC) was purchased from Boehringer Ingelheim and dried on magnesium sulfate in tetrahydrofuran (THF), sublimated and stored in a glove box prior to use. Allyl alcohol (99 %), 1,3-bis(2,6-diisopropylphenyl)-imidazol-2-ylidene (NHC, 97

%), cysteamine (95 %), 2,2-dimethyloxy-2-phenylacetophenone (DMPA, 99 %), Fmoc-rink amide MBHA resin (1.1 mmol/g loading capacity), (benzotriazol-1-yloxy)tripyrrolidinophosphonium hexafluorophosphate (PyBOP, 98 %), triisopropylsilane (TIS, 99 %), *N*,*N*-diisopropylethylamine (DiPEA, 99.5 %) and piperidine (99.5 %) were purchased from Sigma-Aldrich and used as received. All Fmoc-protected amino acid derivatives (99 %) were obtained from Iris Biotech. Active, human, recombinant matrix metalloproteinase-2 (MMP-2) enzyme was purchased from Calbiochem. The enzyme was aliquoted and stored at -80 °C prior to use.

Synthesis of ene-functionalized $PTMC_n$

In a typical experiment, TMC was dissolved in dry THF (2 M) and added drop-wise to a solution of allyl alcohol (12 mM, 20 mM, 28 mM) and NHC (1 mM) in dry THF under inert atmosphere. The reaction was left stirring for 90 min at room temperature and quenched with methanol. PTMC was precipitated in ice-cold methanol and purified by centrifugation (10 min, 8000 rpm). The degree of polymerization was measured by end-group analysis of ^{1}H NMR spectrum. PTMC of DP 13, 21 and 33 were produced and dispersities were determined by SEC to be 1.08, 1.11 and 1.13, respectively, with yields of 85 %, 80 %, and 82 %, respectively. ^{1}H NMR (DMSO, 400 Hz) δ(ppm)= 2.0 (C(O)OCH$_2$C$\underline{H_2}$CH$_2$OC(O)), 4.2 (C(O)OC$\underline{H_2}$CH$_2$C$\underline{H_2}$OC(O)), 4.59 (H$_2$C=CH-C$\underline{H_2}$-), 5.29 ($\underline{H_2}$C=CH-CH$_2$-), 5.89 (H$_2$C=C$\underline{H}$-CH$_2$-).

Synthesis of PVGLIG peptide

The βAPVGLIGβAC (βAla-Pro-Val-Gly-Leu-Ile-Gly-βAla-Cys) (PVGLIG) peptide was grown and cleaved from the rink amide MBHA resin by traditional Fmoc/*t*-Bu solid phase chemistry. Briefly, the synthesis proceeded with successive rounds of deprotection and amino acid coupling. Coupling steps were performed using a solution of the Fmoc-protected amino acid (0.2 M), PyBOP (0.45 M) and DiPEA (2 M) in DMF for 40 min. Deprotection was performed with piperidine/DMF (1:4) and monitored by UV-Vis spectroscopy. The final peptide product and remaining protecting groups were cleaved from the solid support with a mixture of TFA/H_2O/TIS (95/2.5/2.5). The peptide was precipitated in diethyl ether and purified by semi-preparative RP-HPLC on a C18 column (Waters SunFire™ C18 5 μm, 10 x 250 mm). The structure was confirmed by ^{1}H NMR and ESI-MS and HPLC. Theoretical molecular weight = 798.44 g/mol, experimental m/z: [M+H]+ = 799.4. ^{1}H NMR (Figure 14) (DMSO, 400 Hz) δ= 0.95 (Combined 18 Leu, Ile and Val proton signal). Full synthetic scheme and chemical structures of all reagents used are shown in Figures 11 and 12 below.

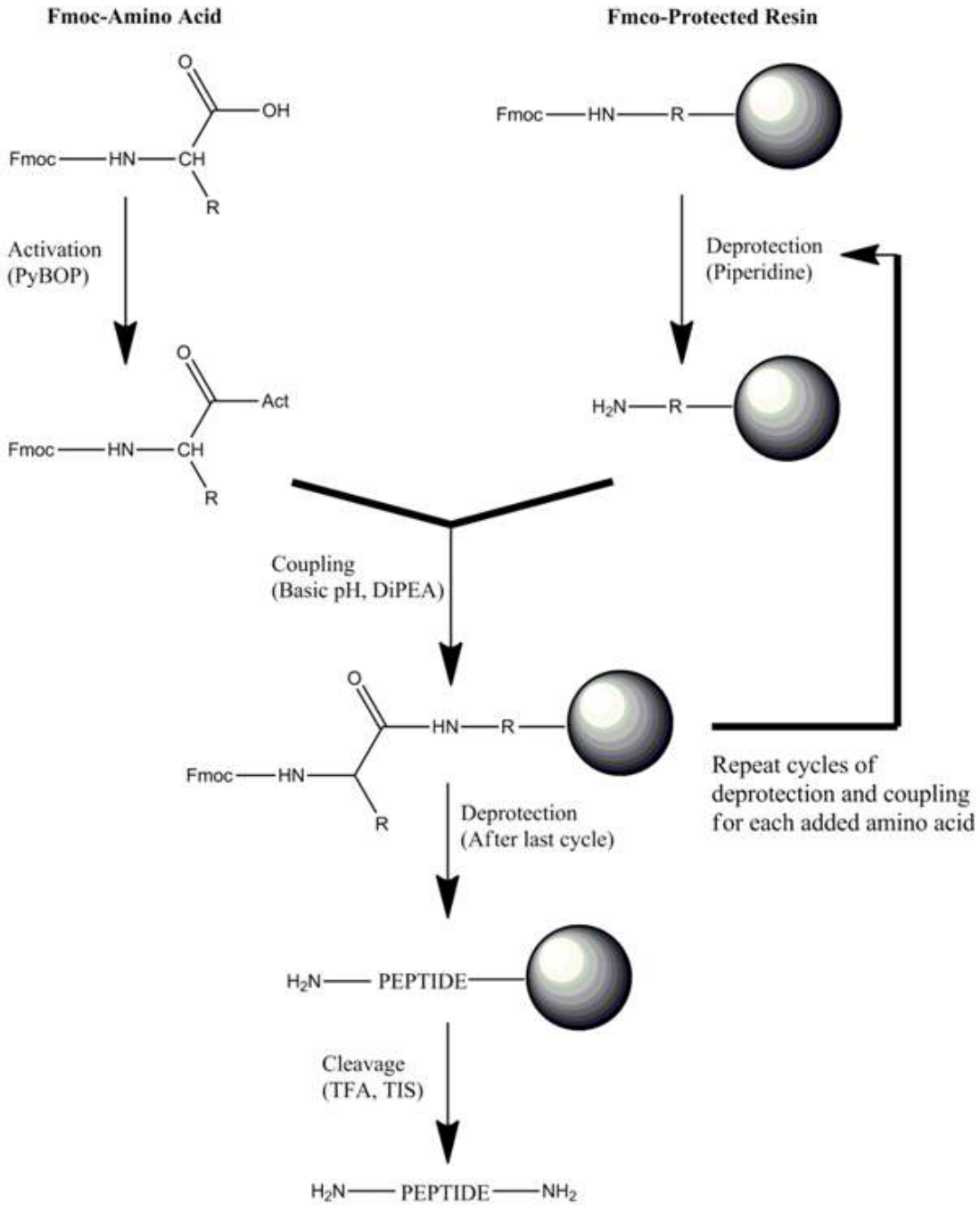

Figure 81 General synthesis protocol for synthesis of a peptide by Fmoc chemistry

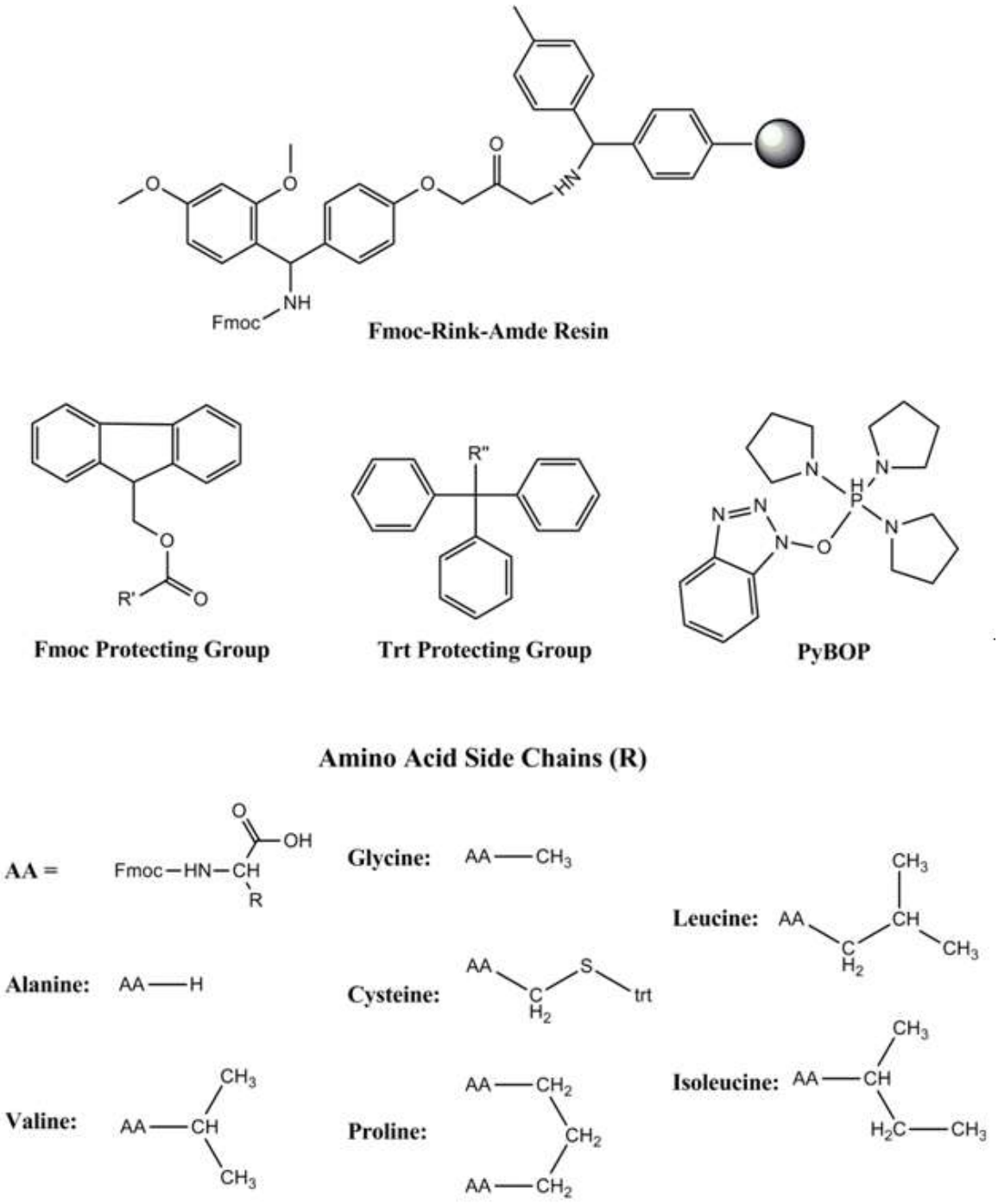

Figure 92 Chemical structure of all reaction reagents and amino acids used in preparation of PVGLIG

Polymer-peptide conjugation by thiol-ene click chemistry

Coupling of the ene-functionalized PTMC with the thiol group of the *C*-terminal cysteine residue of PVGLIG was achieved by UV-initiated thiol-ene click chemistry. In a typical experiment, PTMC (DP 13, 21, 33) (1 eq, 5 mM), PVGLIG (2 eq, 10 mM) and DMPA (1 eq, 5 mM) were dissolved in minimal DMF and irradiated with UV light (λ = 365 nm) for 1 h with stirring. The coupled product (PTMC-*b*-PVGLIG) was precipitated in ice-cold acetonitrile, centrifuged out and dried overnight under vacuum. Successful coupling was confirmed by ^{1}H NMR and SEC. ^{1}H NMR (DMSO, 400 Hz) δ(ppm)= 0.95 (PVGLIG), 2.0 (PTMC backbone), 4.2 (PTMC backbone).

Self-Assembly of diblock conjugates by nanoprecipitation

Self-assembly of $PTMC_n$-*b*-PVGLIG was performed *via* a nanoprecipitation method. PTMC-*b*-PVGLIG (5 mg) was dissolved in DMSO (500 µL). With vigorous stirring (700 rpm), water (4.5 mL) was added over 15 s. The nanoparticle suspension was then purified by dialysis against water over 3 days (MWCO = 13 000), with regular water changes. Structure morphology was probed with dynamic and static light scattering and TEM.

^{1}H NMR.

All measurements were done using a Brukner Adsvance spectrometer operating at 400 MHz. All measurements were carried out at room temperature with a fixed (7.5 s) relaxation time. d-DMSO was used as a reference signal (δ=2.5 ppm).

Size-exclusion chromatography

All SEC measurements were performed in dimethylformamide (DMF) with LiBr (1 g/L) as the eluent. The flow rate was fixed at 0.8 mL/min. Two 7.5 mm x 300 mm PLgel, 5 µm Mixed-D columns (Polymer Laboratories) were coupled to a guard column, 7.5 mm x 50 mm, PLgel, 5 µm (Polymer Laboratories). The system was equipped with a differential refractive index (RI) detector. Calibration was done with polystyrene standards.

Dynamic light scattering (DLS) and static light scattering (SLS)

DLS and SLS measurements were performed with a Brookhaven Laser Light Scattering system with a BI200SMv2 goniometer with a vertically polarized helium-neon diode laser at a wavelength of 636 nm and a BI-9000AT digital correlator with a 125 ns initial measurement time. Samples were kept at constant temperature (25 °C) for the duration of measurements. Measurements were taken every 10 ° between 60 ° and 140 °. SLS measurements were analyzed in a Berry plot to obtain the radius of gyration.

Degradation of $PTMC_n$-*b*-PVGLIG nanostructures by MMP-2 active enzyme

Degradation of the assembled structures was performed *in situ* and conducted in DLS cells at 37 °C. In a typical experiment active MMP-2 enzyme (10 nM) was added to suspensions of $PTMC_n$-*b*-PVGLIG (n= 13, 21 or 33) self-assembled hybrids (10 µM) in buffer (50 mM Tris pH 7.5, 10mM $CaCl_2$, 0.2 M NaCl). Degradation of the structures was followed by monitoring the scattered intensity (that is directly proportional to the size and weight of the nanoparticles) measured by DLS at 90° over a 48 h period.

Transmission electron microscopy (TEM)

TEM images were recorded with a Philips CM10 TEM microscope using a 60 keV acceleration voltage. Samples were prepared by depositing one droplet of the dispersed nanoparticles onto a carbon-formvar grid (200 mesh coated with copper) and allowed to dry. No additional staining was performed.

Micro differential scanning calorimetry (μDSC)

Thermograms were recorded using a VP-DSC Microcalorimeter from MicroCal, LLC. Measurements were performed on 0.8 mL of 10 mM solutions of dispersed nanoparticles. Solutions were first stabilized at 10 °C prior to scanning. Measurements were taken between 10 °C and 60 °C with a scan rate of 20 °C/hour with 10 min isotherms at 10 °C and 60 °C. Two heating and one cooling scans were recorded.

Synthesis of PTMCs, PVGLIG and $PTMC_n$-*b*-PVGLIG Hybrids

In order to produce a series of polymer-peptide hybrids, the PTMC and PVGLIG peptide precursors were synthesized separately and conjugated *via* thiol-ene click chemistry. The PVGLIG peptide was synthesized by traditional Fmoc/*t*-Bu solid phase chemistry with several additional amino acid residues. Namely, one β-alanine residue at both *C*- and *N*- terminal ends was included to act as a short spacer surrounding the Pro-Val-Gly-Leu-Ile-Gly cleavable sequence. A cysteine residue was also added at the *C*-terminal end to provide a thiol group suitable for the subsequent coupling to the polymer by thiol-ene reaction. The calculated molecular weight of the peptide was 798.44 $g.mol^{-1}$. The ESI mass spectrum of peptide figured

two peaks at m/z= 799.4 and 821.5 corresponding to the monocharged hydrogen and sodium cations, $(M+H)^+$ and $(M+Na)^+$, respectively (Figure 13a). DLS measurements showed no aggregation of the isolated peptide. The ^1H NMR spectrum of PVGLIG with peak assignments can be seen in Figure 14.

PTMC was synthesized using a one-step, metal-free ring-opening polymerization (ROP) utilizing allyl alcohol as the initiator and 1,3-bis(2,6-diisopropylphenyl)-imidazol-2-ylidene, a particular *N*-heterocyclic carbene (NHC) as the organic catalyst, to yield the final ene-functionalized polymer[174–176].

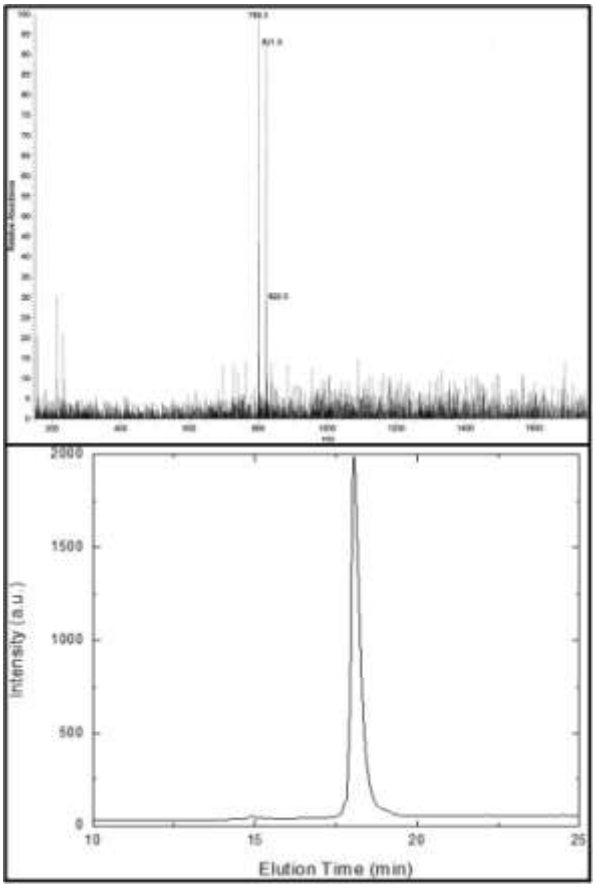

Figure 103 a) ESI-MS spectrum of purified PVGLIG peptide and b) HPLC trace of purified PVGLIG peptide

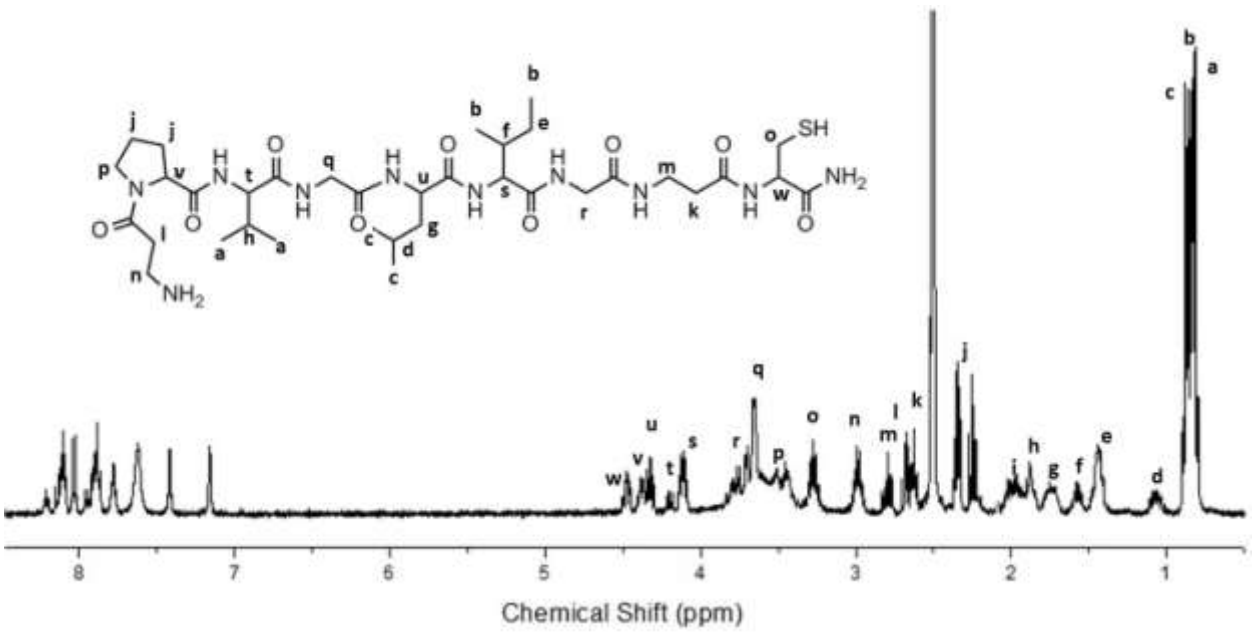

Figure 14 ^{1}H NMR spectrum of purified PVGLIG peptide (d-DMSO). Peaks from the backbone amine groups can be seen between 7 ppm and 8.5 ppm

Prior to synthesis, several preliminary studies were done in order to optimize reaction conditions for future syntheses. The kinetics of the reaction was studied by taking aliquots at key time points during the reaction and performing end-chain analysis of the ^{1}H NMR spectra obtained to determine the degree of polymerization (DP) and GPC to determine the respective polydispersity index (PDI). Figure 15 below summarizes the evolution of the polymer DP and PDI over time. It was observed that within 60 min the polymer could reach 88 % of the targeted DP and 90 % within 90 min. Further reaction time did not produce polymers closer to the target DP.

Interestingly, with increasing reaction time a consistent increase in PDI was observed by GPC. This increase continued even after polymerization of the main chains had stopped as seen

by the evolution of the DP during the same time course. The evolution of the degree of polymerization and the polydispersity can be seen in Figure 15. This increase in PDI is attributed to the formation of side-reaction products. The polymer is known to trans-esterify and this transester product can be seen on the ^{1}H NMR. At longer reaction times the polydispersity increases due to this transesterification process. Because of this side reaction the choice was made to quench reactions after 1 hour to limit the formation of unwanted by-products.

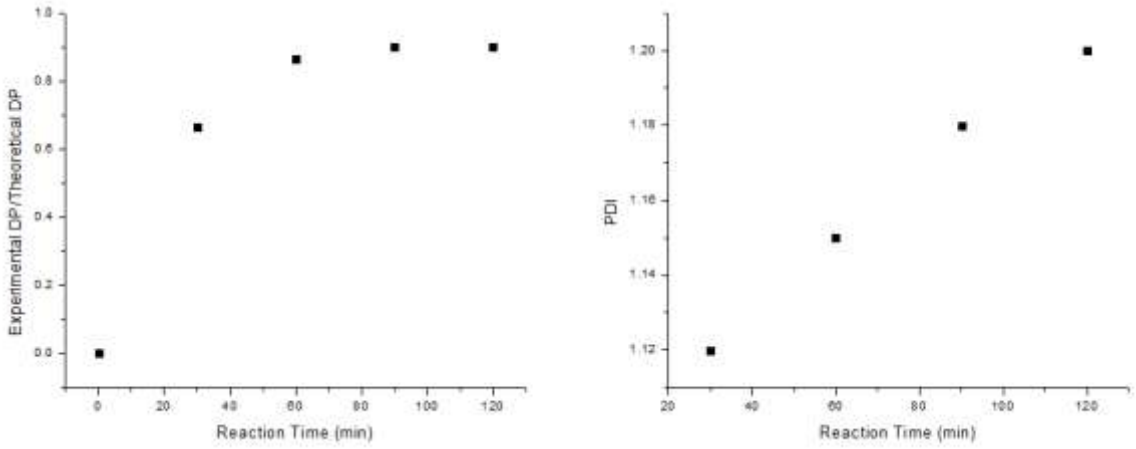

Figure 115 Evolution of the degree of polymerization over time (left). Evolution of the polydispersity of PTMC over reaction time (right)

PTMCs with chain length of 13, 21 and 33 and monomer conversion of approximately 88% (corresponding to one hour reaction time) and narrow dispersities (1.08, 1.11 and 1.13 respectively) were thus synthesized. The SEC trace is shown in Figure 20 for $PTMC_{13}$ as an example, revealing a low dispersity and monomodal distribution of PTMC chains. Longer reaction times led to increased trans-esterification side reactions[177], which results in substantially

higher dispersities approaching 1.30. By limiting the reaction time, the dispersity value could be kept relatively low and molecular weight could be targeted with reasonable precision. Typical ^{1}H NMR spectra of $PTMC_{13}$, $PTMC_{21}$ and $PTMC_{33}$ are shown in Figures 16, 17 and 18 respectively in which the terminal protons of the ene-functional group can be detected as 2 signals on the spectra at $\delta = 5.32$ and 5.81 ppm. In addition, a signal corresponding to the proton adjacent to the terminal hydroxyl group can be seen at $\delta = 3.48$ ppm, confirming the terminal functionalization of PTMC chains. In subsequent coupling reactions, these peaks were used as a probe to account of the coupling to the peptide. No signal due to side reactions such as trans-esterification reactions was detected on the spectrum. Further evidence of the polymer structure and quantitative introduction of the ene moiety was provided by MALDI-TOF mass spectrometry (Figure 19), showing a single distribution of peaks, with a peak-to-peak mass increment of 102.1 g/mol corresponding to the molecular weight of one TMC unit. Peaks appeared at $m/z = 102.1n + M_{termi} + 23$, n being the degree of polymerization, 23 the molecular weight of the sodium ion generated during the ionization process and M_{termi} the molecular weight of allyloxy and ene end groups.

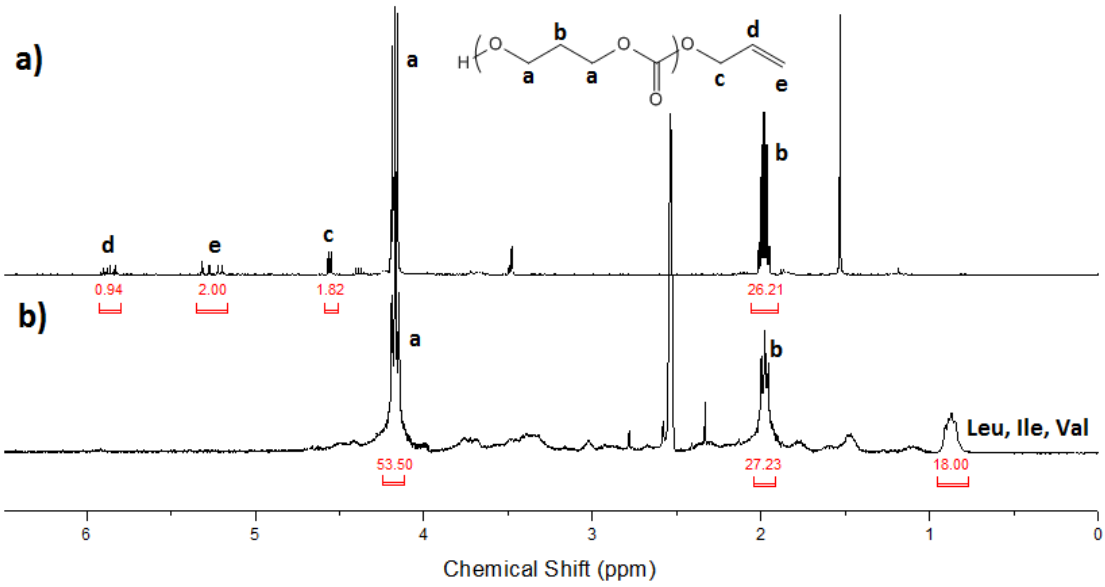

Figure 126 ^{1}H NMR spectra of a) $PTMC_{13}$ and b) $PTMC_{13}$-*b*-PVGLIG showing disappearance of the "ene" functionality and one-to-one coupling of $PTMC_{13}$ and PVGLIG

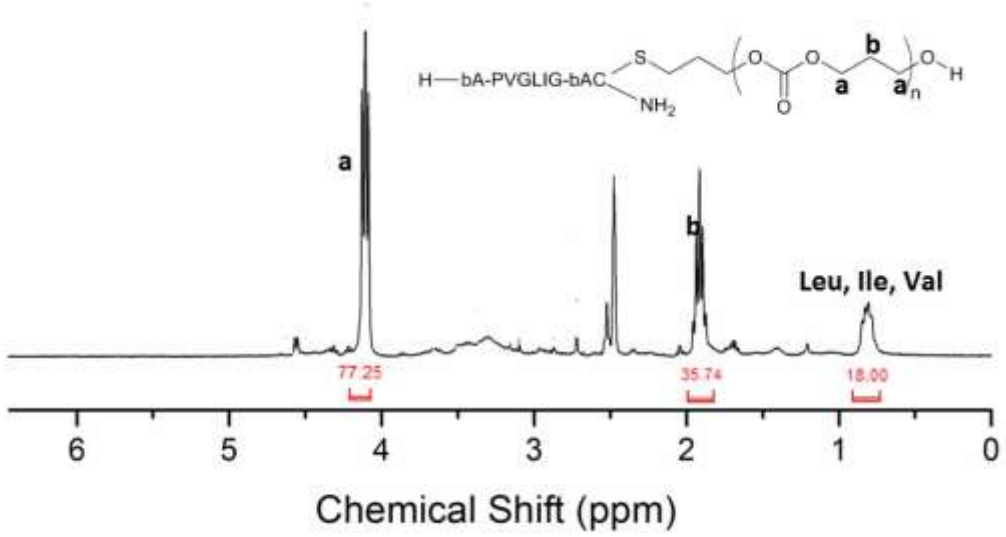

Figure 137 ^{1}H NMR spectra of $PTMC_{21}$-*b*-PVGLIG

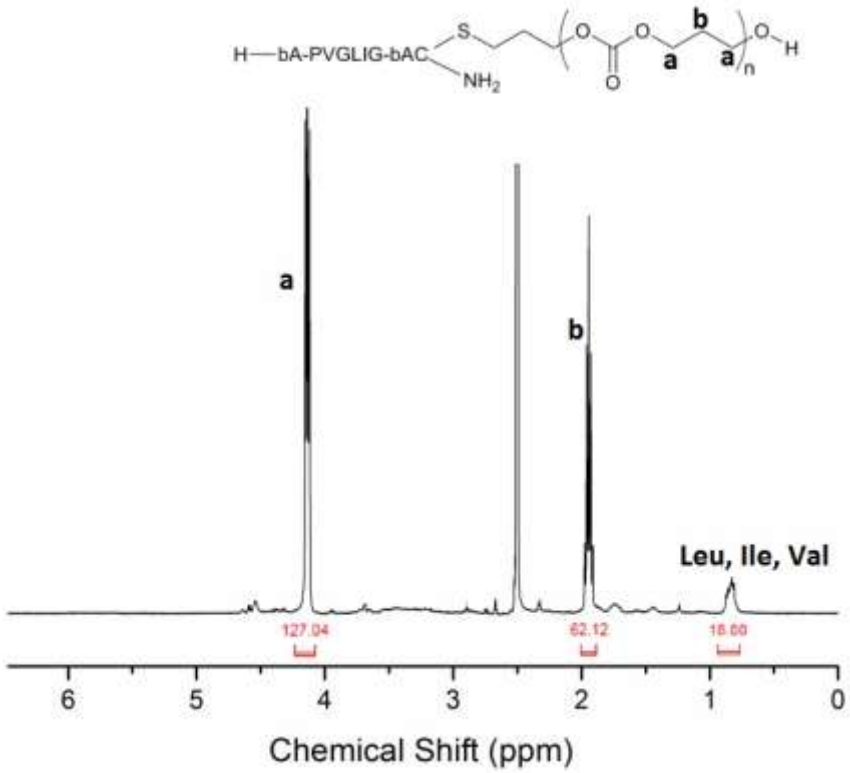

Figure 148 ^{1}H NMR spectra of PTMC$_{33}$-*b*-PVGLIG

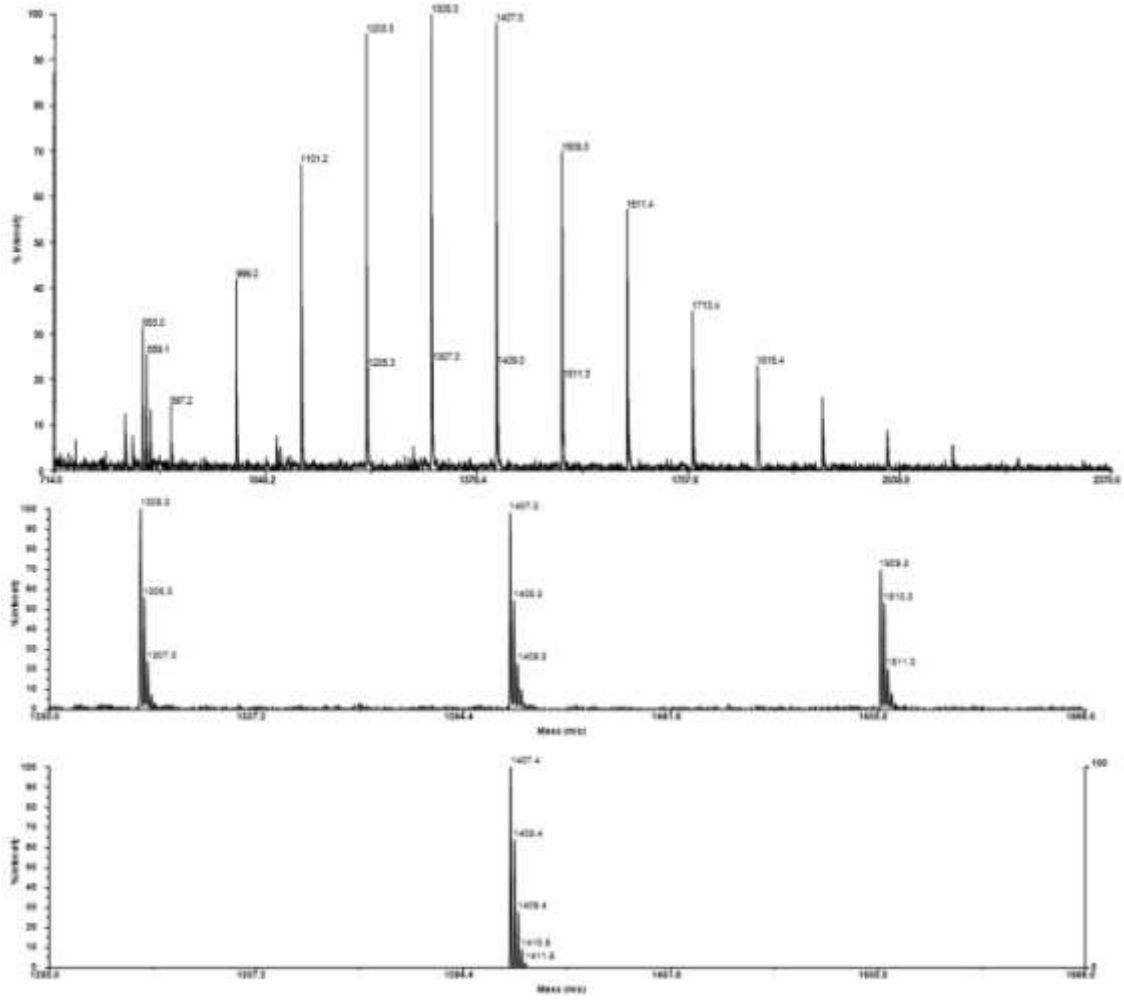

Figure 159 Full MALDI-TOF spectrum of $PTMC_{13}$

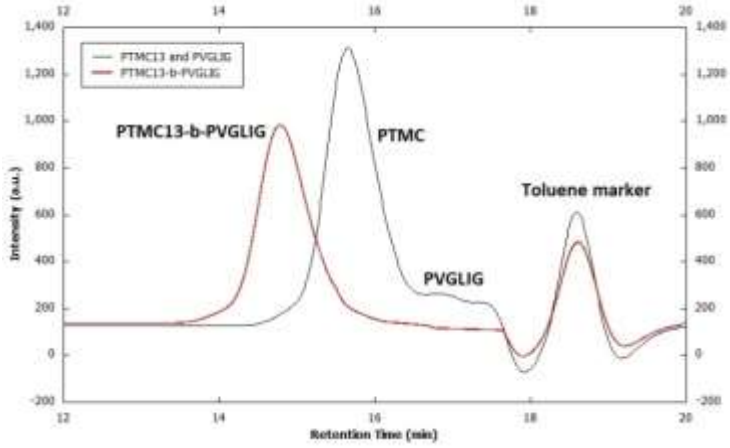

Figure 20 SEC trace in DMF with a toluene flow marker of $PTMC_{13}$ and PVGLIG prior to the coupling reaction and the $PTMC_{13}$-*b*-PVGLIG conjugate product (RI detection).

The successful coupling of the different PTMC segments and PVGLIG was accomplished *via* a thiol-ene click reaction[178–180] between the terminal ene-function of the PTMC and the thiol group of the cysteine residue of the peptide, used in excess (2 equiv.), as shown in Scheme 1. The excess of peptide was subsequently removed by extensive dialysis against water. The successful coupling between the PTMC and the peptide was confirmed by monitoring the disappearance of the "ene" peaks seen on the ^{1}H NMR spectra, at δ = 5.32 and 5.81ppm, and the marked shift in retention time on the SEC trace (Figure 20). The presence of the PTMC backbone peaks and the peptide peaks in the ^{1}H NMR of the coupled product after dialysis confirmed the successful coupling.

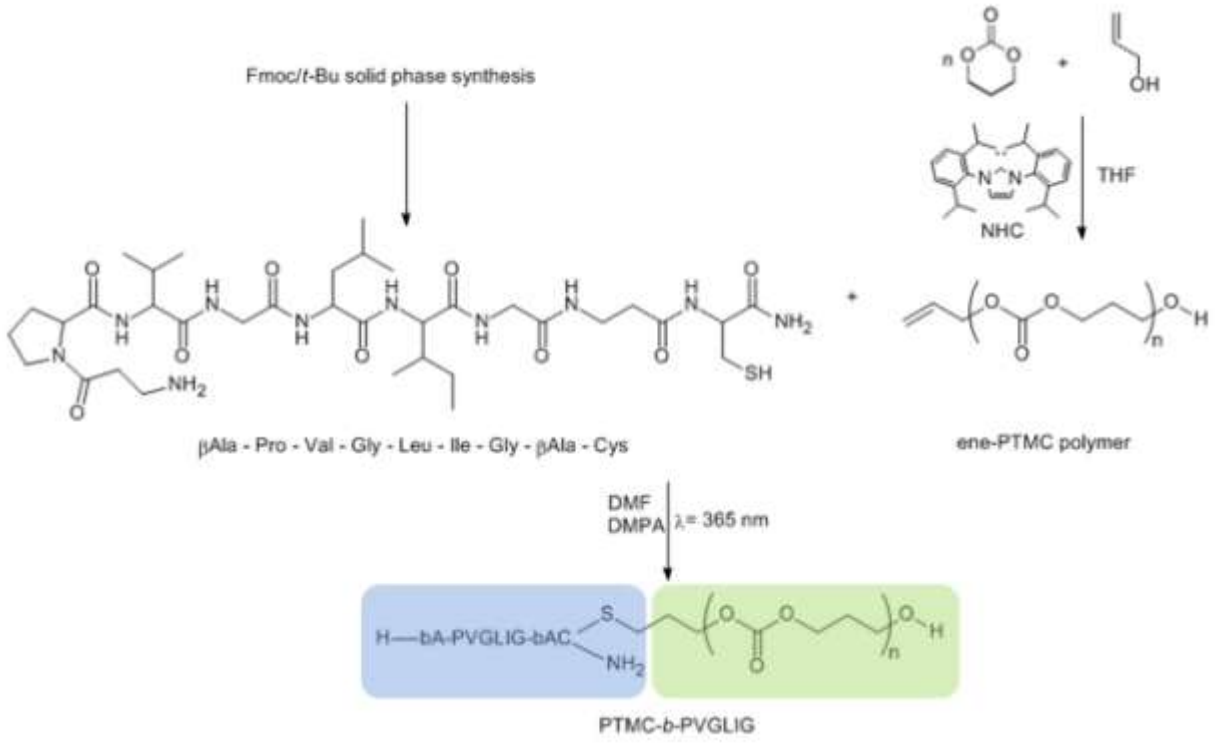

Scheme 1 Synthesis of $PTMC_n$-*b*-PVGLIG coupling via UV-initiated thiol-ene "click" reaction

Table 2 Characteristics of self-assembled polymer-peptide hybrid structures.

Hybrid	f^a(%)	$R_G{}^b$ (nm)	$R_H{}^c$ (nm)	PDI	R_G/R_H	Structure
$PTMC_{13}$-*b*-PVGLIG	38	73.7	68.8	0.19	1.05	Vesicle
$PTMC_{21}$-*b*-PVGLIG	28	65.5	52.6	0.31	1.25	LCM[d]
$PTMC_{33}$-*b*-PVGLIG	19.5	42.4	61.9	0.24	0.685	Core-shell

(a) hydrophilic weight fraction of the conjugate, (b) radius of gyration, (c) hydrodynamic radius, (d) large compound micelles

In addition, the integration of ^{1}H NMR peaks shows a 1:1 ratio between PTMC and the peptide, indicating a one-to-one coupling. This UV-initiated "click" reaction thus provides a versatile method for coupling large macromolecules in non-stringent conditions. A series of polymer-peptide hybrids were then produced by coupling PVGLIG with PTMC of DP 13, 21 and 33.

Self-Assembly of $PTMC_n$-*b*-PVGLIG Hybrids

After self-assembly in aqueous solution by nanoprecipitation and purification by dialysis, the obtained nanoparticles were analyzed by DLS, SLS and TEM. The results obtained from the light scattering are summarized in Table 1. As a result of their unique hydrophilic weight fraction (*f*), each of the hybrids formed stable, well-defined nanoparticles of differing morphology[13,17,181]. Complete DLS and SLS data can be found in Figure 21. All three self-assembled particles showed narrow size distributions over multiple scattering angles; as well, the values of the decay constant (Γ) for all particles exhibited linear q^2 dependence, the hallmark of purely diffusive motion related to the presence of spherical objects. Additionally, Berry plots generated from SLS data over a broad angle range displayed a linear relationship between $(I^{-1})^{-1/2}$ and q^2. All three hybrid systems yielded stable and well-defined nanostructures.

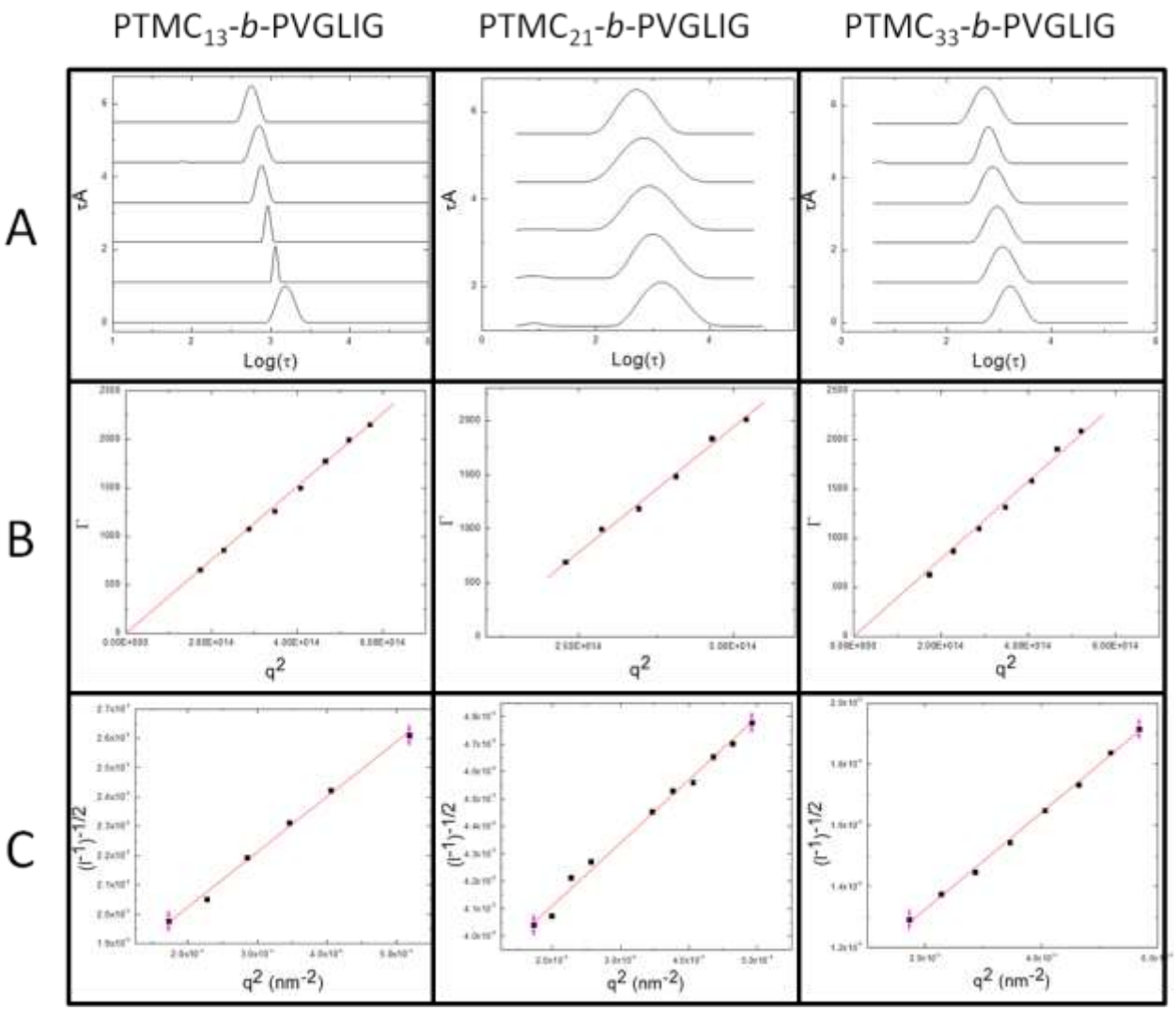

Figure 2116 A) Distribution plots, B) Decay times and C) Berry plots for all hybrids using multi-angle DLS and SLS

Careful examination of TEM micrographs of each hybrid nanostructure was also performed to determine the particle morphology. Typical micrographs are shown in Figure 22 along with schematic representations of each nanostructure for visualization. Based on both the R_G/R_H ratios obtained by light scattering and TEM observations, one can conclude that $PTMC_{13}$-*b*-PVGLIG produced vesicles, while $PTMC_{21}$-*b*-PVGLIG gave rise to large compound micelles (LCM) and $PTMC_{33}$-*b*-PVGLIG produced core-shell particles. The hydrophilic weight fraction

(f) of the hybrids was attributed entirely to the PVGLIG peptide, which had the same segment length in each conjugate. The change in f resulted from the increasing size of the hydrophobic PTMC block. By varying the hydrophobic weight fraction of the conjugates, these hybrids self-assembled into nanostructures of varying morphologies. Eisenberg and Discher[17] have previously demonstrated the importance of f in the morphology of self-assembled particles from flexible and neutral copolymers. In this study, similar effects were evidenced with the polymer-peptide hybrids, with the peptide playing the role of a hydrophilic polymer block. The hydrophilic weight fraction of $PTMC_{13}$-*b*-PVGLIG is 38 % and is consistent with a vesicular morphology and a cylindrical time averaged molecular shape of the diblock system. $PTMC_{21}$-*b*-PVGLIG and $PTMC_{33}$-*b*-PVGLIG have a lower f value and require denser packing of hydrophobic blocks within the nanostructure. As a result of the solvent displacement preparation, the assembled structures are not necessarily in thermodynamic equilibrium, allowing for highly dense regions of PTMC in the structures (seen as dark regions on the TEM images) compared to relatively less dense PVGLIG regions.

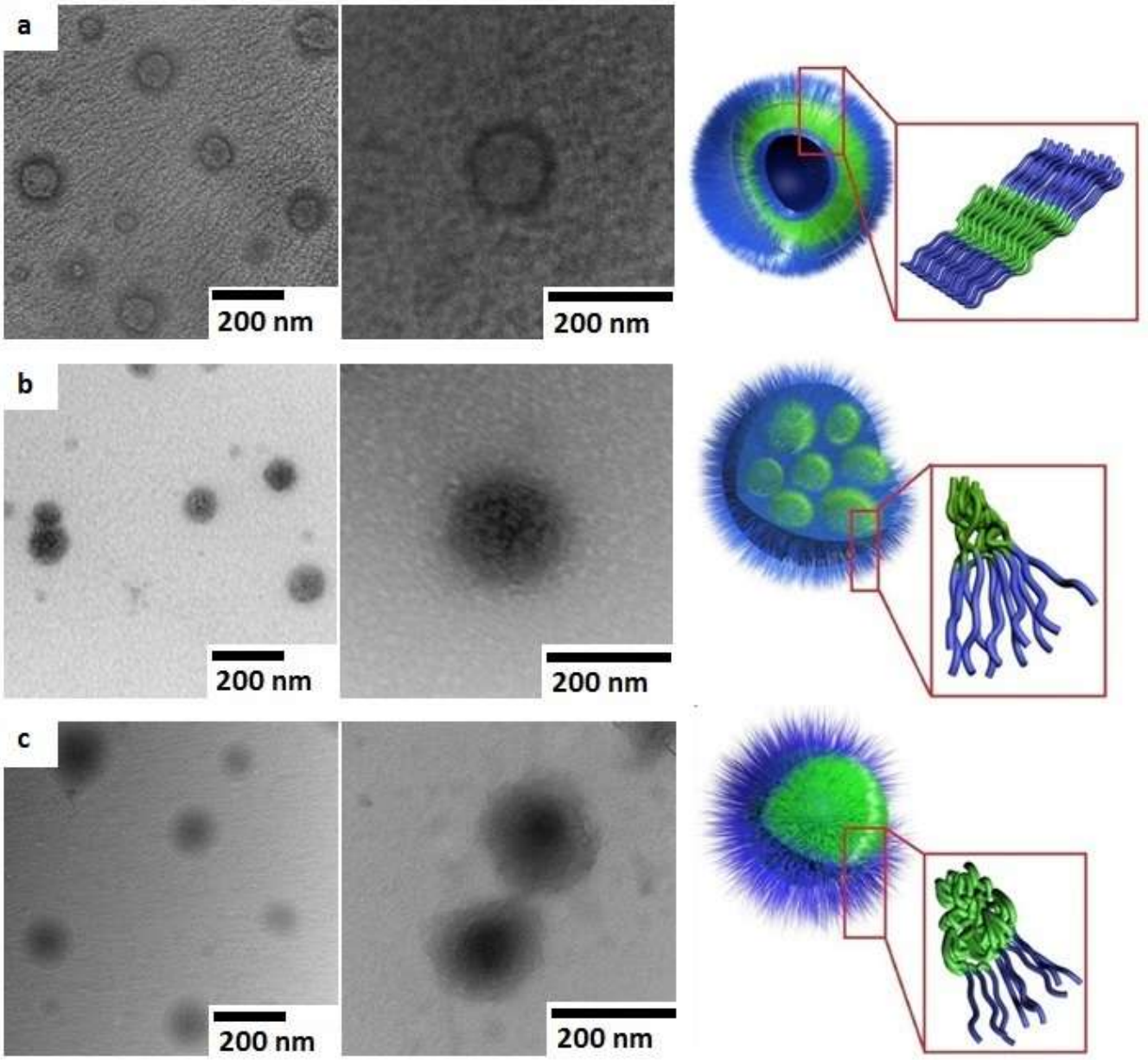

Figure 17 TEM micrographs and structural schematic of a) vesicle nanoparticles assembled from $PTMC_{13}$-*b*-PVGLIG, b) Large compound micelle nanoparticles assembled from $PTMC_{21}$-*b*-PVGLIG and c) core-shell nanoparticles assembled from $PTMC_{33}$-*b*-PVGLIG. In the schematics PTMC is represented in green and PVGLIG in shown in blue.

In addition, the tendency for PTMC to crystallize could have a dominant influence in the self-assembly process, as previously reported[40,182]. The phase transitions (melting point, $T_{m,}$ taken at the peak for simplicity) of each of the hybrid self-assembled structures have been measured in solution by μDSC thermograms (Figure 23, table 2). This crystallization observed with PTMC has a significant influence on the nanostructure morphologies, leading to structure morphologies not in line with the *f* values[70,183]. The extent to which this crystallization and the self-assembly method influences the structure morphology is currently under investigation. The nanoprecipitation process and the nature of PTMC, together allow for the hybrids with low *f* to form the variety of nanostructure morphology observed.

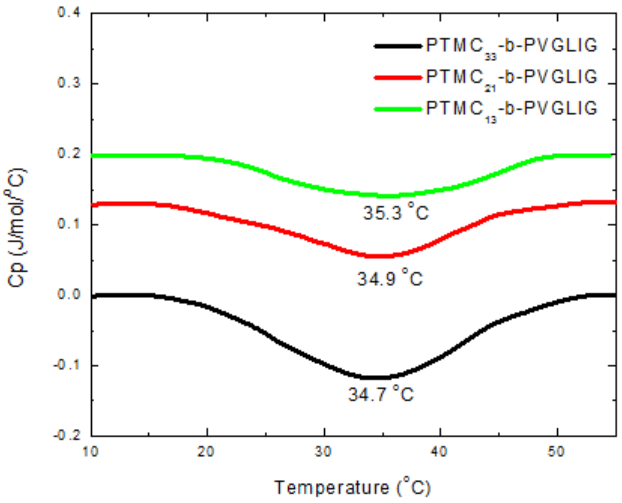

Figure 183 μDSC thermograms of three self-assembled hybrid conjugates during the first heating scan from 10 °C to 60 °C at a scan rate of 20 °C/hour after a 30 min isotherm at 10 °C.

Table 3 Thermal characteristics by µDSC of self-assembled hybrids.

Conjugate	T_m (°C)	Melting Enthalpy (J/g)[a]	Melting Enthalpy (J/mol)
$PTMC_{13}$-*b*-PVGLIG	35.3	4.57	5.94
$PTMC_{21}$-*b*-PVGLIG	34.9	2.45	5.15
$PTMC_{33}$-*b*-PVGLIG	34.7	2.68	8.84

(a) Normalized to PTMC mass in the conjugate

Degradation of Hybrid Particles by MMP-2

Enzymatic degradation was monitored by DLS by measuring the reduction in the scattered light intensity over time, which was correlated with a decrease in particle concentration and molecular weight. $PTMC_n$-*b*-PVGLIG nanostructures were subjected to degradation by MMP-2 active enzyme over a period of 48 hours, which is known to specifically cleave the PVGLIG peptide between the glycine and leucine residues[146]. Dynamic light scattering measurements at 90° were taken at t = 0, 24 h and 48 h. The resulting decrease in the scattering intensity is shown in Figure 24.

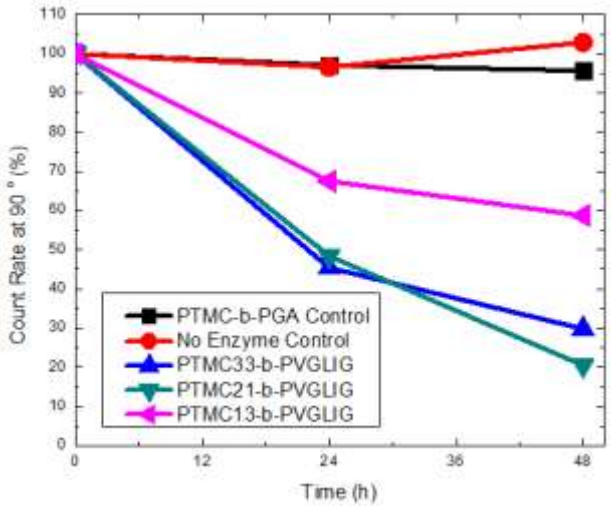

Figure 19 Light-scattering intensity variation during degradation of $PTMC_{13}$-b-PVGLIG, $PTMC_{21}$-*b*-PVGLIG and $PTMC_{33}$-*b*-PVGLIG nanostructures by MMP-2 active enzyme. $PTMC_{30}$-*b*-PGA_{13} vesicles in the presence of MMP-2 are used as a control. $PTMC_{13}$-*b*-PVGLIG vesicles with no enzyme present are used as a negative control.

All the particles (core-shell, LCM and vesicles) displayed significant degradation after 24 and 48 hours. Scattering intensity was below 30 % of the initial for both the core-shell and LCM particles formed from $PTMC_{33}$-*b*-PVGLIG and $PTMC_{21}$-*b*-PVGLIG, respectively, but it was significantly higher (near 60 %) in the case of vesicles formed from $PTMC_{13}$-*b*-PVGLIG. This might be due to the presence of cleavable PVGLIG at both the exterior and interior surfaces of the vesicles. It is likely that the peptide at the interior surface of the vesicles is not highly accessible to MMP-2 and is not cleaved by the enzyme. $PTMC_{13}$-*b*-PVGLIG vesicles in buffer, without the presence of MMP-2, were used as a control to support the stability of the vesicles in solution. In addition, vesicles from a previous study assembled from $PTMC_{30}$-*b*-PGA_{13}[40] in the presence of MMP-2 were used as a negative control. The lack of degradation observed of the

PGA poly(amino acid) by MMP-2 supports the selectivity of the enzyme towards the PVGLIG peptide.

TEM images were taken of each of the three structures after degradation by MMP-2, in order to confirm the structure disruption. The obtained images can be seen in Figure 25 and show significant loss of structure in all three cases. Cleavage of the peptide sequence results in loss of a portion of the hydrophilic weight fraction. This post-assembly modification results in instability of the structures and disassembly and aggregation of the system. In the case of the vesicles, some structures appear to be partially intact. This is likely due to the reduced degradation in the vesicles.

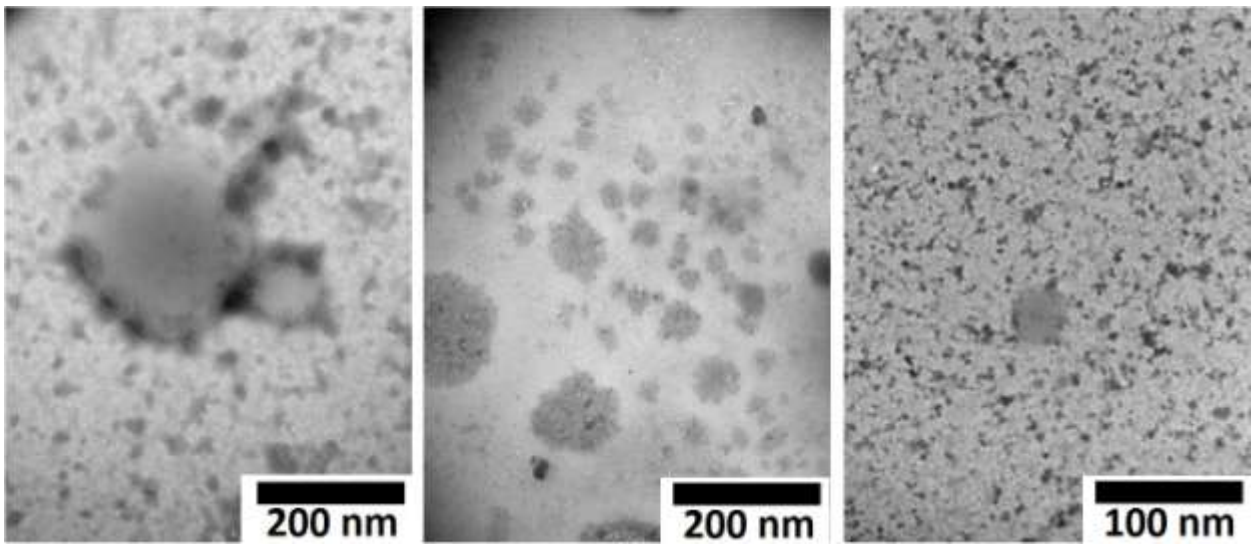

Figure 205 TEM micrographs of degraded vesicles (left), LCMs (center) and core-shell (right) structures after extended incubation with MMP-2 active enzyme

Conclusions

A combination of organo-catalyzed ring-opening polymerization, peptide synthesis and thiol-ene click chemistry was used to successfully access various structurally well-defined polymer-peptide hybrids comprised of PTMC and the MMP-2 peptide substrate PVGLIG. Click chemistry was used to couple the as-made PVGLIG peptide to varying block length PTMC featuring a terminal ene functional group to form the PTMC-*b*-PVGLIG hybrids. The amphiphilic nature of the di-block system allows for the self-assembly of $PTMC_n$-*b*-PVGLIG by nanoprecipitaiton yielding stable monodispersed structures of varying morphology. With the enzyme-cleavable peptide as a structural element in the hybrids, these particles are selectively degradable by the tumor-associated enzyme MMP-2. Significant disruption of all structure morphologies was observed after incubation with MMP-2 over a 48 h period. These MMP-sensitive structures represent the first step towards a targeted drug delivery system for the tumor microenvironment. The unique morphologies provide valuable insight into the mechanism of self-assembly of complex polymer-peptide hybrid molecules.

Chapter 4 Tailored Drug-Release from Multi-Block Polymer-Peptide Hybrid Vesicles

Introduction

Amphiphilic block copolymers have been the dominant class of materials of interest for an increasingly broad range of applications in nanotechnology including health science, technology, energy and informatics[11–13,17,184]. Their prevalence in these fields stems from the unique and wide range of properties achievable by varying the chemistry and types of polymers used as well as their innate ability to self-assemble into a variety of particle morphologies. Specifically, stimuli-responsive materials have gained particular interest due to their ability to respond selectively to the varying conditions of living organisms[18,19]. Structures assembled form this class of materials have been shown to respond to changes in temperature, pH, oxidation conditions as well as chemical and enzymatic environments[6,35,36,88,139,142,164].

Among block copolymers, those consisting of poly(amino acid)s are particularly attractive and have been exploited to more closely mimic biological systems. Several such synthetic polypeptide-based copolymers have recently been developed, but are limited in their ability to interact with biological systems[28,29,168,183]. To address this issue, recently, many self-assembled systems, which seek to move one step further by incorporating biologically relevant molecules as structural elements, have been developed[4–7]. Such approaches represent a new step towards bio-mimicry and show great promise within nanomedicine.

Hybrid systems comprised of synthetic polymers and biologically relevant polypeptides can be tailored to be multi-functional, responding to multiple stimuli in a concerted manner.

They exploit the unique properties of each structural block to create a multi-functional self-assembled system[1,181].

Within this context this study seeks to engineer a triblock hybrid system consisting of the synthetic polymer poly(trimethylene carbonate) (PTMC)[45], the poly(amino acid) poly(glutamic acid) (PGA)[89], and the biologically relevant peptide Pro-Val-Glu-Leu-Ile-Glu (PVGLIG)[146]. PTMC is a semi-crystalline polymer which has been used extensively in self-assembled systems. Due to its melting temperature, structures assembled from this polymer show temperature sensitivity within biologically relevant ranges[45]. PGA is a poly(amino acid) with a pH-sensitivity due to its change in protonation state associated with a change in conformation[40,89,185,186]. Finally, the PVGLIG peptide is one of the known substrates for the tumour associated enzyme MMP-2, and has been used with success to disrupt nanostructures and localize conjugates within tumor microenvironments[3,146–148]. This system is capable of self-assembling into stable vesicles which show responsive drug release, sensitive to temperature, pH and the tumor-associated enzyme matrix metalloproteinase 2 (MMP-2)[145,147,148]. This multi-responsive property arises from the sensitivities of each individual block.

Experimental

Materials

Trimethylene carbonate (1,3-dioxane-2-one: TMC) was purchased from Boehringer Ingelheim and dried on magnesium sulfate in tetrahydrofuran (THF), recrystallized and stored in a glove box prior to use. Allyl alcohol (99 %), 1,3-bis(2,6-diisopropylphenyl)-imidazol-2-ylidene (NHC,

97 %), cysteamine (95 %), 2,2-dimethyloxy-2-phenylacetophenone (DMPA, 99 %), Fmoc-rink amide MBHA resin (1.1 mmol/g loading capacity), (benzotriazol-1-yloxy)tripyrrolidinophosphonium hexafluorophosphate (PyBOP, 98 %), triisopropylsilane (TIS, 99 %), N,N-diisopropylethylamine (DiPEA, 99.5 %), piperidine (99.5 %) and imipramine hydrochloride (IMI, 99 %) were purchased from Sigma-Aldrich and used as received. All Fmoc-protected amino acid derivatives (99 %) and γ-benzyl-L-gluatmate N-carboxy anhydride (BLG-NCA) were obtained from Isochem France and used as received. Hydrobromic acid (HBr, 33 wt %), was purchased from Acros Organics and used as received. Trifuoroacetic acid (TFA, 99.9 %) was purchased from Caledon Laboratory Chemicals. For synthesis, dimethylformamide (DMF) and tetrahydrofuran (THF) were dried prior to use, all other solvents were used as received. Active, human, recombinant matrix metalloproteinase-2 (MMP-2) enzyme was purchased from Calibiochem. The enzyme was aliquoted and stored at -80 °C prior to use.

Synthesis of ene-functionalized $PTMC_{50}$

Ene-functionalized $PTMC_{50}$ was synthesized according to a previously described method[3]. Briefly, recrystalized TMC was dissolved in dry THF (2 M) and added drop-wise to a solution of allyl alcohol (45 mM) and 1,3-bis(2,6-diisopropylphenyl)-imidazol-2-ylidene (NHC) (1 mM) in dry THF under inert atmosphere. The reaction was left stirring for 90 min at room temperature and quenched with methanol. $PTMC_{50}$ was precipitated in ice-cold methanol and purified by centrifugation. The degree of polymerization was measured by end-group analysis of ^{1}H NMR spectrum. $PTMC_{50}$ was produced with a polydispersity of 1.15 at a yield of 88 %. ^{1}H NMR (DMSO-d6, 400 Hz) δ(ppm)= 2.0 (quintuplet) ($C(O)OCH_2C\underline{H_2}CH_2OC(O)$), 4.2 (triplet)

(C(O)OC$\underline{H_2}$CH$_2$C$\underline{H_2}$OC(O)), 4.59 (doublet) (H_2C=CH-C$\underline{H_2}$-), 5.29 (multiplet) ($\underline{H_2}$C=CH-CH$_2$-), 5.89 (multiplet) (H_2C=C$\underline{H}$-CH$_2$-).

Synthesis of PVGLIG peptide

PVGLIG was synthesized according to a previously described method[3]. The βAPVGLIGβAC (βAla-Pro-Val-Gly-Leu-Ile-Gly-βAla-Cys) (PVGLIG) peptide was grown and cleaved from a solid resin by traditional Fmoc/*t*-Bu solid phase chemistry. Briefly, the synthesis proceeded with successive rounds of deprotection and amino acid coupling. Coupling was done by washing of the deprotected peptide (or resin in the case of the first amino acid addition) with a solution of the protected amino acid (0.2 M), PyBOP (0.45 M) and DiPEA (2 M) in DMF for 40 min. Deprotection of the resin and peptide was confirmed by UV-Vis spectroscopy and coupling was confirmed by testing for primary amines (TNBS test). The final peptide product and any remaining protecting groups were cleaved from the solid support with a mixture of TFA/H_2O/TIS (95/2.5/2.5). The peptide was precipitated in diethyl ether and purified by semi-preparative RP-HPLC on a C18 column (Waters SunFire™ C18 5 μm, 10 x 250 mm). The peptide was characterized thoroughly in previous chapters and the ^{1}H NMR with all peaks assigned is given in Figure 14. (DMSO, 400 Hz) δ= 0.95 (Combined 18 Leu, Ile and Val proton signal).

Polymerization of BLG-NCA from PVGLIG macroinitiator

PBLG was grown from the amine terminus of PVGLIG via ROP using the peptide as a macroinitiator. In a glove box under inert conditions, BLG-NCA (225 mM) and PVGLIG (15 mM) were dissolved in dry DMF and left stirring for 48 h. The solution was removed from the glove box and PVGLIG-*b*-$PBLG_{15}$ was precipitated in diethyl ether. The precipitate was removed by centrifugation (10 min, 8000 rpm) and washed repeatedly with diethyl ether. The final product was dispersed in water and put on dialysis (MWCO = 2500), to remove any remaining PVGLIG, for 3 days with frequent changes of dialysis media. The final PVGLIG-*b*-$PBLG_{15}$ was freeze dried to obtain a white powder. ^{1}H NMR (DMSO-d6, 400 Hz) δ= 7.18 (d) 5H, C(O)CH[$(CH_2)_2$C(O)OCH_2Ph]; δ= 5.09 (m) 2H, C(O)CH[$(CH_2)_2$C(O)OCH_2Ph]; δ= 4.41 (m) 1H, C(O)C<u>H</u>[$(CH_2)_2$C(O)OCH_2Ph]; δ=2.45 (m) 2H, C(O)CH[(CH_2CH_2)C(O)OCH_2Ph]; δ=1.95 (m) 2H, C(O)CH[(CH_2CH_2)C(O)OCH_2Ph]; δ= 0.95 (m) 18H, PVGLIG.

Acid hydrolysis of PVGLIG-*b*-$PBLG_{15}$ to PVGLIG-*b*-PGA_{15}

The benzyl side chain of PVGLIG-*b*-$PBLG_{15}$ was cleaved by acid hydrolysis to produce PVGLIG-*b*-PGA_{15}. In a typical cleavage experiment PVGLIG-*b*-$PBLG_{15}$ (50 mg) was dissolved in TFA (3 mL) and HBr (50 µL) and left stirring for 2 h. PVGLIG-*b*-PGA_{15} was precipitated in diethyl either and isolated by filtration. The product was dissolved in water and purified by dialysis (MWCO = 1200 Da) against water for 2 days with frequent water changes. The final PVGLIG-*b*-PGA_{15} product was freeze dried to produce a white powder. ^{1}H NMR (DMSO-d6, 400 Hz) δ= 4.41 (m) 1H, C(O)C<u>H</u>[$(CH_2)_2$C(O)OH]; δ=2.45 (m) 2H,

C(O)CH[($CH_2C\underline{H_2}$)C(O)OH]; δ=1.95 (m) 2H, C(O)CH[($C\underline{H_2}CH_2$)C(O)OH]; δ= 0.95 (m) 18H, PVGLIG.

Coupling of PVGLIG-*b*-PGA_{15} to $PTMC_{50}$ via thiol-ene click chemistry

Coupling of the ene-functionalized $PTMC_{50}$ with the thiol group of the cysteine residue of PVGLIG-*b*-PGA_{15} was achieved *via* a previously developed method[3], by UV-initiated thiol-ene click chemistry. $PTMC_{50}$ (1 eq, 5 mM), PVGLIG-*b*-PGA_{15} (2 eq, 10 mM) and DMPA (1 eq, 5 mM) were dissolved in DMF (3 mL) and irradiated with UV light (λ = 365 nm) for 120 min with stirring. Additional initiator was added consistently using a syringe pump loaded with DMPA (3 mL, 5 mM) at an injection rate of 1.5 mL/h. The coupled product ($PTMC_{50}$-*b*-PVGLIG-*b*-PGA_{15}) was precipitated in water. Unreacted $PTMC_{50}$ was removed by precipitating the reaction mixture in water followed by burst centrifugation (1 min at 2000 rpm). The unreacted $PTMC_{50}$ readily precipitates out of solution leaving a cloudy suspension, which was dialysed against water for 3 days (MWCO = 12 000) with regular changes to remove any excess PVGLIG-*b*-PGA_{15}. The final product was freeze-dried to produce a powder at 18 % yield. Successful coupling was confirmed by ^{1}H NMR and GPC. ^{1}H NMR (DMSO-d6, 400 Hz) δ= 4.41 (m) 1H, C(O)C$\underline{H}$[$(CH_2)_2$C(O)OH]; δ= 4.2 (s) 4H (C(O)OC$\underline{H_2}CH_2C\underline{H_2}$OC(O)); δ=2.45 (m) 2H, C(O)CH[($CH_2C\underline{H_2}$)C(O)OH]; δ= 2.0 (s) 2H (C(O)O$CH_2C\underline{H_2}CH_2$OC(O)); δ=1.95 (m) 2H, C(O)CH[($C\underline{H_2}CH_2$)C(O)OH]; δ= 0.95 PVGLIG.

Vesicle self-assembly and drug encapsulation by nanoprecipitation

Self-assembly of imipramine-loaded vesicles from $PTMC_{50}$-*b*-PVGLIG-*b*-PGA_{15} was performed *via* a previously reported nanoprecipitation method[40]. $PTMC_{50}$-*b*-PVGLIG-*b*-PGA_{15} (10 mg) and

imipramine hydrochloride (35 % feed weight ratio) were dissolved in DMSO (500 µL). With vigorous stirring (700 rpm), buffer pH = 9 (4.5 mL) was added over 15 s. The nanoparticle suspension pH was reduced by dialysis against buffer pH 7.4 over 30 min (MWCO = 13 000), with one buffer change. The dialysed mixture was purified by 3 rounds of ultrafiltation (pore size 25 nm) and dispersion and the volume was reduced to 2 mL (5 mg/mL). Structure morphology was probed with dynamic and static light scattering and TEM. Drug loading was measured by UV-Vis Spectroscopy to be 37 % by monitoring wavelength 309 nm. The UV-Vis spectrum and structure of the free drug is shown in Figure 26, with a strong absorption band clearly visible.

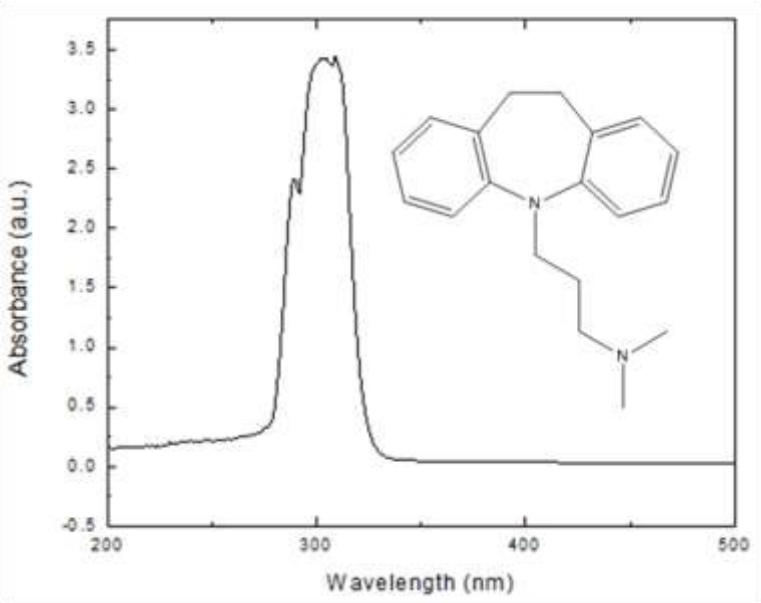

Figure 216 UV-Visible absorption spectrum of free IMI in water with molecular structure. Strong absorption band can be seen at 309 nm

Degradation of $PTMC_{50}$-*b*-PVGLIG-*b*-PGA_{15} vesicles by MMP-2 active enzyme

Degradation of the assembled vesicles was performed *in situ* and conducted in DLS cells at 37 °C. In a typical experiment active MMP-2 enzyme (10 nM) was added to suspensions of $PTMC_{50}$-*b*-PVGLIG-*b*-PGA_{15} self-assembled vesicles (10 μM) in buffer (50 mM Tris pH 7.5, 10 mM $CaCl_2$, 0.2 M NaCl). Degradation of the structures was monitored by following the change in scattering intensity by DLS at 90° over a 120 h period.

Drug release measurements

Drug-loaded vesicles were taken in a cellulose dialysis tube (MWCO: 12 000 g/mol). The dialysis tube, containing 5 mL of IMI-loaded vesicles (0.3 mg/mL) solution was introduced into in vitro release medium containing 50 mL Tris buffer (10mM Tris, pH 7.4). The assemblies were kept at different temperatures (15 °C, 22.5 °C, 26 °C, 38 °C, 45 °C and 55 °C) measured in the dialysis tubes and two pH values (pH 7.4 and pH 5.5 (37 °C)) during release. For release study at pH 5.5, the pH of the IMI-loaded vesicle solution was adjusted just after dialysis by adding concentrated HCl. Then, 5 mL of this solution was introduced into in vitro release medium containing 50 mL Acetate buffer (10 mM Acetate, pH 5.5). In all cases, sink conditions were maintained by replacing 2 mL of the release medium with fresh media at each sampling point. The amount of drug released was estimated from the measurement of the residual drug in the vesicles at each sampling point by spectrophotometry measurements (λ = 251 nm) of an aliquot taken outside the dialysis bag. The drug concentration could be directly calculated from the

measured absorbance by comparison to a prepared calibration curve. The amount of drug released was calculated from the amount of drug initially present in the vesicles and the amount of drug retained in the vesicles at each sampling point. Each experiment was carried out in duplicate and average values plotted.

Size-exclusion chromatography

All SEC measurements were performed in dimethylformamide (DMF) with LiBr (1 g/L) as the eluent. The flow rate was fixed at 0.8 mL/min. Two 7.5 mm x 300 mm PLgel, 5 µm Mixed-D columns (Polymer Laboratories) were coupled to a guard column, 7.5 mm x 50 mm, PLgel, 5 µm (Polymer Laboratories). The system was equipped with a differential refractive index (RI) detector. Calibration was done with polystyrene standards.

^{1}H NMR

All measurements were done using a Brukner Advance spectrometer operating at 400 MHz. All measurements were carried out at room temperature with a fixed (7.5 s) relaxation time. DMSO-d6 was used as a reference signal (δ=2.5 ppm).

UV-Visible spectroscopy

Measurements of drug release concentration were taken using a Varian (Carey 100 Bio) UV-Visable spectrophotometer. Drug concentrations were determined by comparing absorbance values at the drug absorbance peak to a calibration curve. Total drug release was considered to be 100 % based on encapsulation efficiency measured.

Dynamic light scattering (DLS) and static light scattering (SLS)

DLS and SLS measurements were performed with a Brookhaven Laser Light Scattering system with a BI200SMv2 goniometer with a vertically polarized helium-neon diode laser at a wavelength of 636 nm and a BI-9000AT digital correlator with a 125 ns initial measurement time. Samples were kept at constant temperature (25 °C) for the duration of measurements. Measurements were taken every 10° between 60° and 140°. SLS measurements were analyzed in a Berry plot to obtain the radius of gyration.

Transmission electron microscopy (TEM)

TEM images were recorded with a Philips CM10 TEM microscope using a 60 keV acceleration voltage. Samples were prepared by depositing one droplet of the dispersed nanoparticles onto a carbon-formvar grid (200 mesh coated with copper) and allowed to dry. No additional staining was performed.

Micro differential Scanning calorimetry (μDSC)

Thermograms were recorded using a VP-DSC MicorCalorimeter from MicroCal, LLC. Measurements were performed on 0.8 mL of 10 mM solutions of dispersed nanoparticles. Solutions were first stabilized at 10 °C prior to scanning. Measurements were taken between 10 °C and 60 °C with a scan rate of 20 °C/hour with 10 min isotherms at 10 °C and 60 °C. Two heating and one cooling scans were recorded.

Synthesis of PVGLIG, polymers and tri-block Hybrid

With the aim of targeting a vesicle structure with a final hydrophilic weight fraction of 35 %[17], PVGLIG peptide was synthesized and used as a macromolecular initiator for the ROP of BLG-NCA to produce PVGLIG-*b*-$PBLG_{15}$. PVGLIG-*b*-PGA_{15} was produced by acid hydrolysis of the PBLG benzyl function. Finally, ene-functionalized $PTMC_{50}$ was coupled to the thiol function of the cysteine residue of PVGLIG to produce the final $PTMC_{50}$-*b*-PVGLIG-*b*-PGA_{15} triblock system. The complete synthetic strategy can be seen in scheme 2 below.

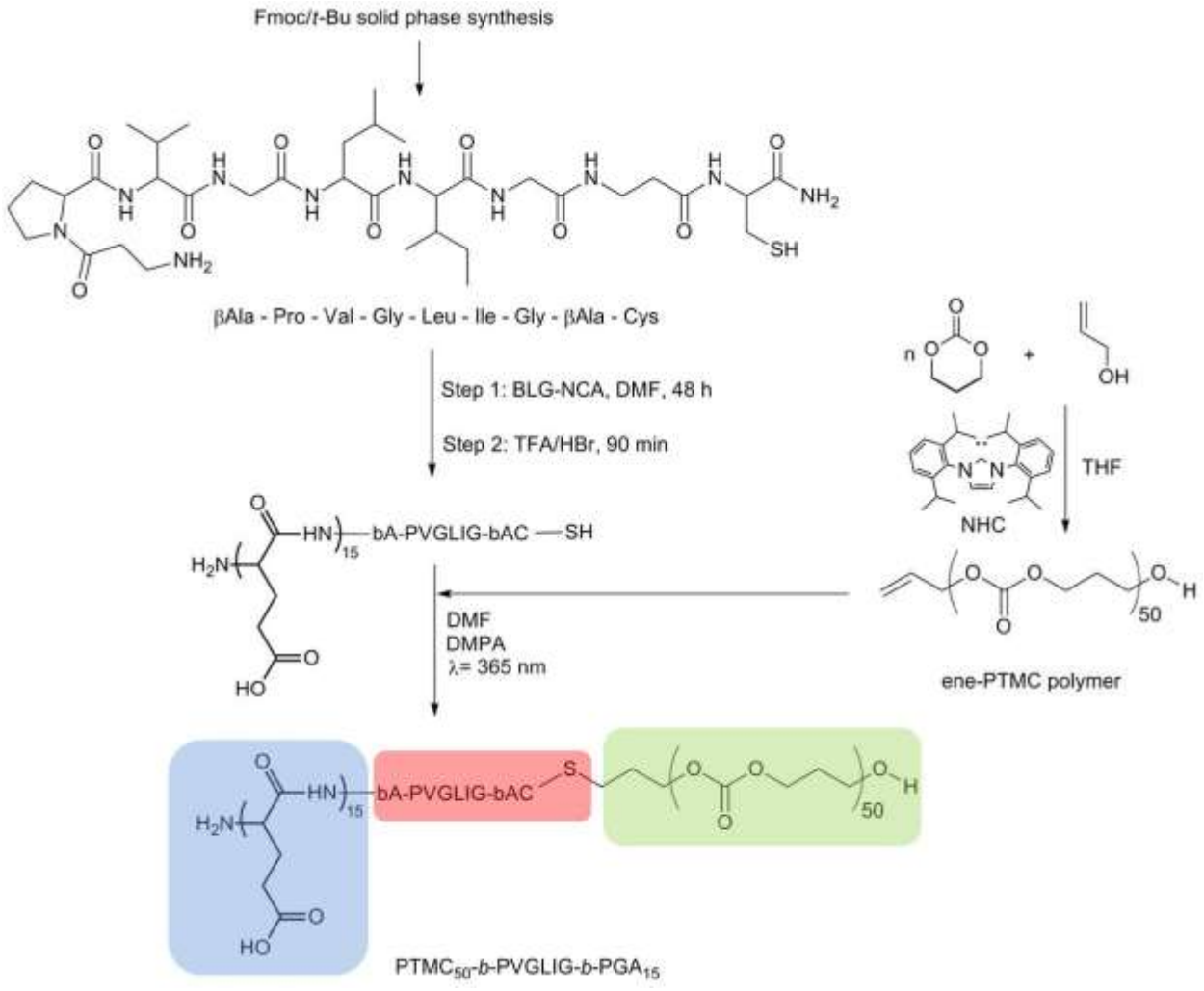

Scheme 2 Synthetic strategy for $PTMC_{50}$-*b*-PVGLIG-*b*-PGA_{15}

The synthetic strategy relies on a sequence order to grow and couple multiple blocks into a single copolymer. This strategy required specific functionalization of each block, including addition of the thiol-containing cysteine residue to PVGLIG and the ene-functionalization of the PTMC block. In addition, the N-terminus of the PVGLIG peptide was required for initiation of the ring-opening of the BLG-NCA monomer. Deprotection of the carboxyl group by TFA/HBr, was done prior to coupling with PTMC in order to avoid any degradation of the PTMC back bone, which is also susceptible to hydrolysis in highly acidic environments.

The PVLGIG peptide was synthesized and well characterized based on a previously reported study. Briefly, the PVGLIG peptide was synthesized by traditional Fmoc/*t*-Bu solid phase chemistry. β-Alanine residues at both *C*- and *N*- terminal ends were included as spacers surrounding the PVGLIG cleavable sequence. A cysteine residue was also added at the *C*-terminal end to provide a thiol group suitable for the subsequent coupling to the polymer by thiol-ene reaction[179].

PVGLIG peptide was used as an initiator for the ROP of BLG-NCA. By adjusting the PVGLIG:BLG-NCA ratio a block length of 15 was targeted successfully with a reaction time of 48 h. The monomer conversion was > 90 % over the full reaction time, allowing for easy targeting of specific molecular weights. Unreacted monomer was removed by precipitation of the conjugate in diethyl ether. The product was dried and dispersed in water. In order to remove any unreacted PVGLIG, the mixture was put on dialysis against water for 3 days with frequent water changes. The purified product was freeze-dried to produce a white powder.

In the ^{1}H NMR spectrum of PVGLIG-*b*-PBLG$_{15}$ seen in Figure 27, a signal can be seen at 0.95 ppm corresponding to the side-chain methyl and ethyl protons of the peptide val, leu and ile residues. The presence of this signal after dialysis is indicative of PVGLIG with polymerized PBLG$_{15}$. Additionally, the benzyl side chain from the PBLG produces two strong signals at 5.05 ppm and 7.2 ppm. Additional signals from the PBLG backbone and side chain can be observed in the ^{1}H NMR (Figure 27). PVGLIG-*b*-PGA$_{15}$ was subsequently produced by acid hydrolysis of the benzyl side-chains of the PBLG block, followed by precipitation in diethyl ether, filtration and multiple rounds of washing with diethyl ether. The loss of the benzyl groups can be observed by monitoring the disappearance of the corresponding ^{1}H NMR peaks at 7.2 and 5.05ppm , seen in Figure 27.

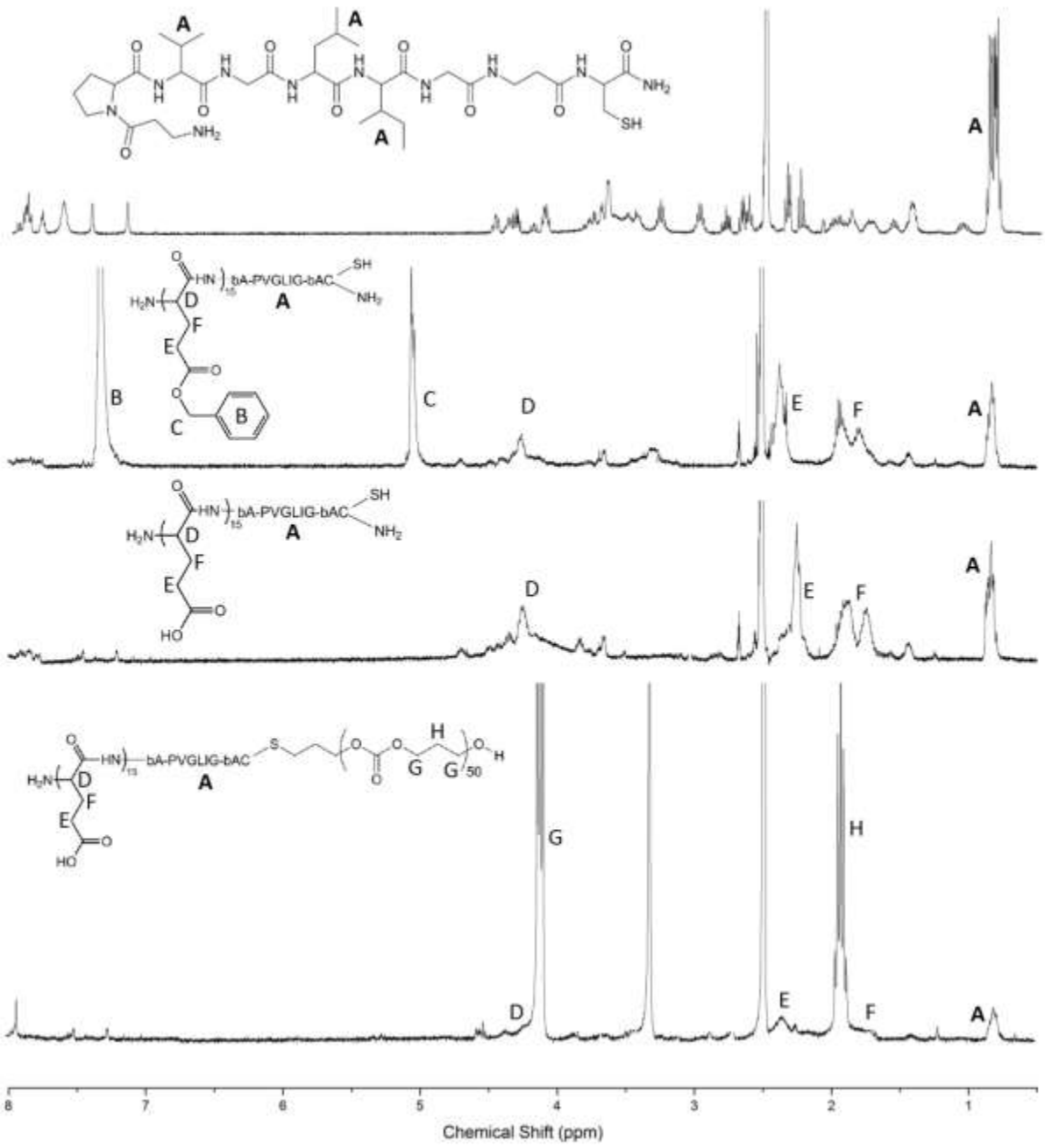

Figure 227 ^{1}H NMR spectra in DMSO-d6 at 400 Hz (from top to bottom) of PVGLIG, PVGLIG-*b*-PBLG$_{15}$, PVGLIG-*b*-PGA$_{15}$, PTMC$_{50}$-*b*-PVGLIG-*b*-PGA$_{15}$ after purification at each step, showing the step-wise synthesis of the final triblock conjugate

$PTMC_{50}$-*b*-PVGLIG-*b*-PGA_{15} was produced by a UV-initiated thiol-ene coupling reaction between the terminal ene function of the PTMC and the cysteine residue of the PVGLIG-*b*-PGA_{15}. Similar reactions had been performed in a previous study with some success[3]; however, due to the increased size of the two macromolecular blocks, initial attempts at the reaction resulted in extremely low yield. As a result of the large molecular weight, the reactive ends have limited accessibility. In addition, the reactive radical produced by the initiator has an extremely short life-time, also contributing to a poor yield. To aid the reaction, a constant supply of DMPA initiator was supplied to the reaction mixture gradually for the duration of the reaction. This process allowed increased exposure of the blocks to the reactive radical initiator resulting in a reaction yield of 18 %, higher than previously achieved. Unreacted $PTMC_{50}$ was removed by successive rounds of precipitation in water and centrifugation. Unreacted PVGLIG-*b*-PGA_{15} was removed by dialysis against water. The ^{1}H NMR spectrum (Figure 27) of the final product shows the presence of peaks corresponding to the backbone protons of $PTMC_{50}$ at 2.00 ppm and 4.00 ppm, as well as the peaks previously observed for PVGLIG-*b*-PGA_{15}.

Figure 28 shows the SEC traces for all products produced. A narrow size-distribution of the $PTMC_{50}$ and PVGLIG-*b*-PGA_{15} precursors can be observed. The triblock showed a clear shift to lower elution time, with no trace from the two isolated blocks, evidencing the success of the coupling and purification steps.

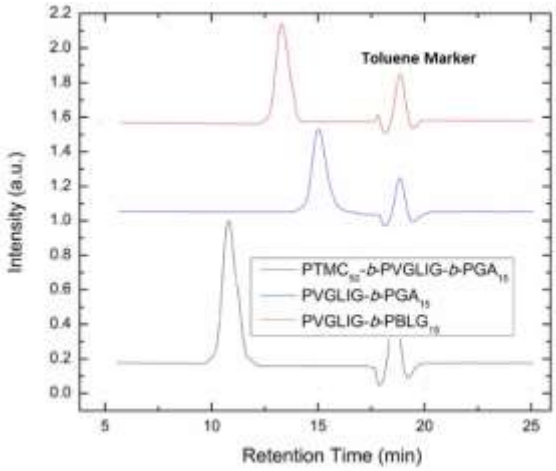

Figure 238 SEC traces of PVGLIG-*b*-PBLG$_{15}$, PVGLIG-*b*-PGA$_{15}$ and PTMC$_{50}$-*b*-PVGLIG-*b*-PGA$_{15}$ showing the step-wise production of the final triblock copolymer in DMF, measured with a refractive index detector.

Self-Assembly and Characterization of PTMC$_{50}$-*b*-PVGLIG-*b*-PGA$_{15}$ Tri-block Vesicles and Degradation by MMP-2

After self-assembly by nanoprecipitation, vesicles produced by the triblock conjugate were isolated by dialysis and analyzed by DLS, SLS and TEM imaging. Light scattering measurements showed a R_G value of 86 nm and an R_H of 94 nm giving a R_G/R_H of 0.92, that can be consistent with a vesicle morphology. The structures showed narrow size distributions over multiple scattering angles and linear q^2 dependance of the decay constant and $(I^{-1})^{-1/2}$ (the complete data set from DLS and SLS measurements can be found in Figure 29). TEM imaging confirmed the vesicle morphology of the structures. Typical micrographs and schematic representation are shown in Figure 30.

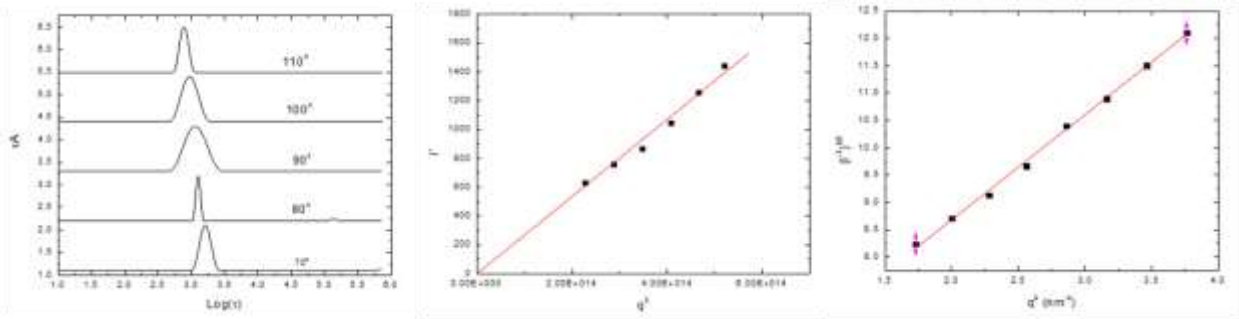

Figure 249 A) Distribution plots, B) Decay times and C) Berry plots for triblock conjugates using multi-angle DLS and SLS

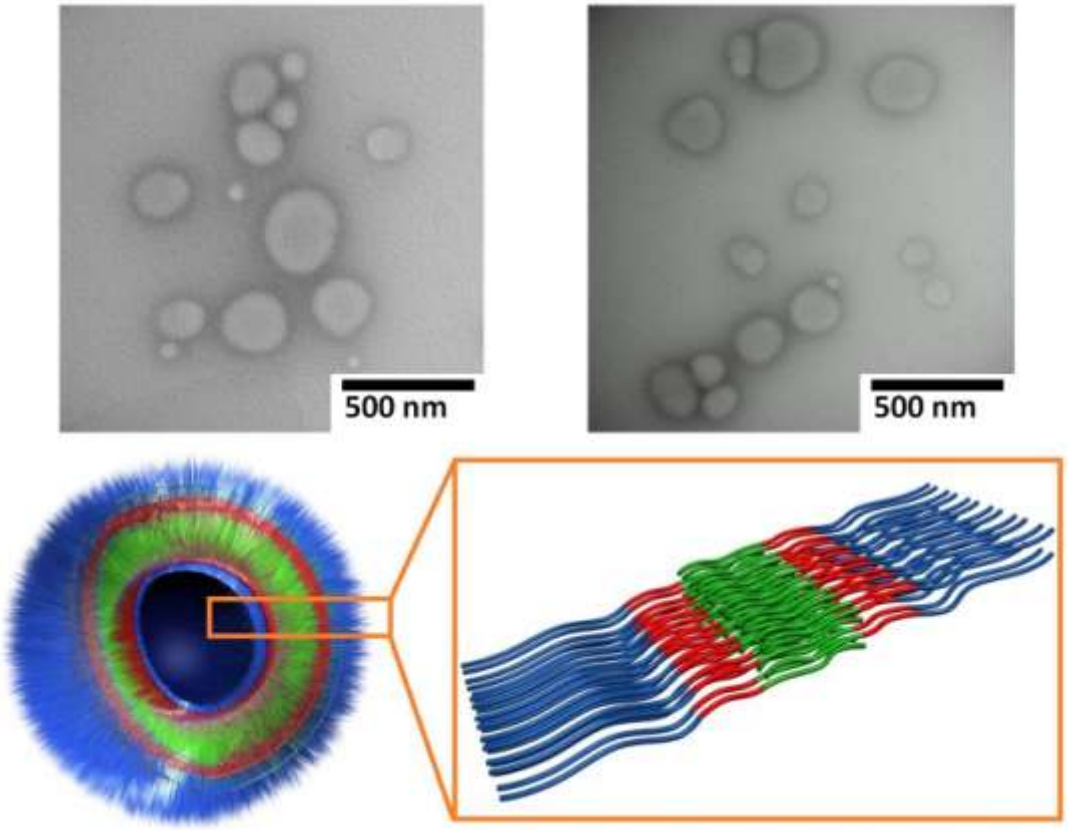

Figure 30 TEM micrographs of vesicles self-assembled from $PTMC_{50}$-*b*-PVGLIG-*b*-PGA_{15} triblock conjugates with schematic representation for visualization showing $PTMC_{50}$ (green), PVGLIG (red) and PGA_{15} (blue).

Degradation of the vesicle structure can be monitored by following the decrease in light scattering intensity as measured by light scattering. Tri-block vesicles were subjected to enzymatic degradation by MMP-2 over a 120 hour period with light scattering measurements taken every 24 hours. The observed decrease in scattering intensity was plotted in Figure 31. The vesicles showed slow but significant degradation, with scattered intensity decreasing to 60 %. The cancer-associated enzyme MMP-2 has been previously shown to be capable of cleaving a peptide substrate within a variety of nanostructure morphologies assembled from diblock conjugates, when the substrate is exposed on the particle surface[3]. In the case of these $PTMC_{50}$-*b*-PVGLIG-*b*-PGA_{15} vesicles the PVGLIG substrate links two polymer blocks, limiting its accessibility. In addition due to the vesicle morphology the PVGLIG peptide is present at both the exterior and interior surfaces of the structure; it is likely that the interior of the vesicle is inaccessible to MMP-2. As a result the degradation of the vesicles is slowed requiring longer time frame for cleavage of the substrate compared to structures of other morphology and composition.. To prove the selectivity of MMP-2 to the PVGLIG peptide $PTMC_{30}$-*b*-PGA_{13} vesicles were used as a negative control and show no degradation by MMP-2 over the same time frame.

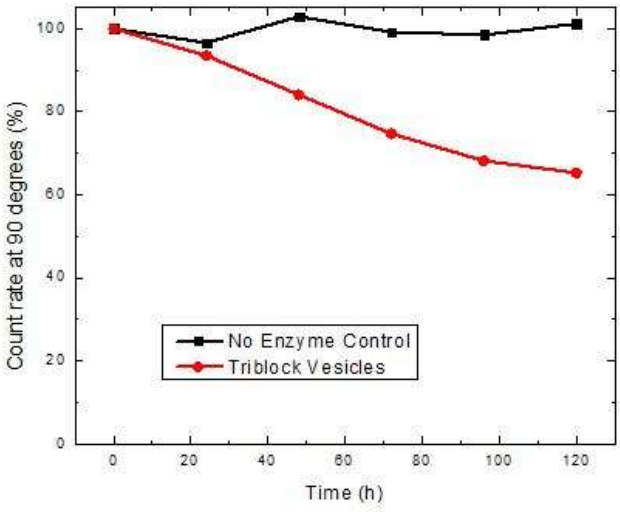

Figure 251 Light scattering intensity was measured by DLS at 90 degrees of vesicles assembled from PTMC$_{50}$-*b*-PVGLIG-*b*-PGA$_{15}$ triblock conjugate as well as vesicles assembled from PTMC$_{30}$-*b*-PGA$_{13}$ as a control after incubation with MMP-2 active enzyme at 20 nM.

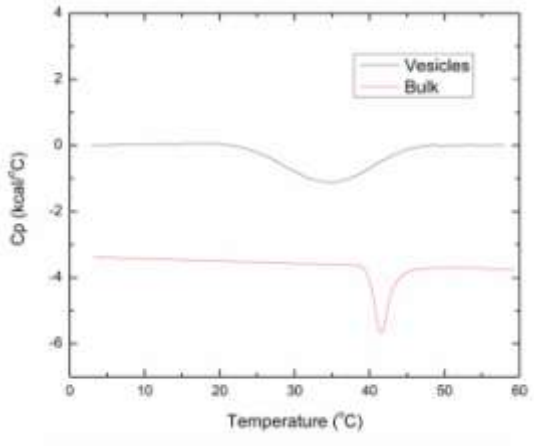

Figure 32 DSC trace of PTMC$_{50}$-*b*-PVGLIG-*b*-PGA$_{15}$ bulk material showing a Tm of 40.5 °C and µDSC trace taken of a suspension of vesicles (100 mM) self-assembled from PTMC$_{50}$-*b*-PVGLIG-*b*-PGA$_{15}$ in water showing a T_m of 35.5 °C.

The nanoprecipitation process is necessary for self-assembly of these structures due to the crystalline nature of the PTMC block. The crystalline nature of PTMC has previously been shown to play an important role in the self-assembly of a variety of stable structures[3,40,187]. This crystallinity is present in the bulk material and is maintained in the vesicle structure as evidenced by the melting temperature transition observed on a micro DSC trace seen in Figure 32. Above the melting temperature, the vesicle morphology is maintained, however, it is believed that some fluidization of the membrane occurs.

The light scattering intensity of the vesicles at 90 degrees was monitored over a range of temperatures and the resulting data is show in Figure 33. A clear discontinuity is seen in the trend as the temperature approaches the T_m of the PTMC block. This change in the light scattering trend results from the fluidization of the PTMC membrane core. The intercept of the two linear regions correlates well with the transition observed in the μDSC curves. This change in scattering intensity likely results from changes in the refractive index of the PTMC membrane component. As the copolymer undergoes a transition at its melting point from semi-crystalline to amorphous, the apparent refractive index changes accordingly, resulting in a discontinuity in the observed scattering intensity. This change in scattered light intensity is indicative of a possible change in membrane structure. The effect of temperature on the membrane integrity is investigated in greater detail in the following chapter of this report.

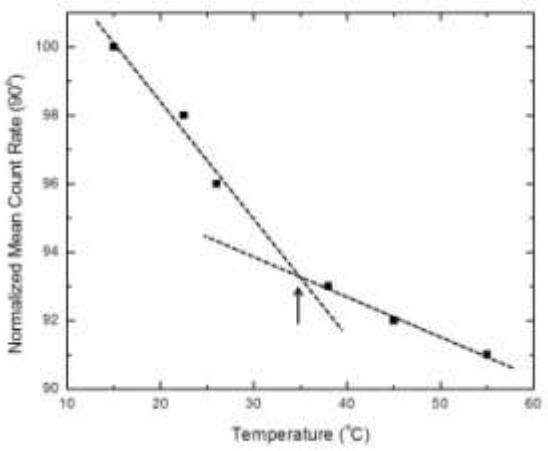

Figure 33 Change in scattering intensity measured by DLS at 90 degrees of $PTMC_{50}$-*b*-PVGLIG-*b*-PGA_{15} vesicles in water between 15 °C and 55 °C.

Drug-Loading and Release of ImiHy from Vesicles

Drug-loading with imipramine hydrochloride was achieved during the nanoprecipitation process with a feed weight ratio of 30 %. Due to electrostatic interactions between the positively charged drug and the negatively charged PGA_{15} block, encapsulation was done at pH 9.5, above the pKa of imipramine (8.9) to avoid precipitation of the system. The pH was reduced to 7.4 by successive rounds of ultrafiltration and dispersion. The final round of ultafiltration concentrated the loaded vesicles to a concentration of 5 mg/mL.

The imipramine was encapsulated into the vesicle with an encapsulation efficiency of 37 %. This was determined by measuring the concentration of imipramine in the filtrate following purification and concentration of the loaded vesicles. Drug concentrations were determined by

UV/vis spectroscopy following the absorption band of IMI at 309 nm in the filtrate obtained (Figure 26). The release of IMI *in vitro* was subsequently studied under a variety of conditions, varying pH, temperature and under the presence of MMP-2. The release was measured by taking 2 mL samples from the release medium and observing the absorbance peak of IMI by UV/Vis spectroscopy. In each case the removed volume was replaced in order to maintain sink conditions within the release media. The compiled release data is shown in Figure 34. Release studies showed that drug diffusion from the vesicles is sensitive to both pH and temperature; as well, drug release is enhanced in the presence of the tumor-associated enzyme MMP-2.

The release of IMI from the tri-block vesicles was measured at 6 temperatures ranging from 15 °C to 55 °C. In all cases, the drug release rate increases with increasing temperature. Notably there is a significant discontinuity in release rate as the melting temperature of the PTMC block is approached. Release of IMI from the vesicles is relatively slow, increasing nominally with temperature in the lower three release temperatures (15, 22.5 and 26 °C). As the release temperature approaches the melting temperature of the PTMC block there is a sharp increase in the release rate. This is consistent with the postulated fluidization of the membrane, resulting in a marked increase in the diffusion of IMI from the vesicles.

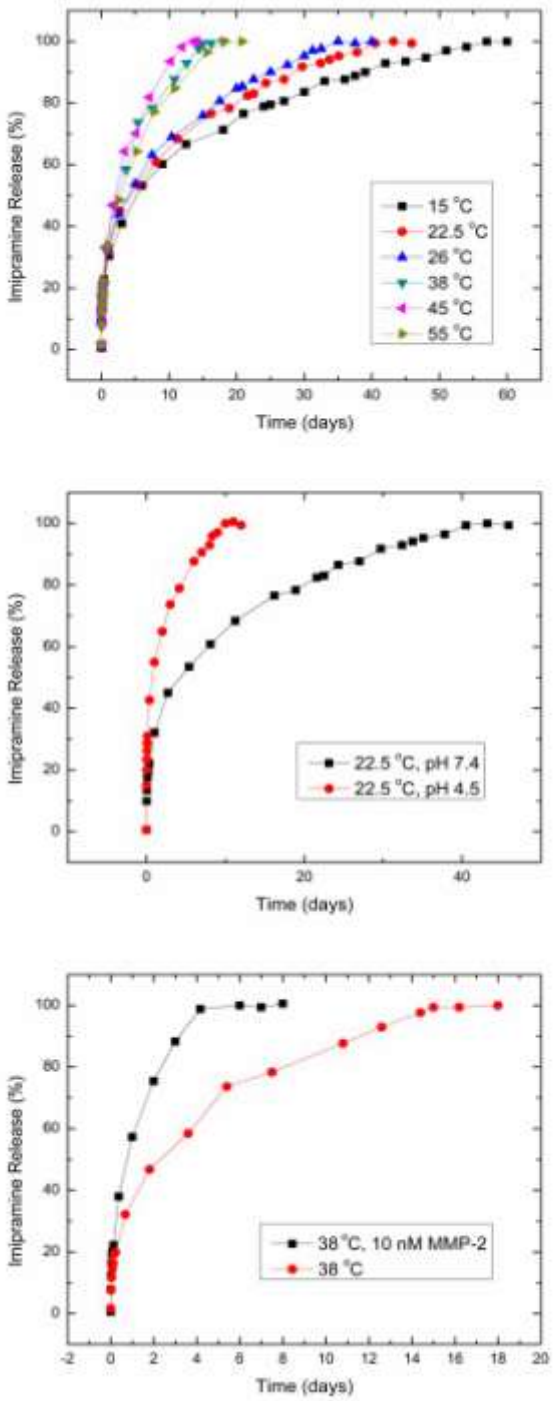

Figure 34 Release of imipramine from PTMC$_{50}$-*b*-PVGLIG-*b*-PGA$_{15}$ vesicles under changing temperature and pH conditions as well as in the presence of MMP-2 active enzyme.

Release of IMI was measured at room temperature in both neutral and low pH conditions (pH 4.5). There is a significant increase in release rate under low pH conditions, reflecting the pH-sensitivity of the PGA block. As the pH is reduced towards the pKa of the PGA block, electrostatic forces between the drug and PGA are reduced allowing for faster diffusion from the vesicles.

Finally, the vesicles showed significantly enhanced release in the presence of MMP-2 at 38 °C. With no enzyme present, total release of the drug was achieved after approximately 16 days. In the presence of 20 nM MMP-2, the same level of release was achieved within 4 days, with a nearly linear release profile. The release profiles with and without MMP-2 are similar during the initial 8 hours of measurements, however begin to diverge significantly by 12 and more so 24 hours, reflecting the slow cleavage of the PVGLIG block. In addition, as the peptide is cleaved, liberating the drug, we observe a change in the release profile to a more linear release rate compared to release not in the presence of MMP-2.

Conclusions

A triblock polymer-peptide conjugate consisting of a semi-crystalline synthetic polymer (PTMC), a pH-sensitive poly(amino acid) (PGA) and a biologically relevant peptide (PVGLIG) was successfully synthesized using thiol-ene coupling and organo-catalyzed ROP. Thiol-ene coupling between two macromolecules was achieved with efficiency by introducing a constant supply of the radical-producing initiator throughout the reaction mixture under constant UV exposure. Vesicles self-assembled from this system by a nanoprecipitation technique showed

significant changes in release of imipramine under varied conditions. Thermal, pH and enzyme sensitivities derived from the individual polymer, poly(amino acid) and peptide blocks, respectively, were observed in the final structures. Notably, vesicles show a significant increase in release rate under temperatures in excess of the melting temperature of $PTMC_{50}$. The vesicles were cleavable in the presence of the tumor-associated enzyme MMP-2, and showed a corresponding enhanced release under these conditions. Such a multi-functional system comprised of multiple conjugated blocks represents a new step towards biomimetic systems and holds potential for further development into clinically relevant drug-delivery systems.

Chapter 5 Temperature-Induced Structural Changes in Hybrid Vesicles

Introduction

Since their inception, self-assembled structures have gained considerable attention in a broad range of applications, due to their remarkable versatility[188]. Such structures have been produced from a variety of materials, including phospholipids, polymers, peptides and protein fragments[2,36,189]. Due to their likeness to natural biological systems, self-assembled systems have been of particular interest in biomedical applications.

Self-assembled structures have been produced in a wide range of morphologies and derived from a wide range of amphiphiles[3,17,164]. Of particular interest have been vesicles formed from amiphiphilic block copolymers. Depending on the nature of the polymer blocks chosen, various morphologies can be achieved with unique properties such as "breathing"[99], "schizophrenic"[92] and can be produced to respond to a spectrum of stimuli[58,66].

Within the realm of vesicular systems, structures have been developed with a broad range of membrane permeability and stability. Efforts have been made to alter the membrane stability by the inclusion of cross-linking agents, allowing for stable vesicles with varying degrees of permeability related to the degree of crosslinking[66]. Polymer blends used to design vesicle systems have been shown to impact the elasticity of the membrane, and biodegradable membranes have had their rates of degradation improved by playing on the molecular weights and compositions of polymers used[134]. In addition, total disruption of the vesicular membrane

has been achieved with a wide range of stimuli-responsive materials[190]. Control over membrane integrity is pivotal in the move towards the design of cell-like structures.

In liposomes, analogous to polymersomes, the phospholipid subunits exhibit a degree of crystallinity which can be exploited for temperature-sensitive drug-delivery[45]. The stimuli-responsive character of liposomes occurs across the chain-melting transition (T_m) as the ordered character of the membrane is lost[67]. In such systems, this transition is exploited as drug release kinetics are more favourable above the T_m. Below the T_m, the hydrophobic chains exhibit a highly ordered state, which is lost above the T_m. [67,68]

In polymeric systems, the phenomenom of membrane crystallinity has been explored by Sanson *et al,* with the $PTMC_{22}$-*b*-PGA_{14} system[45]. This polymersome structure showed the presence of crystalline character in larger vesicles directly related to the membrane integrity. In the case of PTMC, this transition was shown to be non-reversible due to the slow kinetics of recrystillization. The highly ordered chain packing in the crystalline state was not observable after heating beyond the chain-melting temperature. Other polymers, particularly, PEO have showed significant crystalline character in nanostructures[66]. Structures containing PEO have shown to exhibit significant morphological changes when heated past the chain-melting temperature.

In both liposomes and polymersomes heating and cooling across the chain-melting temperature of crystalline regions of the membrane has resulted in significant rearrangement and morphological changes in self-assembled structures. The mechanisms of structural change are the occurance of both fusion and fission events. As structures are heated above the chain melting temperature crystalline regions undergo a micro phase separation and eventual budding and

ejection from the structure resulting in structural fission. The reverse mechanism has been observed for fusion events upon cooling of structures.

The synthetic polymer poly(trimethylene carbonate) (PTMC) has previously been demonstrated to form a wide range of self-assembled morphologies[3,4,113]. PTMC, due to its semi-crystalline nature, can be assembled in a unique nanoprecipitation process to give rise to frozen structures, dependant on the crystallinity of the polymer. This crystalline nature has been shown to provide the structure with a temperature-sensitivity, resulting from the melting of PTMC within the structure[45]. Systems containing PTMC have been shown to produce temperature-sensitive drug delivery systems as a result of their unique properties[89].

In this study, we seek to probe the effect of temperature on the crystallinity and morphology of nanovesicles containing the hydrophobic polymer PTMC and the hydrophilic poly(amino acid) PGA. Stable vesicles from previous studies are subjected to consecutive rounds of heating and cooling and the observed changes in melting temperature and melting enthalpy are monitored. Vesicles are shown to fuse when heated above the melting temperature of the PTMC block and form larger stable vesicles.

Experimental

Materials

The synthetic work to produce $PTMC_{50}$-*b*-PVGLIG-*b*-PGA_{15} and the self-assembly of nanovesicles was described in detail in the previous chapter of this report. The empty (non-drug loaded) vesicles produced from that study were used in all experiments described here.

Thermal fusion of $PTMC_{50}$-*b*-PVGLIG-*b*-PGA_{15} Vesicles

Vesicles suspended in water were heated cycled through rounds of heating and cooling between 60 °C and 10 °C with 120 min periods of equilibration at each extreme prior to analysis. Heating and cooling was done at a rate of 0.5 °C/min. Four cycles of heating and cooling were performed and samples were analyzed after each cycle.

Dynamic light scattering (DLS) and static light scattering (SLS)

DLS and SLS measurements were performed with a Brookhaven Laser Light Scattering system with a BI200SMv2 goniometer with a vertically polarized helium-neon diode laser at a wavelength of 636 nm and a BI-9000AT digital correlator with a 125 ns initial measurement time. Samples were kept at constant temperature (25 °C or 50 °C) for the duration of measurements. Measurements were taken every 10 ° between 60 ° and 140 °. SLS measurements were analyzed in a Berry plot to obtain the radius of gyration.

Transmission electron microscopy (TEM)

TEM images were recorded with a Philips CM10 TEM microscope using a 60 keV acceleration voltage. Samples were prepared by depositing one droplet of the dispersed nanoparticles onto a carbon-formvar grid (200 mesh coated with copper) and allowed to dry. No additional staining was performed.

Micro differential scanning calorimetry (μDSC)

Thermograms were recorded using a VP-DSC MicorCalorimeter from MicroCal, LLC. Measurements were performed on 0.8 mL of 10 mM solutions of dispersed nanoparticles. Solutions were first stabilized at 10 °C prior to scanning. Measurements were taken between 10 °C and 60 °C with a scan rate of 0.5 °C/min with 120 min isotherms at 10 °C and 60 °C.

Temperature-Induced Structural Changes in Hybrid Vesicles

The $PTMC_{50}$-*b*-PVGLIG-*b*-PGA_{15} hybrid vesicles are comprised of a synthetic, hydrophobic polymer PTMC, the poly(amino acid) PGA and the enzyme-sensitive enzyme PVGLIG. The $PTMC_{50}$-*b*-PVGLIG-PGA_{15} self-assembled structures were made and well characterized as described in the previous chapter.

PTMC is a semi-crystalline polymer and has been well studied in the context of self-assembly due to its ability to form a variety of highly stable nanostructures. The $PTMC_{50}$-*b*-PVGLIG-*b*-PGA_{15} bulk material has a melting temperature of 40.5 °C as seen in the DSC trace in Figure 33. The melting temperature is present in the self-assembled vesicles containing $PTMC_{50}$, but the thermal transition has significantly broadened and the T_m shifted to a lower temperature. This shift arises from the curvature of the vesicles and the increased mobility or packing ability of the PTMC chains within the membrane. Although no direct quantitative measurements of membrane crystallinity have been performed it is believed that the decrease in melting temperature observed is a result of a lower degree of crystalinity in the membrane.

Previous studies have shown the size-dependence of the T_m in relation to the vesicle size, achieving a T_m equal to that of the bulk material at vesicle sizes of 5 um and higher[45]. This

results from the comparable degrees of crystallinity and lack of chain constraint in the larger vesicles. Reports from Sanson *et al* on vesicles from $PTMC_{22}$-*b*-PGA_{14}, showed no crystalline character in vesicles below 200 nm in diameter. The vesicles used in this study are in the 200 nm range, and still exhibit a melting temperature. The significantly higher molecular weight of the PTMC block as well as the presence of the PVGLIG peptide (with alternating amine and carbonyl groups capable of hydrogen bonding) may result in a decreased chain mobility and microphase separation of the $PTMC_{50}$ block, favouring crystallization. An increased level of crystallization is also evidenced by the higher T_m (40.5 °C) observed, compared to the T_m reported by Sanson *et al*.

Consecutive µDSC runs were performed between 10 °C and 60 °C with a heating and cooling rate of 0.5 °C/min and 2 hour equilibrations at both high and low temperatures. Peaks for T_m were observed in each run with the T_m increasing during each heating and cooling cycle. The observed heating curves are seen in Figure 35 and the obtained melting temperatures and melting enthalpies are summarized in table 3.

Low molecular weight PTMC is known to crystallize slowly and within vesicle membranes confinement of the PTMC chains contributes to these slow kinetics. For this reason 2 hour isotherms were performed at both the high and low temperature ranges of the µDSC runs. These isotherms may allow for closer association and ordering of the membrane chains and allow for recrystallization of the PTMC upon cooling. This method in addition to the large molecular weight of the PTMC block in the copolymer results in a recrystallization of the PTMC block within the nanostructures. Additionally, the presence of the PVGLIG peptide may contribute to a microphase separation and reduced mobility of the PTMC chains, favouring crystallization.

Table 4 Summary of melting temperatures and melting enthalpies of bulk homopolymer and the vesicle suspensions

Heating cycle	T_m (°C)	Melting Enthalpy (J/mol)
0	34.1	4.5
2	36.0	4.8
4	37.4	5.3
Bulk	40.5	10.3

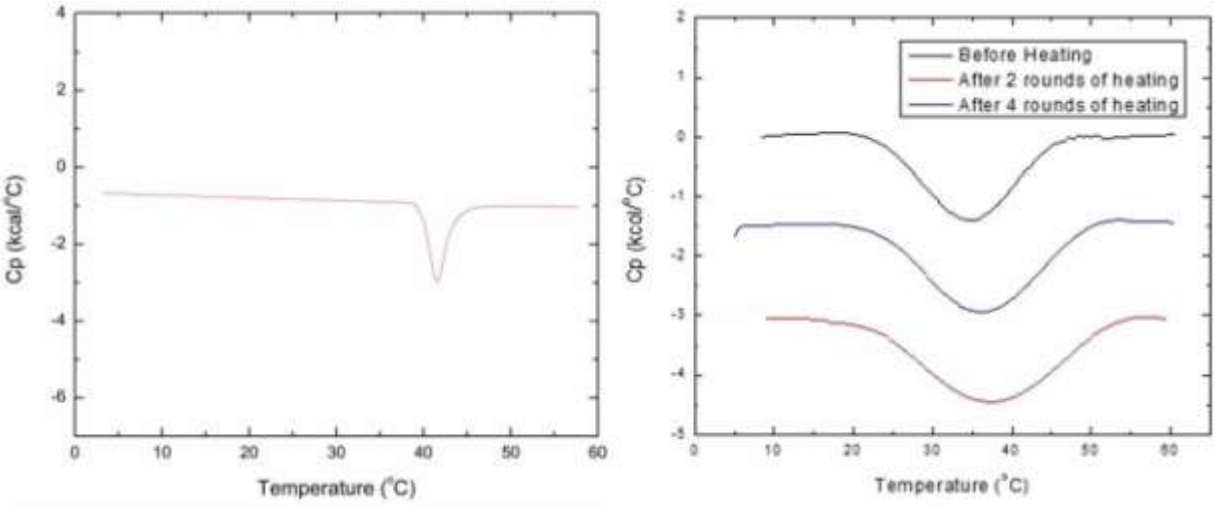

Figure 35 DSC trace of bulk $PTMC_{50}$-*b*-PVGLIG-*b*-PGA_{13} (left) and µDSC traces of vesicle suspensions in water over multiple rounds of heating.

With each cycle of heating and cooling, the melting temperature of the vesicles increases from a low of 34.1 °C of the originally produced vesicles to a high of 37.4 °C after 4 rounds of heating and cooling. This increase in melting temperature is suggestive of an increased stability

of the crystalline phase of the vesicles. In addition, the change in melting temperature is accompanied by an increase in the molar melting enthalpy of the vesicle suspension as well as a broadening of the melting range. As the vesicle melting stems from the degree of crystallinity of the PTMC block in the vesicle membrane, the increasing melting temperature and higher molar melting enthalpy suggests an increased heat capacity and an increased degree of crystallinity of the PTMC block after successive rounds of heating and cooling.

The vesicles prior, during and after 4 rounds of heating were analyzed by DLS and SLS. The full data set from this analysis can be seen in Figure 36 with the size data summarized in table 4. Vesicles prior to heating showed narrow size distributions over a range of angles with a linear q^2 dependance of both the decay constants and $(\Gamma^{-1})^{-1/2}$. These characteristics were also present in samples measured after 4 heating cycles. When light scattering measurements were taken of vesicle samples at 50 °C for the duration of the measurement, the distribution plots were noticeable broader suggesting the structures may no longer be monodispersed.

Prior to heating the vesicles had an R_G of 86 nm and an R_H of 94 nm resulting in an R_G/R_H value of 0.92, consistent with a vesicle morphology. Similarly, after several rounds of heating and cooling, the structures had an R_G of 147 nm and an R_H of 137 nm giving an R_G/R_H value of 1.07, once again consistent with vesicle morphology, suggesting that this morphology is stable throughout the heating process. There is however a significant size increase between the as-made vesicles and the structures after heating. This size increase is consistent with the observed increases in the melting temperature and the molar melting enthalpy. The origin of the size increase is attributed to the possible occurrence of fusion and/or fission events between vesicles and is discussed in greater detail below.The polymer chains within the larger vesicles

have less chain constraint and thus are able to achieve a higher degree of crystallinity within the structure.

DLS and SLS measurements were also taken of the vesicles after the 3rd high temperature isotherm. The samples were maintained at 60 °C for the duration of the DLS and SLS measurements. When measurements were taken of the samples during heating we observed a broad size distribution with a mean R_G of 188 nm and a mean R_H of 77 nm, giving a R_G/R_H of 2.4, suggestive of a non-vesicle morphology. This ratio likely results from the presence of multiple morphologies at high temperature. In this situation the presence of fusion and/or fission events give rise to a non-specific ratio. While the vesicles structure is maintained before and after heating, there is a significant size increase with the vesicles passing through a transition state during the heating and cooling processes. Since the measurements were taken at high temperature while the PTMC chains were no longer in a crystallized state it is likely that these data represent an ill defined state. Due to the limitations of the DLS and SLS measurements it is difficult to draw conclusions from these data alone.

Table 5 Summary of size data obtained from as made vesicles, vesicles under heating and after 4 cycles of heating.

Sample	R_G (nm)	R_H (nm)	R_G/R_H
As made	86	94	0.92
During 2nd heating cycle	188	77	2.4
After 4 heating rounds	147	137	1.07

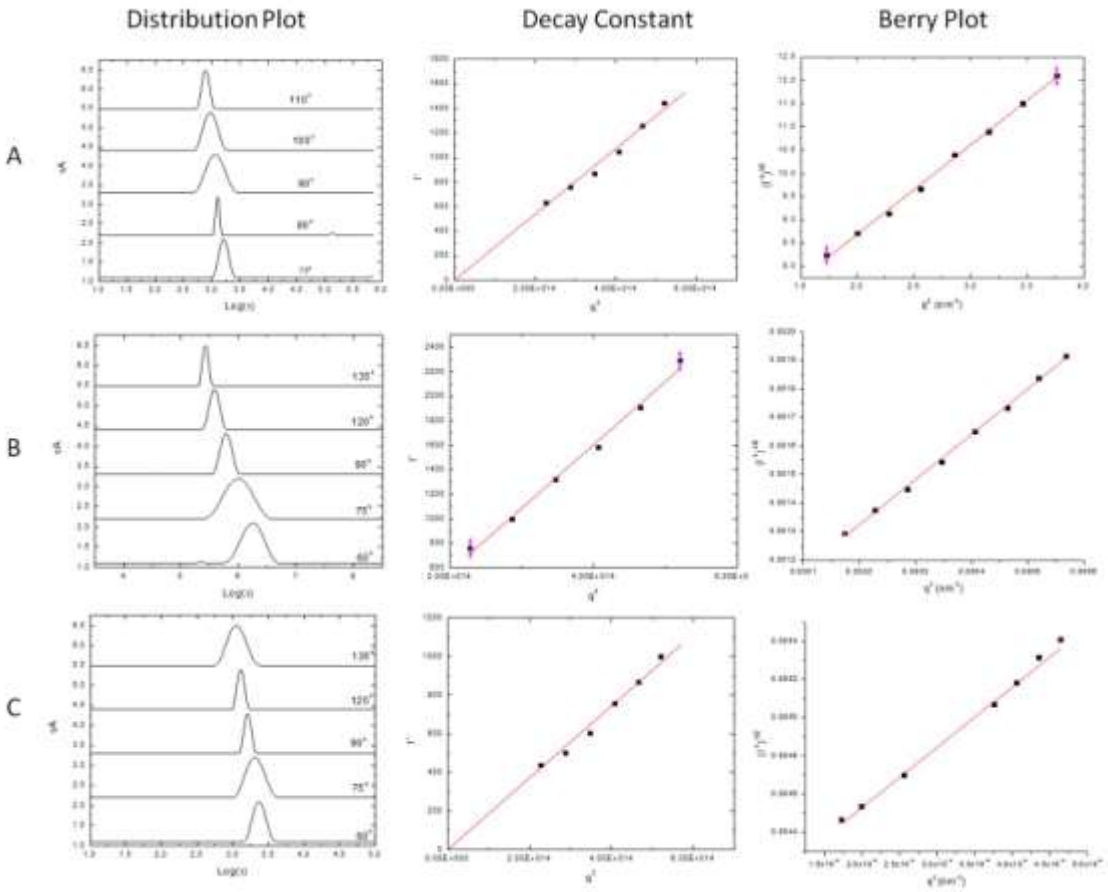

Figure 36 Full DLS (distribution plots and decay constants) and SLS (Berry plots) data set obtained from triblock vesicles prior to heating (A), during heating (B) and after heating (C)

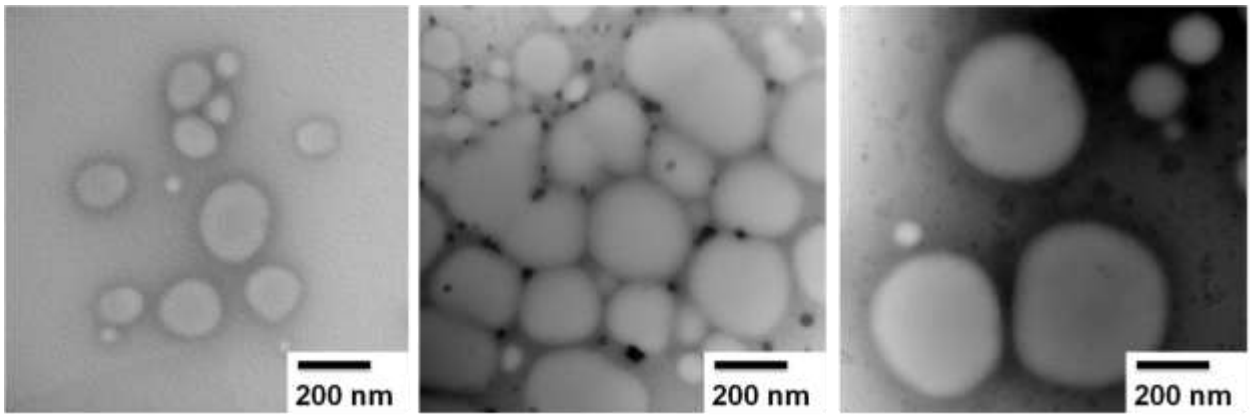

Figure 37 TEM micrographs of triblock nanostructures prior to heating (left), during the 3rd heating (center) and after 4 heating and cooling cycles (right).

In order to probe the morphological changes observed during the heating process, TEM images were taken of the nanostructures before, during and after heating. Typical micrographs from this examination can be seen in Figure 35. Before and after heating cycles, a vesicle morphology and size range consistent with the light scattering data can be seen. The images taken during the heating process appear to be a mix of structures with some intact vesicles of varying sizes clearly visible. There also appears to be fusion and/or fission of vesicles.

Fusion and fission events have frequently been observed in both liposomes and polymersomes. The fusion and fission events arise from a high level of defects in the vesicle membrane due to a mix of crystalline and non-crystalline regions resulting in microphase separation as the membrane approaches its chain-melting temperature. Fission generally occurs during heating when the domains created from phase separation are expelled from the membrane, resulting in an overall decrease in particle size. Fusion occurs by the reverse mechanism upon cooling of systems resulting in an overall increase in particle size. In addition

to the formation of defects during the gel-liquid-crystalline transition, fusion necessarily requires close proximity of particles, and fission can be strongly influenced by membrane curvature.

The overall increase in the vesicle sizes observed suggests that fusion is the dominant mechanism occurring. This process would occur during the cooling cycles. It is possible that due to the small size of the vesicles, the membrane curvature does not favour fission. The deformation observed on DLS/SLS and TEM during high temperature measurements results from these fusion and fission events, resulting in distorted particles and unclear sizes.

Conclusions

Well defined monodispersed vesicles comprised of a triblock $PTMC_{50}$-*b*-PVGLIG-*b*-PGA_{15} system were shown to fuse when heated above the melting temperature of the structurally important, semi-crystalline $PTMC_{50}$ block. The vesicles likely merge to form larger vesicles.. Vesicles produced with larger sizes show an increase in melting temperature and molar melting enthalpy towards that of the bulk material. This increase results from reduced chain constraint derived from the larger size, resulting in a higher degree of crystalline character in the membrane. These results help shed light on the important role that semi-crystalline polymers and PTMC in particular can play in the assembly and stability of nanostructures. This polymer may hold promise for producing nanostructures with temperature-tunable morphologies. By varying the chain length of PTMC and the duration of heating, it may be possible to produce a range of tunable nanostructures.

Chapter 6 Influence of Drug-Carrier Interactions on Encapsulation and Release

Introduction

In recent decades research in nanomedicine has had a particular focus on the encapsulation, controlled and triggered release of payloads[57,88,190]. In order to address this application a wide range of polymers, copolymers and nanoparticle morphology have been developed with varying degrees of success[3,113,128,183]. Research has largely focused on the design of unique nanoparticle carriers capable of transporting and releasing a payload under certain conditions and significant attention was devoted to the careful engineering of the carrier structure.

An increasing number of drug delivery systems comprising varying morphologies that are loaded with a broad range of drugs have been successfully developed[147,149,191]. Notably, the drug loading capacity and drug release rates vary greatly between systems and drugs. Loading efficiencies approaching 70 % were achieved with DOX-loaded PTMC-*b*-PGA vesicles[89], while others showed substantially lower loading capacities. Though efforts have been made to better understand the drug-carrier relationship, for many of these systems drug loading has not been studied in depth.. Such relationships and their impact on drug encapsulation and release should be a focus for the development of efficient drug delivery systems for a broad range of applications.

Significant work in this area has been done by the group of Kataoka[12,103,192], who have showed the increase affinity for ionic micelles for payloads by increasing electrostatic interactions between the carrier and encapsulant. P(asp) was conjugated to PEG for production of polyionic micelles, having a highly charged character. Due to the charged nature of the micelle, oppositely charged drugs and payloads were shown to have a high affinity for the carrier through electrostatic interactions with the charged peptide block. Additionally, in aqueous solutions the charged enzyme lysozyme could become trapped in the micelles leading to the degradation of the structure. This affinity was further enhanced by addition of aromatic groups to the copolymer structure. In the case of this PEG-b-PAsp structure the presence of the charged peptide and the level of interaction between the peptide and the payload and enzyme were key to the structure function.

PEG-SS-PAsp has been developed to not only enhance the solubility of the anticancer drug adriamycin,[106] but additionally to provide a redox-sensitive release mechanism. Within the cytoplasmic environment the disulfide bridge linking the polymer and peptide could be selectively reduced by glutathione. Adriamycine showing strong interaction with the PAsp block through the electrostatics between the carboxyl unit of the peptide and the amine group of the drug. Such drug-carrier interactions are here greatly exploited for the benefit of the delivery system.

Stimuli-responsive drug carriers have been of great interest due to their capacity to tailor the release conditions for each specific application[37,72,190]. In particular, pH-sensitive drug delivery systems have been the focus of numerous studies, and their sensitivity often stems from the presence of titratable charged groups present on the drug, carrier or both. By varying the pH, the degree of protonation can be impacted, which can alter the release kinetics of a drug[89,131].

This type of electrostatically-controlled interaction between drug and carrier can be studied in depth by isothermal titration calorimetry (ITC). Additionally, this technique can be used to probe additional interactions and forces between host and guest such as hydrophobic interactions and van der Waals forces.

By studying the variety of interactions between drug molecules and potential carriers, delivery systems can be customized to maximize the drug-loading capacity and tailor the release kinetics under varying conditions. A more thorough understanding of how interaction between payload molecules and carriers affect loading and release may permit the customization of delivery systems for specific payloads that exhibit the best performance profiles.

Thus, this study seeks to synthesize an amphiphilic copolymer based on the semi-crystalline polymer PTMC and the poly(amino acid) PGA using the synthetic platform described in the previous chapters. This copolymer can be self-assembled into stable monodispersed vesicles. The loading and release of two model drugs (procaine hydrochloride and imipramine hydrochloride) were measured using drug-selective electrodes developed in-house. Using ITC the interactions between model drugs and copolymer carriers were studied with the aim of understanding how these forces impact the loading capacity and release kinetics of each of these drugs.

Experimental

Materials

Trimethylene carbonate (1,3-dioxane-2-one: TMC) was purchased from Boehringer Ingelheim and dried on magnesium sulfate in tetrahydrofuran (THF), sublimated and stored in a glove box prior to use. Allyl alcohol (99 %), 1,3-bis(2,6-diisopropylphenyl)-imidazol-2-ylidene (NHC, 97 %), cysteamine (95 %), 2,2-dimethyloxy-2-phenylacetophenone (DMPA, 99 %) and imipramine hydrochloride (IMI, 99 %) were purchased from Sigma-Aldrich and used as received. γ-benzyl-l-gluatmate N-carboxy anhydride (BLG-NCA) was obtained from Isochem France and used as received. Hydrobromic acid (Hbr, 33 wt %), was purchased from Acros Organics and used as received. Trifuoroacetic acid (TFA, 99.9 %) was purchased from Caledon Laboratory Chemicals. For synthesis dimethylformamide (DMF) and tetrahydrofuran (THF) were dried prior to use, all other solvents were used as received.

Synthesis of ene-functionalized $PTMC_{30}$

Ene-functionalized $PTMC_{30}$ was synthesized according to a previously described method. Briefly, recrystalized TMC was dissolved in dry THF (2 M) and added drop-wise to a solution of allyl alcohol (45 mM) and NHC (1 mM) in dry THF under inert atmosphere. The reaction was left stirring for 90 min at room temperature and quenched with methanol. $PTMC_{30}$ was precipitated in ice-cold methanol and purified by centrifugation. The degree of polymerization was measured by end-group analysis of ^1H NMR spectrum. $PTMC_{30}$ was produced with a polydispersity of 1.13 at a yield of 85 %. ^1H NMR ($CDCl_3$, 400 Hz) δ(ppm)= 2.0

(C(O)OCH$_2$C$\underline{H_2}$CH$_2$OC(O)), 4.2 (C(O)OC$\underline{H_2}$CH$_2$C$\underline{H_2}$OC(O)), 4.59 (H$_2$C=CH-C$\underline{H_2}$-), 5.29 ($\underline{H_2}$C=CH-CH$_2$-), 5.89 (H$_2$C=C$\underline{H}$-CH$_2$-).

Amine-functionalization of PTMC$_{30}$ by thiol-ene coupling

Ene-functionalized PTMC$_{30}$ (1 eq), Cysteamine (3 eq) and DMPA (3 eq) were dissolved in DMF and irradiated with UV light for 15 min. The NH$_2$-PTMC was then precipitated in cold methanol, centrifuged and dried under vacuum. Successful functionalization was confirmed by analysis of ^{1}H NMR spectrum of the dried product. Polydispersity index was experimentally determined by gel permeation chromatography (GPC). ^{1}H NMR (CDCl$_3$, 400 Hz) δ(ppm)= 2.0 (C(O)OCH$_2$C$\underline{H_2}$CH$_2$OC(O)), 2.55 (CH$_2$S$\underline{CH_2}$CH$_2$NH$_2$), 2.75 (CH$_2$SCH$_2$$\underline{CH_2}NH_2$), 3.02 ($\underline{CH_2}SCH_2CH_2NH_2$) 4.2 (C(O)OC$\underline{H_2}CH_2C\underline{H_2}$OC(O)), 4.23 (H$_2$C=CH-C$\underline{H_2}$).

Polymerization of BLG-NCA from PTMC$_{30}$-NH$_2$ macroinitiator

PBLG was grown from the amine terminus of PTMC$_{30}$ via ROP using the PTMC$_{30}$-NH$_2$ as a macroinitiator. In a glove box under inert conditions BLG-NCA and PTMC$_{30}$-NH$_2$ were dissolved in dry DMF with [BLG-NCA]:[PTMC$_{30}$-NH$_2$] = 14, and left stirring for 48 h. The solution was removed from the glove box and PTMC$_{30}$-*b*-PBLG$_{13}$ was precipitated in diethyl ether. The precipitate was removed by centrifugation and washed repeatedly with diethyl ether. ^{1}H NMR (DMSO, 400 Hz) δ= 7.18 (d) 5H, C(O)CH[(CH$_2$)$_2$C(O)OCH$_2$$\underline{Ph}$]; δ= 5.09 (m) 2H, C(O)CH[(CH$_2$)$_2$C(O)OC$\underline{H_2}$Ph]; δ= 4.41 (m) 1H, C(O)C$\underline{H}$[(CH$_2$)$_2$C(O)OCH$_2$Ph]; δ=2.45 (m) 2H, C(O)CH[(CH$_2$C$\underline{H_2}$)C(O)OCH$_2$Ph]; δ=1.95 (m) 2H, C(O)CH[(C$\underline{H_2}$CH$_2$)C(O)OCH$_2$Ph].

Acid hydrolysis of $PTMC_{30}$-*b*-$PBLG_{13}$ to $PTMC_{30}$-*b*-PGA_{13}

The benzyl side chain of $PTMC_{30}$-*b*-$PBLG_{13}$ was cleaved by acid hydrolysis to produce $PTMC_{30}$-*b*-PGA_{13}. In a typical cleavage $PTMC_{30}$-*b*-$PBLG_{13}$ was dissolved in TFA and HBr and left stirring for 2 h. $PTMC_{30}$-*b*-PGA_{13} was precipitated in diethyl either and isolated by filtration. The product was dissolved in water and purified by dialysis against water for 2 days with frequent water changes. The final $PTMC_{30}$-*b*-PGA_{13} product was freeze dried to produce a white powder. ^{1}H NMR (DMSO, 400 Hz) δ= 4.41 (m) 1H, C(O)C<u>H</u>[$(CH_2)_2$C(O)OH]; δ=2.45 (m) 2H, C(O)CH[(CH_2C<u>H_2</u>)C(O)OH]; δ=1.95 (m) 2H, C(O)CH[(C<u>H_2</u>CH_2)C(O)OH].

Vesicle self-assembly and drug encapsulation by nanoprecipitation

Self-assembly of imipramine-loaded and procaine-loaded vesicles from $PTMC_{30}$-*b*-PGA_{13} was performed *via* a previously reported nanoprecipitation method. $PTMC_{30}$-*b*-PGA_{13} (10 mg) and imipramine hydrochloride or procaine hydrochloride (40 % feed weight ratio) were dissolved in DMSO (500 µL). With vigorous stirring, buffer (4.5 mL) pH = 9.5 (for IMI) or pH 7.4 (for PrHy) was added over 15 s. The unbound drug in the IMI-loaded nanoparticle suspension was removed by dialysis against buffer pH 7.4 over 30 min (MWCO = 13 000), with one buffer change. The vesicle suspension mixtures were purified by 3 rounds of ultrafiltation (pore size 25 nm) and the dispersion volume was reduced to 2 mL (5 mg/mL). The structural morphology was probed with dynamic and static light scattering and TEM and the drug loading was measured by drug-selective electrodes.

Drug release measurements

Aliquots of drug-loaded vesicles were dispersed in 50 mL of buffer (pH 7.4 or 4.5) with gentle stirring and drug concentrations were monitored by drug-selective electrodes over a 36 hour period under ambient conditions. Readings of drug concentrations were taken every 10 seconds.

Preparation of drug-selective electrodes

A drug-ion complex was first prepared. Poly(vinyl chloride) (PVC) (0.5 g) was dissolved in THF (30 mL). Separately, procaine hydrochloride (0.955 g for PrHy membrane) or imipramine hydrochloride (1.109 g, for IMI membrane) was dissolved in a 1:9 THF:H_2O mixture (100 mL). The dissolved PVC was then added drop-wise to the drug solution with vigorous stirring and left for 48 h to complex. The complex was then precipitated in cold deionized water and filtered by vacuum filtration. The filtrate was washed several times with deonized water and dried overnight in a vacuum oven.

The prepared complex was used in the preparation of ion-selective membranes. Drug-on complex (either PrHy-PVC or IMI-PVC) was dissolved in THF (15 mL) and the polymeric plasticizer poly(ethylene-co-vinyl acetate-co-carbon monoxide) (PE-co-PVA-co-CO) and NaTPB were dissolved separately in THF (15 mL). The two solutions were mixed and allowed to stir for 10 min. The mixture was then poured into a Petri dish (55 mm diameter) and the solvent was allowed to evaporate over 2 – 3 days. The membrane was then carefully removed from the Petri dish and stored. The selectivity of the membrane is attributed to the presence of the drug ion within the membrane.

The drug membrane was cut-out into a disc and adhered onto the end cap of the electrode body using THF which was placed on the flat concentric surface of the tip. Leakages of the tip with drug membrane were tested by filling the tip with distilled de-ionized water after the THF had been evaporated. After checks for leakages, the end cap with drug membrane was dried and stored in a desiccator and kept from light. Prior to use, the membrane was soaked in a 0.01 M PrHy solution (PrHy membrane) or 0.01 M IMI solution (IMI membrane) for half an hour. Calibration of PrHy and IMI selective probes was conducted over a concentration range of 10^{-5} – 10^{-1} M. Stability of the electrode response was measured at 10^{-3} M of either PrHy or IMI over a 24 h period. Calibration and stability testing can be seen in Figures 38and 39.

Prior to all measurements with the designed drug-selective electrodes, both calibrations and long-term stability testing was performed. Calibration was done over a range of 10^{-5} – 10^{-2} M PrHy (or IMI), and long-term stability testing was conducted over a 24 h period. The results of both of these tests are given below in Figures 38 and 39.

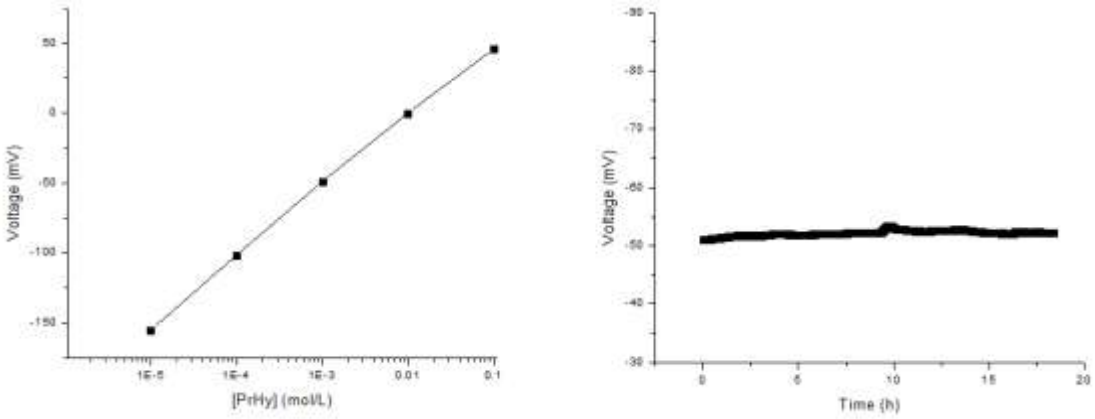

Figure 38 Long-term stability (right) and calibration curve (left) of PrHy-selective electrode

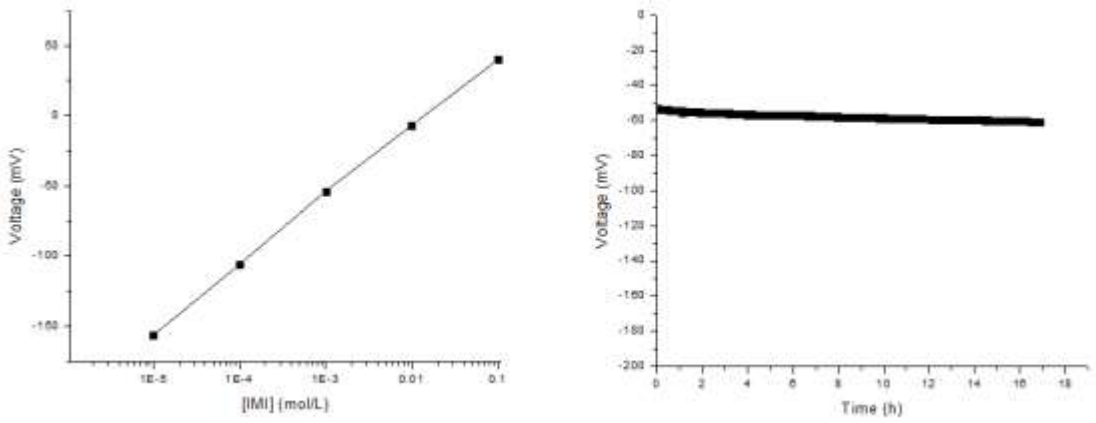

Figure 39 Long-term stability (left) and calibration curve (right) of IMI-selective electrode

PrHy selective electrode was shown to display a linear response within the range of 10^{-5}-10^{-2} M with an average drift of 0.1 mV/h. Likewise the IMI-selective electrode showed a linear response between 10^{-5} – 10^{-2} M with an average drift of 0.3 mV/h over a 16 h period. For the purposes of this project both electrodes are usable within the concentration and time ranges of the planned experiments.

Size-exclusion chromatography

All SEC measurements were performed in dimethylformamide (DMF) with LiBr (1 g/L) as the eluent. The flow rate was fixed at 0.8 mL/min. Two 7.5 mm x 300 mm PLgel, 5 µm Mixed-D columns (Polymer Laboratories) were coupled to a guard column, 7.5 mm x 50 mm, PLgel, 5 µm (Polymer Laboratories). The system was equipped with a differential refractive index (RI) detector. Calibration was performed with polystyrene standards.

^{1}H NMR

All measurements were conducted using a Brukner Adsvance spectrometer operating at 400 MHz at room temperature with a fixed (7.5 s) relaxation time. d-DMSO or $CDCl_3$ was used as a reference signal (δ=2.5 ppm and 7.4 respectively).

Dynamic light scattering (DLS) and static light scattering (SLS)

DLS and SLS measurements were performed with a Brookhaven Laser Light Scattering system with a BI200SMv2 goniometer with a vertically polarized helium-neon diode laser at a wavelength of 636 nm and a BI-9000AT digital correlator with a 125 ns initial measurement time. Samples were kept at constant temperature (25 °C) for the duration of measurements. Measurements were taken every 10 ° between 60 ° and 140 °. SLS measurements were analyzed in a Berry plot to obtain the radius of gyration.

Transmission electron microscopy (TEM)

TEM images were recorded with a Philips CM10 TEM microscope using a 60 keV acceleration voltage. Samples were prepared by depositing one droplet of the dispersed nanoparticles onto a carbon-formvar grid (200 mesh coated with copper) and allowed to dry. No additional staining was performed.

Isothermal titration calorimetry (ITC)

The calorimetric data on the binding interactions between procaine hydrochloride, imipramine hydrochloride and the copolymer $PTMC_{30}$-*b*-PGA_{13} were obtained using a Microcal VP-ITC calorimeter (Northampton, MA). The stock solutions of 10 mM of drug were selected for titration onto 1 mM solution of vesicles. The volume of individual injections varied for each run increasing from a starting volume of 2 µL to a final volume of 20 µL until the total volume was injected and/or saturation was observed. All titrations were conducted at 25.0 °C, with delays between injections varying until a return to the baseline was achieved, generally 200 seconds was sufficient. The microcalorimeter consists of a reference cell and a sample cell of approximately 1.4 mL in volume, and the drug solution was injected from a filled 281.72 µL injection syringe into the sample cell filled with the copolymer solutions. The syringe is tailor-made such that the tip acts as a blade-type stirrer to ensure an efficient mixing at 307 rpm. In this study, we utilized identical injection protocol and same time interval between successive injections for all ITC measurements.

Synthesis of $PTMC_{30}$-*b*-PGA_{13}

The synthesis of $PTMC_{30}$-*b*-PGA_{13} was achieved using a combination of organocatalyzed ROP and thiol-ene coupling. The full synthetic strategy is shown in Scheme 3. Ene-functionalized $PTMC_{30}$ was synthesized using an organic catalyst as described in previous chapters, followed by amine-functionalizations by UV-initiated thiol-ene coupling. The reaction was completed within 10 minutes of exposure to UV light with near total functionalization. The functionalization was monitored by the disappearance of 2 peaks associated with the ene-

functionality on the ^{1}H NMR spectrum at δ = 5.32 and 5.81 ppm and the subsequent appearance of small triplets between 2.5 and 3 ppm associated with the addition of cyateamine to the $PTMC_{30}$. These peaks are visible on the ^{1}H NMR spectra seen in Figure 40.

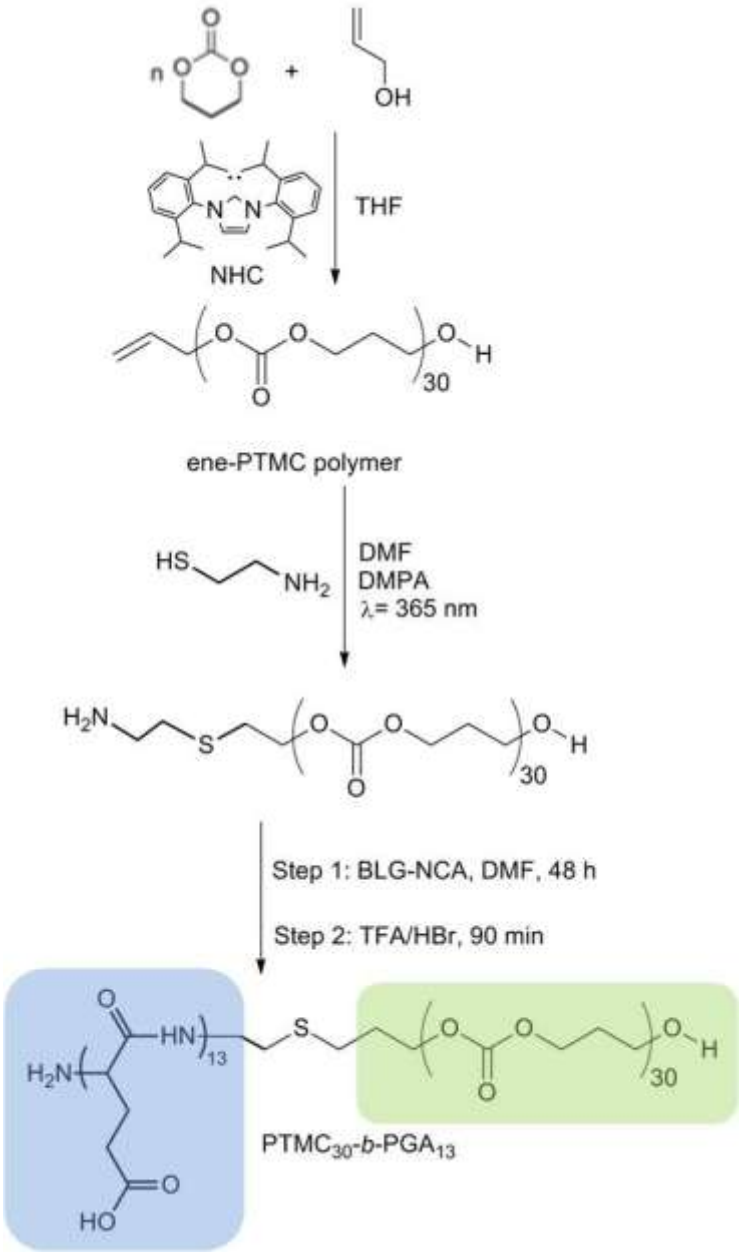

Scheme 3 Synthetic strategy for $PTMC_{30}$-*b*-PGA_{13}

Amine-functionalized $PTMC_{30}$ was used as a macroinitiator for the ring-opening polymerization of BLG-NCA. The reaction proceeded to completion after 48 hours and was purified by precipitation to give $PTMC_{30}$-*b*-$PBLG_{13}$. The appearance of signals from the PBLG on the ^1H NMR spectrum are indicative of the successful polymerization and the degree of polymerization was confirmed by integration of the ^1H NMR signals. A degree of polymerization of 13 was specifically targeted with the goal of producing a final copolymer with a hydrophilic weight fraction (*f*) of 36 %. This value of f was chosen with the intent to produce nanoparticles with a vesicular morphology. In a second step the benzyl pendant group of the PBLG block was cleaved from the copolymer by acid hydrolysis in TFA/HBr. The cleavage was confirmed by the disappearance of the benzyl peaks from the ^1H NMR of the copolymer. The final $PTMC_{30}$-*b*-PGA_{13} copolymer was dried under vacuum.

Self-Assembly and Drug Loading of Vesicles from $PTMC_{30}$-*b*-PGA_{13}

Following the self-assembly by nanoprecipitation and purification, the resulting nanostructures were analyzed by DLS, SLS and TEM. Light scattering analysis showed narrow size distributions over a range of angles, a linear q^2 dependence of the decay rate (Γ). Additionally, the Berry plot showed a linear relationship between $(I^{-1})^{-1/2}$ and q^2. These relationships can be clearly seen in Figure 41.

DLS analysis revealed a R_H value of 77 nm and SLS produced a R_G value of 81.2 nm giving a R_G/R_H value of 1.05, consistent with the expected vesicle morphology. The structures were stable and well-defined. Light scattering analysis was followed by visual inspection by TEM. Typical micrographs are given below in Figure 42 with a schematic representation of the

structure for visualization. The micrographs revealed uniform vesicle structures consistent with the light scattering analysis.

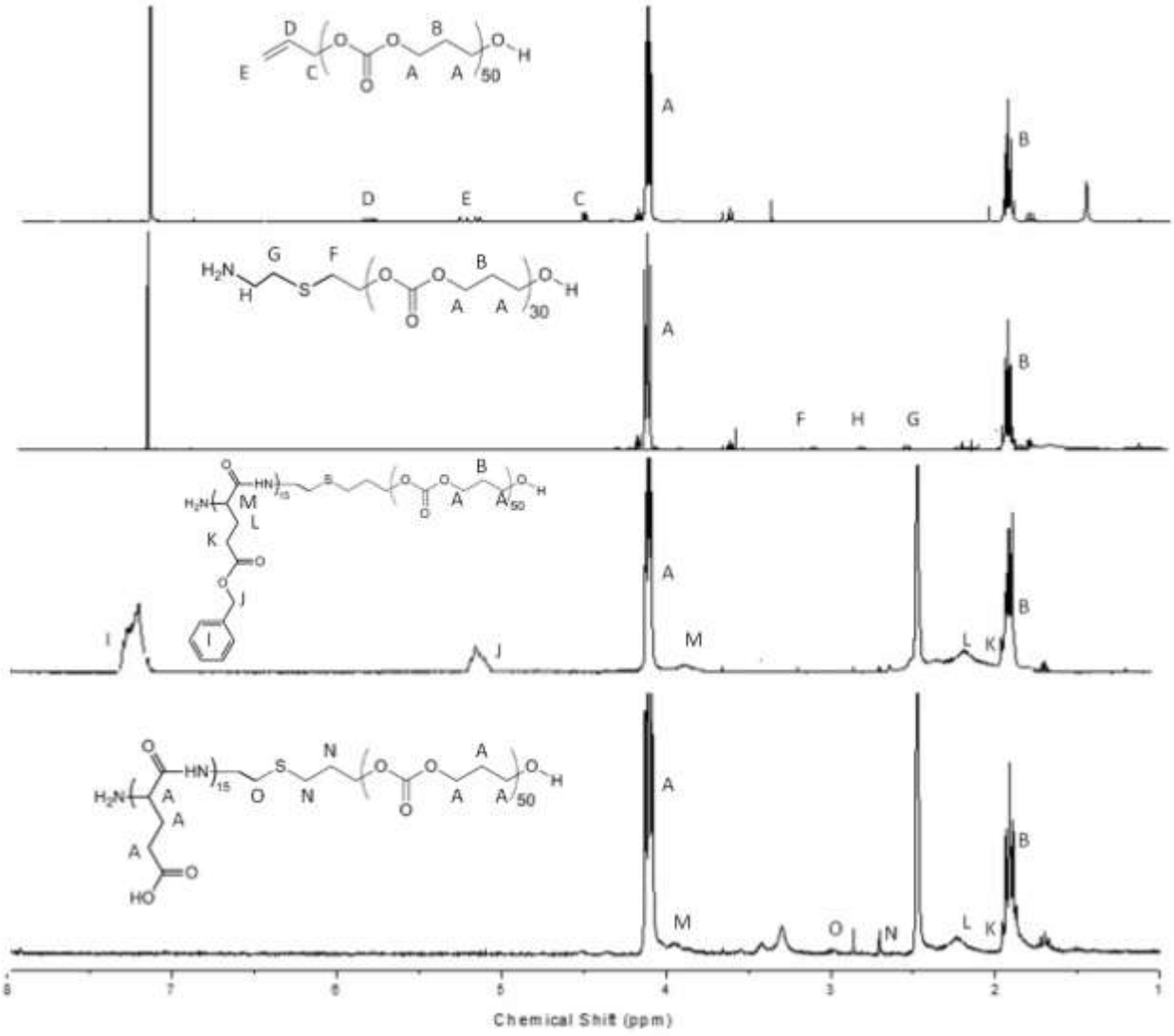

Figure 40 ^{1}H NMR spectra (from top to bottom) of ene-PTMC$_{30}$, PTMC$_{30}$-NH2, PTMC$_{30}$-*b*-PBLG$_{13}$ and PTMC$_{30}$-*b*-PGA$_{13}$ after purification at each step, showing the step-wise synthesis of the final conjugate

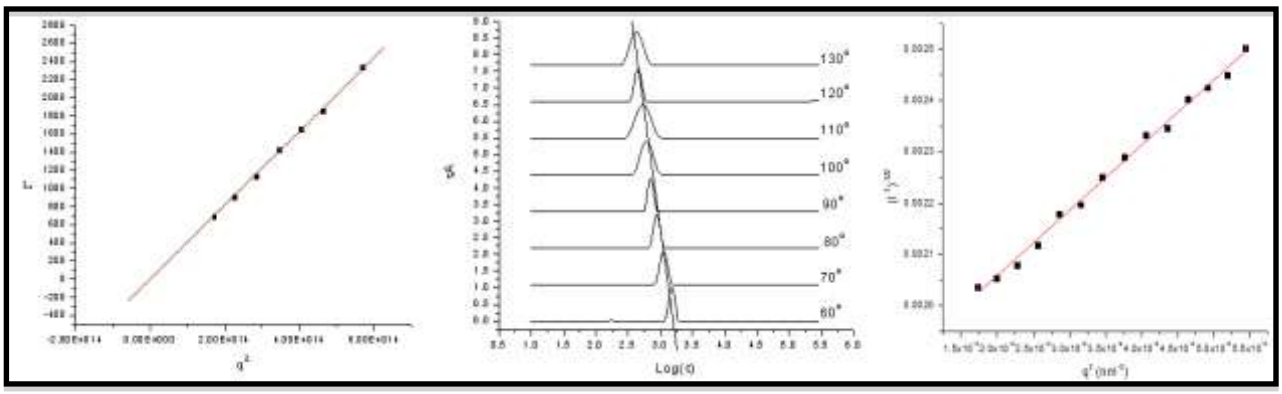

Figure 41 Full DLS and SLS data set showing q^2 dependence of the decay time (left), narrow and well defined distribution over multiple angles (center) and linear progression of $(I^{-1})^{-1/2}$ and q^2 (right)

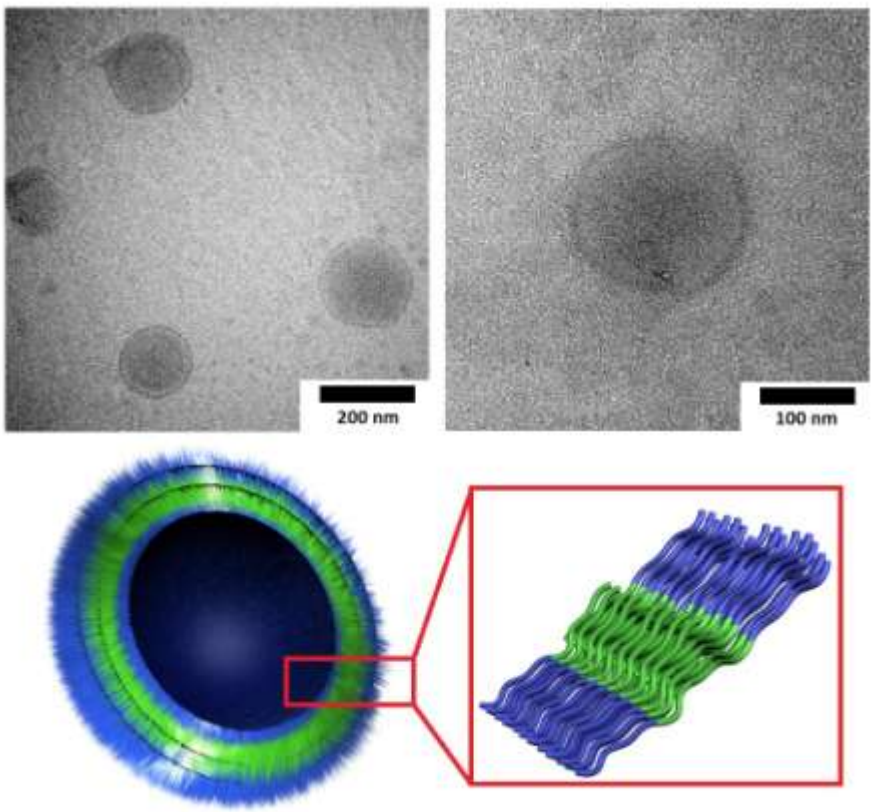

Figure 42 TEM micrographs of $PTMC_{30}$-*b*-PGA_{13} vesicles with schematic representation showing $PTMC_{30}$ (green) and PGA_{13} (blue).

Encapsulation of the model drugs procaine hydrochloride and imipramine hydrochloride was achieved via co-precipitation during the self-assembly process. The amount of drug encapsulated was measured by performing ultrafiltration on the particle suspension and measuring the residual drug content in the filtrate. Procaine was encapsulated at 24 % while imipramine showed 37 % encapsulations and the explanation for the observed difference will be discussed below.

Study of Drug-Carrier Interactions

In order to evaluate the impact of drug-carrier interactions on the encapsulation efficiency and release kinetics of this system, two model drugs were chosen for evaluation; procaine hydrochloride (PrHy) and imipramine hydrochloride (IMI). The chemical structure of both drugs is given in Figure 43. Both drugs are amphiphilic and possess surfactant-like characteristics, though the hydrophobic region of procaine is less significant than that of imipramine. Additionally, though both drugs have a titratable tertiary amine, the charge on the tertiary amine in the procaine structure is considerably shielded by the surrounding ethyl groups. This effect is not present with imipramine. The similarities and difference in the structure of the two drugs makes them ideal models to compare the effects of drug-carrier interactions.

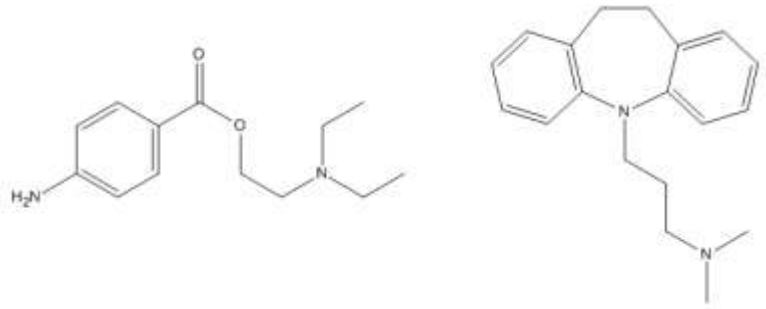

Figure 43 Chemical structure of model drugs PrHy (left) and IMI (right)

In order to measure the magnitude and characteristics of interaction between the two model drugs and the $PTMC_{30}$-*b*-PGA_{13} copolymer vesicles, the drugs were titrated into a dispersion of the copolymer vesicles by ITC at pH 7.4, 9.5 and 4.5.

At pH 7.4, heat changes recorded from the titration of procaine were small relative to the much larger heat changes observed from the titration of imipramine under similar conditions. The raw data from this titration is shown in Figure 44. Additionally, when the enthalpy values were extracted and plotted (Figure 44), the titration of imipramine revealed a significant heat transition resulting in saturation of all interaction sites and the curve could be fitted to a two-site interaction model, where it was dominated by the electrostatic interaction. The interaction models were established by the ITC software and involved selecting the number of sites and varying the thermodynamic parameters over a sequence of iterations, until an appropriate fit was achieved. In the case of imipramine, this was consistent with the expected strong electrostatic interactions between the positively charged amine group on the drug and the negatively charged carboxyl group on the copolymer. In contrast, the titration of procaine hydrochloride showed no major transitions and the data could be fitted to a one-site interaction model. Due to the structure

of PrHy we concluded that the minimal interaction was attributed to shielded charge and the significantly reduced hydrophobic group relative to IMI.

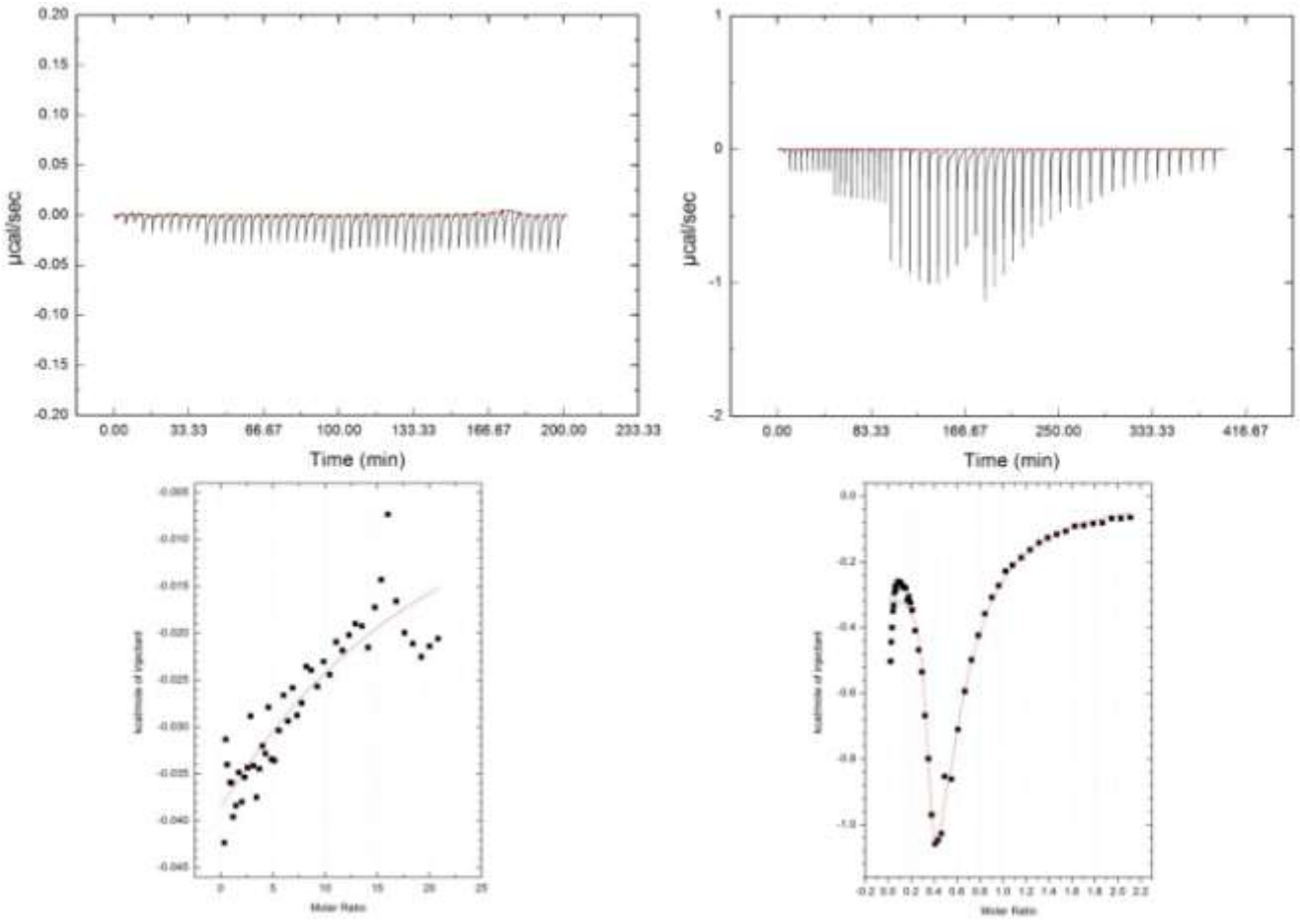

Figure 44 Full ITC data set obtained at pH 7.4 showing raw heat curves from titration of PrHy (top left) and IMI (top right) with corresponding enthalpy curves below fitted to interaction site models.

The minimal interaction observed may be responsible for the comparably lower encapsulation efficiency observed with this system. It is worth noting that due to the dominant electrostatic interaction observed with imipramine encapsulation at pH 7.4, the complexes

formed precipitated from solution. Hence, encapsulation of imipramine was performed at pH 9.5 (above the pKa of both drugs), however the relative importance of drug-polymer interaction is similar at high pH.

Titrations of the two model drugs were performed at pH 9.5 and the raw data and enthalpy curves are shown in Figure 45. At pH 9.5, the titration of procaine again exhibited minimal interaction that is consistent with weak electrostatic interaction and very weak hydrophobic interaction. Imipramine, with a pKa of 8.9, showed significantly reduced interaction at pH 9.5 than at pH 7.4due to the protonation of the drug that eliminated the positive charges resulting in the removal of electrostatic interaction previously present. The enthalpy curve did show a significant transition and could be fitted to a one-site interaction model, that was consistent with hydrophobic interaction forces expected to be present at high pH. This interaction at high pH is responsible for the higher encapsulation efficiency when compared to PrHy.

Finally, titrations of both drugs were performed at pH 4.5, approaching the pKa of the PGA block of the copolymer (4.3). The low pH titrations are similar in interaction to the high pH case and the data set can be seen in Figure 46.

The titration of procaine at low pH again showed minimal interactions with no significant transitions observed in the enthalpy plot. In contrast the titration of imipramine at low pH, significant heat changes with a transition on the enthalpy curve was observed and the data could be fitted to a one-site interaction model. This correlated well with the expected minimal electrostatic interactions and the dominating hydrophobic interactions.

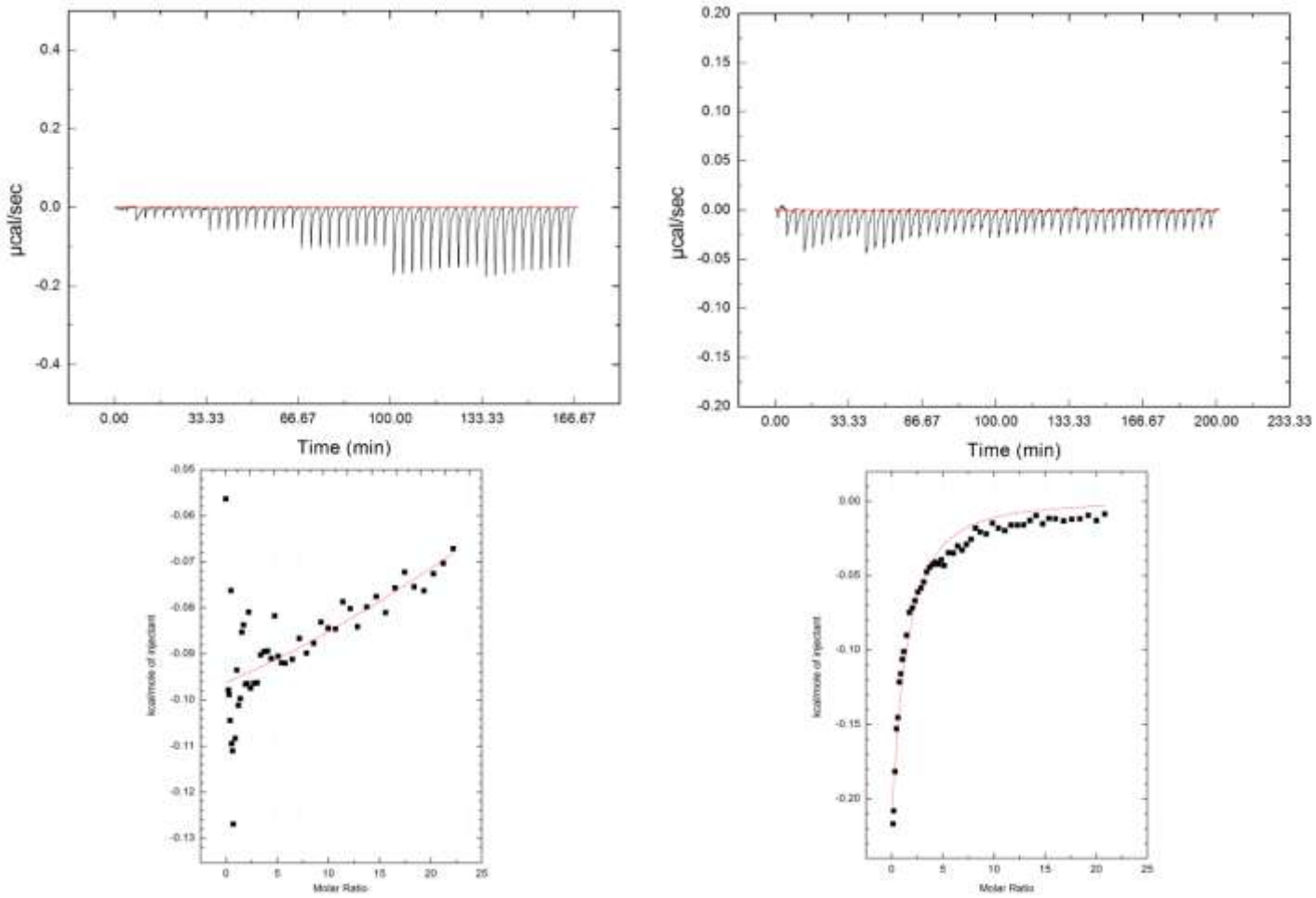

Figure 45 Full ITC data set obtained at pH 9.5 showing raw heat curves from titration of PrHy (top left) and IMI (top right) with corresponding enthalpy curves below fitted to interaction site models.

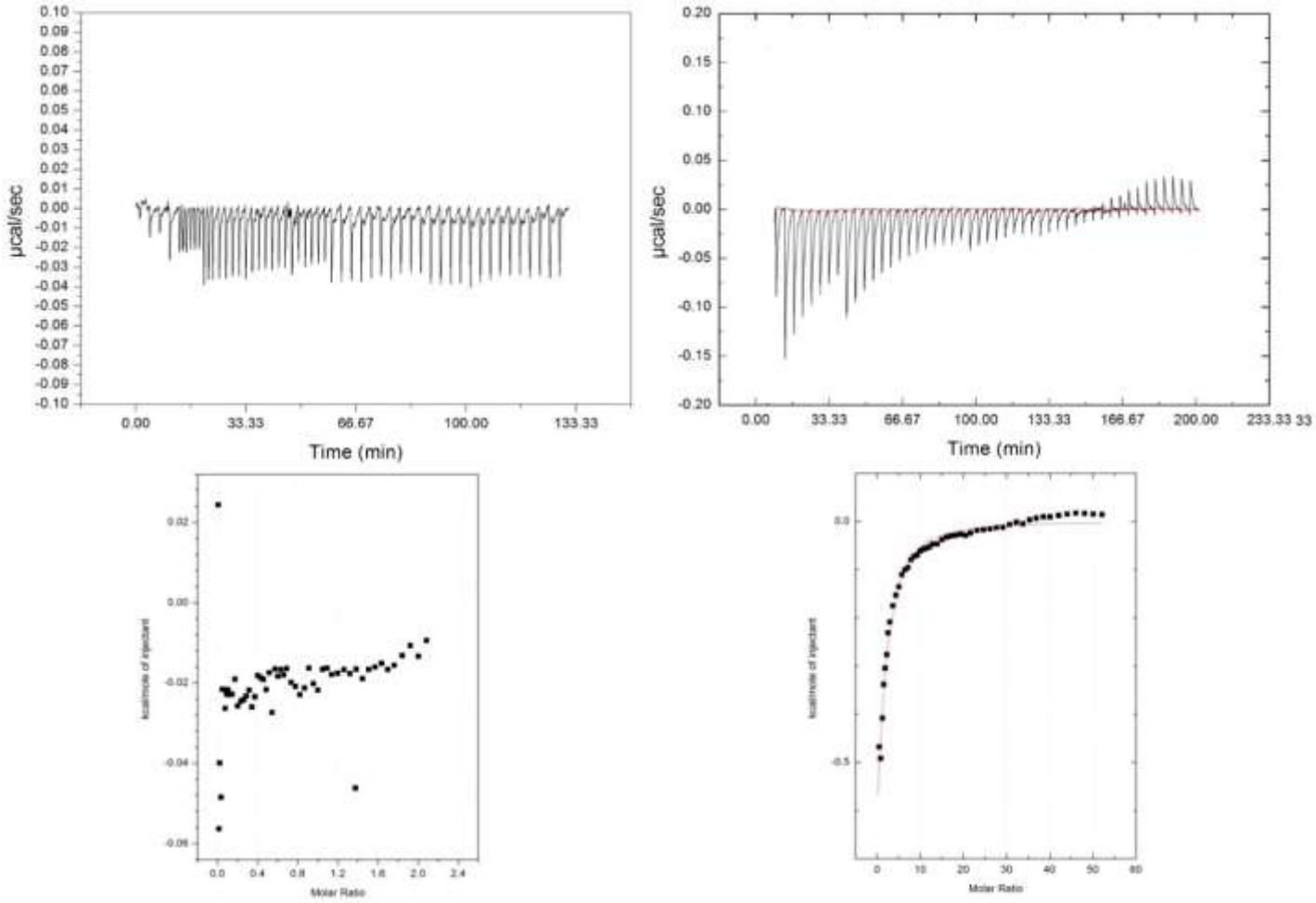

Figure 46 Full ITC data set obtained at pH 4.5 showing raw heat curves from titration of PrHy (top left) and IMI (top right) with corresponding enthalpy curves below fitted to interaction site models.

At all pHs the interaction of imipramine with the copolymer was significantly higher than that of procaine. The weakest interactions observed between imipramine and the copolymer were at pH 9.5 and were nonetheless stronger than the interactions between procaine and the copolymer at all pHs. This difference in the magnitude of interaction has a significant impact on the encapsulation efficiency of the drugs within the polymer vesicles. Procaine was encapsulated at 24 % efficiency while imipramine showed 38 % encapsulation, an increase in encapsulation of

50 %. Due to the hydrophilic nature of procaine, it is believed that the drug is encapsulated into the aqueous hydrophilic cavity of the vesicle. In contrast, since the encapsulation of imipramine was performed at high pH (above the pKa of the drug), where the drug was uncharged and largely hydrophobic, it was likely that the drug molecules were encapsulated within the hydrophobic region of the vesicle membrane. This type of encapsulation has been previously observed with similar systems.

In Vitro Drug Release of Procaine Hydrochloride and Imipramine Hydrochloride

The in vitro release of PrHy from the vesicles was measured at pH 7.4 using a PrHy-selective electrode. The release profile obtained is shown in Figure 47. The release of procaine from the vesicles was quite rapid showing 50 % release after only 30 min and nearly 85 % drug release within 5 hours. As there is little interaction between the drug and vesicles (as evidenced by ITC measurements) there is no strong driving force holding the drug in the vesicles. The release of the drug molecules occurs by simple diffusion of the drug across the vesicle membrane driven by the concentration gradient driving force. With no strong drug-polymer interaction, the drug diffuses against the concentration gradients with relative ease.

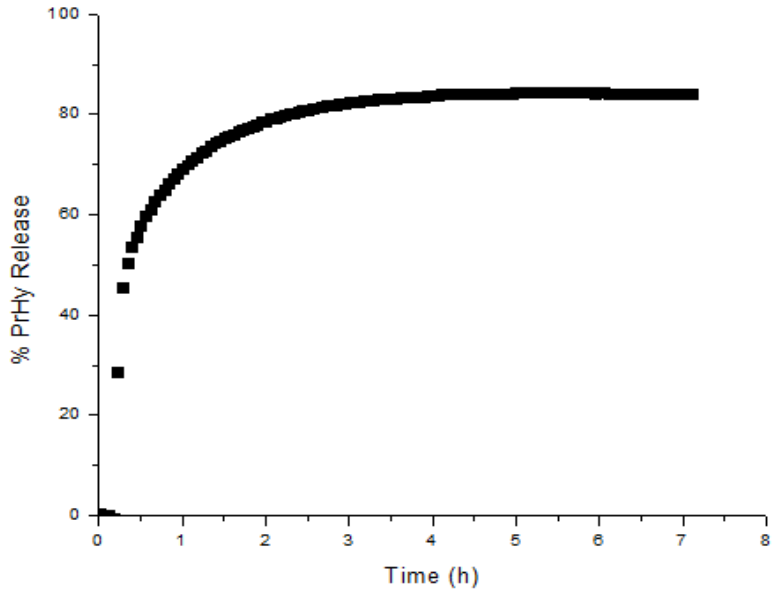

Figure 267 Release of procaine hydrochloride from PTMC$_{30}$-*b*-PGA$_{13}$ vesicles

The release of IMI was measured at pH 7.4 and 4.5 using an IMI-selective electrode. The results are shown in Figure 48. At pH 7.4 the release of IMI was quite slow compared to that of PrHy, showing a 50 % release after approximately 11 h and 70 % release after 24 hours. It is believed that the much slower release of IMI from the vesicles compared to that of procaine resulted from the much stronger interactions present between IMI and the vesicles compared to PrHy and the vesicles as evidenced by ITC measurements. The strong electrostatic interactions between the positively charged drug and the negatively charged internal and external surfaces of the vesicles traps the drug within vesicles (either membrane or cavity) reduced the release and diffusion of the drug molecules from the vesicle to the bulk solution.

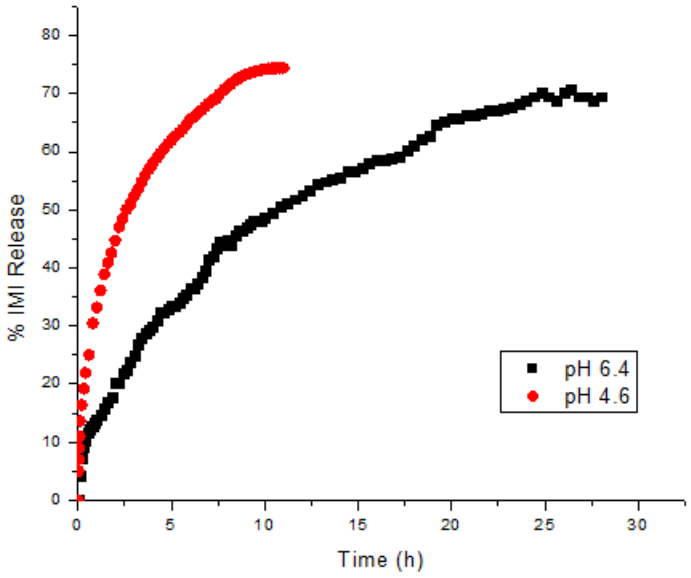

Figure 48 Release of imipramine hydrochloride from $PTMC_{30}$-*b*-PGA_{13} Vesicles

The differences in the release rates between PrHy and IMI correlated very well to the magnitude of interaction between the drugs and the vesicles determined from ITC measurements at pH 7.4. It is believed that drug-polymer interaction plays a key role in the encapsulation and release of drugs from delivery systems and this can be used to select appropriate drug carriers for the encapsulation and delivery of drug molecules. Further studies are needed to confirm this hypothesis.

The release of IMI at pH 4.5, which is close to the pKa of the PGA shell (4.3) of the vesicles, was faster than the release at pH 7.4, showing 50 % release after only 2.5 hours and 75 % release after 10 hours. As described above, the release is largely influenced by the drug-polymer interactions which are predominately hydrophobic at low pH and electrostatic at neutral pH. These interactions are governed by the pH conditions. As the pH of the release media

approaches the pKa of the PGA shell (4.3), the PGA becomes protonated, neutralizing the negative surface charges. The electrostatic interactions between the positive drug and the negative polymer which previously trapped the drug within the vesicles are no longer present (or greatly reduced) allowing for more rapid drug release.

Kataoka et al have previously described a system comprised of PEG-b-PAsp in which the affinity of the system towards a drug and a relevant enzyme was significantly enhanced upon modification.[12,103] Firstly, the addition of aromatic groups to the structure enhanced affinity with the target enzyme, and addition of charged components to the copolymer backbone enhanced the ionic nature to the polymer and directly resulted in a greater affinity between the carrier and the drug. The results presented here are consistent with the general theme of Kataoka's work. In all cases affinity of the drug to the carrier seems to directly correlate to enhanced encapsulation efficiency and enhanced affinity for the drug and other charged species.

Although, the localization of the two drugs used in this study may vary (vesicle core vs vesicle membrane), the general trend relating encapsulation and release rate with the magnitude of interaction between the carrier and drug can be very valuable to the drug delivery community. This is internded as a preliminary study to give insight into the effects of drug-carrier interactions on encapsulation and release to encourage the design of appropriate carriers for specific drugs.

This work provides some insight however, a more comprehensive study should be done in order to compare multiple drugs over a broader array of interaction conditions. In this fashion a more in-depth understanding of release mechanisms and how they relate to interactions between drugs and carriers can be achieved.

Conclusions

$PTMC_{30}$-*b*-PGA_{13} was synthesized by a combination of organo-catalyzed ROP and rapid UV-initiated thiol-ene coupling with high yield. Well-defined mono-dispersed vesicles can be prepared from the copolymer via a nanoprecipitation technique and both procaine hydrochloride and imipramine hydrochloride can be loaded into the vesicles with high efficiency. Interactions of the two model drug with the copolymer were probed by ITC and the data correlated with encapsulation efficiency and drug release rates. Both drugs showed total drug release within 36 hours, with procaine releasing within 5 hours resulting from low interaction of the drug with the carrier. Additionally, the reduction of electrostatic forces at low pH was correlated with enhanced drug release of imipramine from the vesicle carrier. These results point to the inherent need to understand the interaction between drugs and potential carriers in order to tailor the system to high loading efficiency and optimal release rates. ITC has proven to be an invaluable tool to probe this phenomenon and it can be used to select and match drugs with optimal carrier systems.

Chapter 7 Conclusions and Recommendations

In this work a synthetic polymer (PTMC) was combined with a biologically-relevant peptide (PVGLIG) and a poly(amino acid) (PGA) to produce diblock and triblock copolymers capable of self-assembly into a range of well-characterized particle morphologies (Chapters 3 & 4). Then influence of both temperature and pH on drug release was studied with significant stimuli-responsive behaviour observed. Structures containing PVGLIG were subjected to enzymatic degradation by the tumor-associated enzyme MMP-2 and demonstrated selective-degradation in biologically-relevant conditions.

The membrane integrity and occurrence of fission and fusion events was investigated by heating and cooling hybrid vesicles across the chain-melting temperature (Chapter 5). Special attention is paid to discrepancies observed relative to comparable vesicular systems in the literature.

Finally, the work aimed to understand the relationship between drug-carrier interactions and the encapsulation and release of drugs from polymer vesicles (Chapter 6). The interactions between two model drugs and $PTMC_{30}$-*b*-$PTMC_{13}$ vesicles were probed using ITC, and the encapsulation efficiency and drug release of these drugs was monitored using drug-selective electrodes. The observed interactions were correlated with the release rates and encapsulation capacities. In highly charged systems the drug release rate is largely governed by electrostatic interactions. The following conclusions can be drawn from this work.

General Contributions

$PTMC_n$-*b*-PVGLIG diblock nanostructures

A combination of organo-catalyzed ring-opening polymerization, peptide synthesis and thiol-ene click chemistry was used to successfully access various structurally well-defined polymer-peptide hybrids comprised of PTMC and the MMP-2 peptide substrate PVGLIG. Synthesis of ene-functionalized PTMC by use of an *N*-heterocyclic carbene catalyst and functionalized alcohol initiator had not previously been reported and offers a facile strategy for production of PTMC with other functionalities. Click chemistry was used to successfully couple the as-made PVGLIG peptide to varying block length PTMC featuring a terminal ene functional group to form the $PTMC_n$-*b*-PVGLIG hybrids. The amphiphilic nature of the di-block system allows for the self-assembly of $PTMC_n$-*b*-PVGLIG by nanoprecipitation yielding stable monodispersed structures of varying morphology. The observed morphologies were not consistent with traditional structural morphologies based on the hydrophobic/hydrophilic balance. This discrepancy stems from the presence of the semi-crystalline PTMC block and the nanoprecipitation process used for self-assembly, which can freeze the structure morphology outside of thermodynamic equilibrium.

With the enzyme-cleavable peptide as a structural element in the hybrids, these particles are selectively degradable by the tumor-associated enzyme MMP-2. Significant disruption of all structure morphologies was observed after incubation with MMP-2 over a 48 h period. These MMP-sensitive structures represent the first step towards a targeted drug delivery system for the

tumor microenvironment. The unique morphologies provide valuable insight into the mechanism of self-assembly of complex polymer-peptide hybrid molecules.

$PTMC_{50}$-*b*-PVGLIG-*b*-PGA_{15} multi-functional vesicles

The unique synthetic strategy used for synthesis of diblock hybrid conjugates was here expanded to produce a triblock system consisting of PTMC, a pH-sensitive poly(amino acid) (PGA) and a biologically relevant peptide (PVGLIG). Thiol-ene coupling between two macromolecules was achieved with efficiency by introducing a constant supply of the radical-producing initiator throughout the reaction mixture under constant UV exposure. Vesicle self-assembled from this system by a nanoprecipitation technique showed significant changes in release of imipramine under varied conditions. Thermal, pH and enzyme sensitivities derived from the individual polymer, poly(amino acid) and peptide blocks, respectively, were observed in the final structures. Notably, vesicles show a significant increase in release rate under higher temperatures in excess of the melting temperature of $PTMC_{50}$. Additionally, drug-release could be enhanced under low pH conditions. The vesicles were cleavable in the presence of the tumor-associated enzyme MMP-2, and showed a corresponding enhanced release under these conditions. Very few systems have been reported in literature in which an enzyme-specific peptide is used as a linker within the structure of a polymersome. In this respect the structures produced in this work are unique. Such a multi-functional system comprised of multiple conjugated blocks represents a new step towards biomimetic systems and holds potential for further development into clinically relevant drug-delivery systems.

Thermally-induced structural changes in hybrid vesicles

Well defined monodispersed vesicles comprised of a triblock $PTMC_{50}$-*b*-PVGLIG-*b*-PGA_{15} system were shown to fuse when heated above the melting temperature of the structurally important, semi-crystalline $PTMC_{50}$ block. The vesicles likely merge to form larger vesicles. The observed crystalline behaviour in these small vesicles is in contrast to previous reports by Sanson et al which demonstrate that structures below 200 nm in size showed no crystalline behaviour. The difference seen in this system is likely due to the presence of the PVGLIG peptide and the increase size of the PTMC block. These two factors may contribute to a microphase separation of crystalline and gel regions as temperatures approach the chain-melting temperature of the copolymer. Vesicles produced with larger sizes show an increase in melting temperature and molar melting enthalpy towards that of the bulk material. This increase results from reduced chain constraint derived from the larger size, resulting in a higher degree of crystalline character in the membrane.

Unlike previously reported systems, after melting of the membrane, the crystalline character was reversible with T_m being observed in consecutive DSC scans. Compared to previously published literature the equilibrations performed at both high and low extremes of heating and cooling cycles likely allow sufficient time for the slow recrystallization of PTMC within the vesicle membrane. In addition, the presence of PVGLIG and the larger molecular weight of PTMC likely contribute to the crystalline character of the vesicles. These results help shed light on the important role semi-crystalline polymers in general and PTMC in particular can play in the assembly and stability of nanostructures. This polymer may hold promise for producing nanostructures with temperature-tunable morphologies. By varying the chain length of

PTMC and the duration of heating, it may be possible to produce a range of tunable nanostructures.

Drug-carrier interaction and the implications for encapsulation and release

The synthetic strategy employed in the previous chapters to generate diblock and triblock hybrid conjugates was modified here to produce a copolymer from PTMC and the poly(amino acid) PGA. $PTMC_{30}$-*b*-PGA_{13} was synthesized by a combination of organocatalyzed ROP and rapid UV-initiated thiol-ene coupling with high yield. Well-defined mono-dispersed vesicles can be prepared from the copolymer *via* a nanoprecipitation technique and both procaine hydrochloride and imipramine hydrochloride can be loaded into the vesicles with high efficiency. Interactions of the two model drug with the copolymer were probed by ITC and the data correlated with encapsulation efficiency and drug release rates. Both drugs showed total drug release within 36 hours, with procaine releasing within 5 hours resulting from low interaction of the drug with the carrier. Additionally, the reduction of electrostatic forces at low pH was correlated with enhanced drug release of imipramine from the vesicle carrier. The electrostatic character of both the nano-vesicles and the model drugs was shown to have a significant impact on both drug encapsulation and release. These results point to the inherent need to understand the interaction between drugs and potential carriers in order to tailor the system to high loading efficiency and optimal release rates. ITC has proven to be an invaluable tool to probe this phenomenon and it can be used to select and match drugs with optimal carrier systems.

Recommendations for Future Work

Based on the results of the research presented above, the impact of the crystalline nature of copolymers should be further investigated in the context of both self-assembly and temperature-induced morphology changes. Additionally, the potential for the produced enzyme-cleavable systems for use as drug delivery systems should be further pursued. In addition, a more comprehensive look at a broader range of drug-carrier combinations should be done to better understand the role of differing interactions on the efficacy of drug delivery systems. The following recommendations are proposed.

The role of PTMC and semi-crystalline polymers in self-assembly

The $PTMC_n$-*b*-PVGLIG diblock structure synthesized in this work were capable of forming nanostructure morphologies inconsistent with what would be classically expected based on their hydrophilic weight fraction. This phenomenon has been attributed to the presence of the semi-crystalline PTMC block in the structures and the nanoprecipitation process used for self-assembly. Assembling structures from a much larger series of copolymers with varying PTMC block sizes may yield additional unexpected morphologies and give insight into how PTMC can be used for more controlled production of particle morphology. Indeed, apart from the vesicle morphologies all other structures produced were not expected and retroactive analysis of their structure was performed. These structures were not predicted or targeted. A larger study, involving a range of copolymers with carefully controlled molecular weights could help to understand the possible morphologies that can be produced from PTMC containing copolymers.

In this way, structure morphology can be more carefully controlled, and specific structural morphologies can be targeted.

As well, variations on the experimental protocol for nanoprecipitation can be altered to play on the morphology of specific copolymers. In doing this, the degree of crystallinity within the nanostructure could potentially be increased or decreased and maybe further give rise to additional particle morphologies. Self-assembly of semi-crystalline conjugates above the chain-melting temperature may also give more predictable particle morphologies as the major influencing factor (chain crystallization) is not present.

Temperature-tunable morphology in nanostructures

As discussed in the literature review of this report, temperature has been used as an indirect inducer of morphology changes in structures containing semi-crystalline copolymers. These morphology changes were directly linked to the chain-transition temperature exhibited in structures with a crystalline nature. The structures produced in this work all exhibit this same transition, however, only the triblock systems was investigated in depth. Given the range of morphologies observed from the diblock copolymers produced, I would recommend that the effect of temperature and the chain-melting temperature be investigated. Work by Li *et al* has shown a compound micelle to core-shell transition in PEO-*b*-PE compound micelles upon heating above the T_m. Similar morphological changes may be observed with the range of structures produced in this work. Moreover, a thorough study on these structures could lead to particles with temperature-tunable morphologies, in which a specific structural architecture can be targeted by temperature adjustments.

In the same way that triblock systems were produced in this work, other triblock systems consisting of multiple crystalline blocks, with differing chain-melting temperatures, could give rise to structures with inducible, step-wise morphology changes. In the recommendations discussed, the goal should be to gain more control over the particle morphology so that nanoparticles can be produced in a more targeted and predictable way.

Diblock and triblock hybrids as drug delivery systems

One of the primary goals of this work was to produce vesicle structures capable of responsive and controlled drug release. This goal was achieved, and enhanced drug release was shown under changing temperature and pH conditions and importantly in the presence of the tumor-associated enzyme MMP-2. This triblock system holds potential to be further developed into a drug delivery system by pairing it with drugs particularly relevant to cancer therapy. Additionally, given the vesicle nature of the structure it is possible to load both hydrophilic and hydrophobic drugs into the carrier. This is one of the main advantages of the vesicle morphology, but has not yet been explored in this work. With multiple payloads loaded (in the membrane core and in the aqueous cavity), the release of each could be carefully controlled independently and in response to different stimuli (pH to release drugs from the aqueous cavity and temperature to release drugs from the membrane for example.).

While the triblock system developed showed multi-responsive character, the vesicles produced from the diblock conjugates may also hold potential for further development. These structures showed significantly faster degradation in the presence of MMP-2 compared to the analogous triblock vesicles. This more rapid cleavage would likely result in a more prominent

enhancement of drug release compared to what was observed in the triblock vesicles. I would recommend that the $PTMC_{13}$-*b*-PVGLIG vesicles be further investigated for controlled and induced drug release in the presence of MMP-2.

References

(1) Morell, M.; Puiggalí, J.*Polymers*; **2013**, 5, 188–224.

(2) Kopeček, J.; Yang, J. *Angew. Chem. Int. Ed. Engl.* **2012**, *51*, 7396–417.

(3) Bacinello, D.; Garanger, E.; Taton, D.; Tam, K. C.; Lecommandoux, S. *Biomacromolecules* **2014**, 4, 1882-1888

(4) Drappier, C.; Wirotius, A.-L.; Bathany, K.; Ibarboure, E.; Condassamy, O.; Garanger, E.; Lecommandoux, S. *Polym. Chem.* **2013**, *4*, 2011.

(5) Mathews, A. S.; Ahmed, S.; Shahin, M.; Lavasanifar, A.; Kaur, K. *Bioconjug. Chem.* **2013**, *24*, 560–70.

(6) Li, J.; Ge, Z.; Liu, S. *Chem. Commun.*. **2013**, *49*, 6974–6.

(7) Jabbari, E.; Yang, X.; Moeinzadeh, S.; He, X. *Eur. J. Pharm. Biopharm.* **2013**, *84*, 49–62.

(8) Elsabahy, M.; Wooley, K. L. *Chem. Soc. Rev.* **2012**.

(9) Sawant, R. M.; Hurley, J. P.; Salmaso, S.; Kale, a; Tolcheva, E.; Levchenko, T. S.; Torchilin, V. P. *Bioconjug. Chem.* **2006**, *17*, 943–9.

(10) Sanson, C.; Diou, O.; Thevenot, J.; Ibarboure, E.; Soum, A.; Brulet, A.; Miraux, S.; Thiaudiere, E.; Tan, S.; Brisson, A.; Dupuis, V.; Sandre, O.; Lecommandoux, S. *AC Nano*.. **2011**, 1122–1140.

(11) Jain, S.; Bates, F. S. *Science).* **2003**, *300*, 460–4.

(12) Kwon, G. S.; Kataoka, K. *Adv. Drug Deliv. Rev.* **2012**, *64*, 237–245.

(13) Xiong, X.-B.; Binkhathlan, Z.; Molavi, O.; Lavasanifar, A. *Acta Biomater.* **2012**, *8*, 2017–33.

(14) Antonietti, M.; Förster, S. *Adv. Mater.* **2003**, *15*, 1323–1333.

(15) Du, J.; O'Reilly, R. K. *Soft Matter* **2009**, *5*, 3544.

(16) Smart, T.; Lomas, H.; Massignani, M.; Flores-merino, M. V; Perez, L. R.; Battaglia, G. *Nano Today*. **2008**, *3*, 38–46.

(17) Discher, D. E.; Eisenberg, A. *Science.* **2002**, *297*, 967–73.

(18) Rodriguezhernandez, J.; Checot, F.; Gnanou, Y.; Lecommandoux, S. *Prog. Polym. Sci.* **2005**, *30*, 691–724.

(19) Rösler, A.; Vandermeulen, G. W. M.; Klok, H.-A. *Adv. Drug Deliv. Rev.* **2012**, *64*, 270–279.

(20) Chen, W.; Meng, F.; Cheng, R.; Zhong, Z. *J. Control. Release* **2010**, *142*, 40–6.

(21) Photos, P. J.; Bacakova, L.; Discher, B.; Bates, F. S.; Discher, D. E. *J. Control. Release* **2003**, *90*, 323–34.

(22) Discher, B. M.; Won, Y. Y.; Ege, D. S.; Lee, J. C.; Bates, F. S.; Discher, D. E.; Hammer, D. *Science* **1999**, *284*, 1143–6.

(23) Lomas, H.; Du, J.; Canton, I.; Madsen, J.; Warren, N.; Armes, S. P.; Lewis, A. L.; Battaglia, G. *Macromol. Biosci.* **2010**, *10*, 513–30.

(24) Pangburn, T. O.; Petersen, M. a; Waybrant, B.; Adil, M. M.; Kokkoli, E. *J. Biomech. Eng.* **2009**, *131*, 074005.

(25) Christian, D. a; Cai, S.; Bowen, D. M.; Kim, Y.; Pajerowski, J. D.; Discher, D. E. *Eur. J. Pharm. Biopharm.* **2009**, *71*, 463–74.

(26) Meeuwissen, S.; Kim, K. T.; Chen, Y.; Pochan, D. J.; van Hest, J. C. M. *Angew. Chem. Int. Ed. Engl.* **2011**, *50*, 7070–3.

(27) Carlsen, A.; Lecommandoux, S. *Curr. Opin. Colloid Interface Sci.* **2009**, *14*, 329–339.

(28) Lalatsa, A.; Schätzlein, A. G.; Mazza, M.; Le, T. B. H.; Uchegbu, I. F. *J. Control. Release* **2012**, *161*, 523–36.

(29) Ma, Y.; Jiang, X.; Zhuo, R. *J. Polym. Sci. Part A Polym. Chem.* **2013**, *51*, 3917–3924.

(30) Park, S.-I.; Lee, E.-O.; Yang, H.-M.; Park, C. W.; Kim, J.-D. *Colloids Surf. B. Biointerfaces* **2013**, *110*, 333–8.

(31) Kim, S.-H.; Shum, H. C.; Kim, J. W.; Cho, J.-C.; Weitz, D. *J. Am. Chem. Soc.* **2011**, *133*, 15165–71.

(32) Bermudez, H.; Brannan, A. K.; Hammer, D. A.; Bates, F. S.; Discher, D. E. *Macromol.* **2002**, *4*, 8203–8208.

(33) Discher, D. E.; Ortiz, V.; Srinivas, G.; Klein, M. L.; Kim, Y.; Christian, D.; Cai, S.; Photos, P.; Ahmed, F. *Prog. Polym. Sci.* **2007**, *32*, 838–857.

(34) Battaglia, G.; Ryan, A. J.; Tomas, S. *Methods* **2006**, 4910–4913.

(35) Danhier, F.; Feron, O.; Préat, V. *J. Control. Release* **2010**, *148*, 135–46.

(36) Cabane, E.; Zhang, X.; Langowska, K.; Palivan, C. G.; Meier, W. *Biointerphases* **2012**, *7*, 9.

(37) Stuart, M. a C.; Huck, W. T. S.; Genzer, J.; Müller, M.; Ober, C.; Stamm, M.; Sukhorukov, G. B.; Szleifer, I.; Tsukruk, V. V; Urban, M.; Winnik, F.; Zauscher, S.; Luzinov, I.; Minko, S. *Nat. Mater.* **2010**, *9*, 101–13.

(38) Aranda-Espinoza, H.; Bermudez, H.; Bates, F.; Discher, D. *Phys. Rev. Lett.* **2001**, *87*, 208301.

(39) Dischera, B. M.; Hammera, D. A.; Batesb, F. S.; Discher, D. *Curr. Opin. Colloid Interface Sci*. **2000**, *5*, 125–131.

(40) Sanson, C.; Schatz, C.; Le Meins, J.-F.; Brûlet, A.; Soum, A.; Lecommandoux, S. *Langmuir* **2010**, *26*, 2751–60.

(41) Garanger, E.; Lecommandoux, S. *Angew. Chem. Int. Ed. Engl.* **2012**, *51*, 3060–2.

(42) Palivan, C. G.; Fischer-Onaca, O.; Delcea, M.; Itel, F.; Meier, W. *Chem. Soc. Rev.* **2012**, *41*, 2800–23.

(43) Lin, J. J.; Ghoroghchian, P. P.; Zhang, Y.; Hammer, D. A. *Langmuir*. **2006**, 3975–3979.

(44) Gaitzsch, J.; Appelhans, D.; Gräfe, D.; Schwille, P.; Voit, B. *Chem. Commun.*. **2011**, *47*, 3466–8.

(45) Sanson, C.; Le Meins, J.-F.; Schatz, C.; Soum, A.; Lecommandoux, S. *Soft Matter* **2010**, *6*, 1722.

(46) Lee, J. S.; Zhou, W.; Meng, F.; Zhang, D.; Otto, C.; Feijen, J. *J. Control. Release* **2010**, *146*, 400–8.

(47) Lee, R.-S.; Chen, W.-H. *React. Funct. Polym.* **2011**, *71*, 455–462.

(48) Ryu, J.-H.; Roy, R.; Ventura, J.; Thayumanavan, S. *Langmuir* **2010**, *26*, 7086–92.

(49) Ghosh, S.; Yesilyurt, V.; Savariar, E. *J. Polym.* **2009**, 1052–1060.

(50) Achilleos, D. S.; Hatton, T. A.; Vamvakaki, M. *J. Am. Chem. Soc.* **2012**, *134*, 5726–9.

(51) Jin, H.; Zheng, Y.; Liu, Y.; Cheng, H.; Zhou, Y.; Yan, D. *Angew. Chem. Int. Ed. Engl.* **2011**, *50*, 10352–6.

(52) Goodwin, A. P.; Mynar, J. L.; Ma, Y.; Fleming, G. R.; Fréchet, J. M. J. *J. Am. Chem. Soc.* **2005**, *127*, 9952–3.

(53) Lee, S. J.; Lee, H. J.; Moon, M.-J.; Vu-Quang, H.; Lee, H.-J.; Muthiah, M.; Che, H.-L.; Heo, S. U.; Jeong, H. J.; Jeong, Y. Y.; Park, I.-K. *J. Nanosci. Nanotechnol.* **2011**, *11*, 7057–7060.

(54) Lecommandoux, S.; Sandre, O.; Chécot, F.; Rodriguez-Hernandez, J.; Perzynski, R. *Adv. Mater.* **2005**, *17*, 712–718.

(55) Napoli, A.; Boerakker, M. J.; Tirelli, N.; Nolte, R. J. M.; Sommerdijk, N. J. M.; Hubbell, J. *Langmuir* **2004**, *20*, 3487–91.

(56) Meng, F.; Engbers, G. H. M.; Feijen, J. *J. Control. Release* **2005**, *101*, 187–98.

(57) Lee, J. S.; Feijen, J. *J. Control. Release* **2011,** 101, 206.

(58) Kita-Tokarczyk, K.; Grumelard, J.; Haefele, T.; Meier, W. *Polymer.* **2005**, *46*, 3540–3563.

(59) Zhang, L.; Eisenberg, A. *Macromolecules* **1996**, 3168–3181.

(60) Stoenescu, R.; Graff, A.; Meier, W. *Macromol. Biosci.* **2004**, *4*, 930–5.

(61) Battaglia, G.; Ryan, A. J.; Building, D.; Hill, B.; Sheffield, S. *J Phys Chem B.* **2006**, 10272–10279.

(62) Won, Y.; Brannan, A. K.; Davis, H. T.; Bates, F. S. *J Phys Chem* B. **2002**, 3354–3364.

(63) Blanazs, A.; Armes, S. P.; Ryan, A. J. *Macromol. Rapid Commun.* **2009**, *30*, 267–77.

(64) Israelachvili, J. N.; Ninham, B. W. *Biochim Biophys Acta.***1977**, *470*, 185–201.

(65) Choucair, A.; Soo, P. L.; Eisenberg, A. *Polymer.* **2005**, 9308–9313.

(66) Discher, B. M.; Bermudez, H.; Hammer, D.; Discher, D. E.; Won, Y.-Y.; Bates, F. S. *J. Phys. Chem. B* **2002**, *106*, 2848–2854.

(67) Leekumjorn, S.; Sum, A. K. *Biochim. Biophys. Acta* **2007**, *1768*, 354–65.

(68) Kraske, W. V; Mountcastle, D. B. *Biochim Biophys Acta.* **2001**, *1514*, 159–164.

(69) Mihut, A. M.; Crassous, J. J.; Schmalz, H.; Ballauff, M. *Colloid Polym. Sci.* **2010**, *288*, 573–578.

(70) Qiu, H.; Cambridge, G.; Winnik, M. a; Manners, I. *J. Am. Chem. Soc.* **2013**, *135*, 12180–3.

(71) Li, T.; Wang, W. J.; Liu, R.; Liang, W. H.; Zhao, G. F.; Li, Z.; Wu, Q.; Zhu, F. M. *Macromolecules.* **2009**, 3804–3810.

(72) Chécot, F.; Brûlet, A.; Oberdisse, J.; Gnanou, Y.; Mondain-Monval, O.; Lecommandoux, S. *Langmuir* **2005**, *21*, 4308–15.

(73) Kukula, H.; Schlaad, H.; Antonietti, M.; Förster, S. *J. Am. Chem. Soc.* **2002**, *124*, 1658–63.

(74) Nardin, C.; Hirt, T.; Meier, W. *Langmuir.* **2000**, 1035–1041.

(75) Nardin, C.; Thoeni, S.; Widmer, J.; Winterhalter, M.; Meier, W. *Chem. Commun.* **2000**, 1433–1434.

(76) Shen, H.; Eisenberg, A. *Macromolecules.* **2000**, 2561–2572.

(77) Shen, H.; Eisenberg, A. *J Phys Chem B.* **1999**, 9473–9487.

(78) Waku, T.; Matsusaki, M.; Kaneko, T.; Akashi, M. *Macromolecules.* **2007**, 6385–6392.

(79) Castelletto, V.; Gouveia, R. J.; Connon, C. J.; Hamley, I. W. *Eur. Polym. J.* **2013**.

(80) Meng, F.; Zhong, Z.; Feijen, J. *Biomacromolecules* **2009**, *10*, 197–209.

(81) Chung, J. E.; Yokoyama, M.; Yamato, M.; Aoyagi, T.; Sakurai, Y.; Okano, T. *J. Control. Release* **1999**, *62*, 115–27.

(82) Coughlan, D. C.; Corrigan, O. I. *Int. J. Pharm.* **2006**, *313*, 163–74.

(83) Eeckman, F.; Moës, a J.; Amighi, K. *Int. J. Pharm.* **2004**, *273*, 109–19.

(84) Boutris, C.; Chatzi, E. G.; Kiparissides, C. *Polymer.* **1997**, *38*, 2567–2570.

(85) Deshmukh, M. V; Vaidya, A. A.; Kulkarni, M. G.; Rajamohanan, P. R.; Ganapathy, S. *Polymer.* **2000**, *41*, 7951–7960.

(86) Topp, M. D. C.; Dijkstra, P. J.; Talsma, H.; Feijen, J.*Macromolecules.* **1997**, *9297*, 8518–8520.

(87) Lee, E. S.; Na, K.; Bae, Y. H. *J. Control. Release* **2003**, *91*, 103–13.

(88) Meng, F.; Zhong, Z.; Feijen, J. *Biomacromolecules* **2009**, *10*, 197–209.

(89) Sanson, C.; Schatz, C.; Le Meins, J.-F.; Soum, A.; Thévenot, J.; Garanger, E.; Lecommandoux, S. *J. Control. Release* **2010**, *147*, 428–35.

(90) Jung, J.; Lee, I.-H.; Lee, E.; Park, J.; Jon, S. *Biomacromolecules* **2007**, *8*, 3401–7.

(91) Soppimath, K. S.; Tan, D. C.-W.; Yang, Y.-Y. *Adv. Mater.* **2005**, *17*, 318–323.

(92) Rodríguez-Hernández, J.; Lecommandoux, S. *J. Am. Chem. Soc.* **2005**, *127*, 2026–7.

(93) Cheng, R.; Feng, F.; Meng, F.; Deng, C.; Feijen, J.; Zhong, Z. *J. Control. Release* **2011**, *152*, 2–12.

(94) Upadhyay, K. K.; Bhatt, A. N.; Mishra, A. K.; Dwarakanath, B. S.; Jain, S.; Schatz, C.; Le Meins, J.-F.; Farooque, A.; Chandraiah, G.; Jain, A. K.; Misra, A.; Lecommandoux, S. *Biomaterials* **2010**, *31*, 2882–92.

(95) Borchert, U.; Lipprandt, U.; Bilang, M.; Kimpfler, A.; Rank, A.; Peschka-Süss, R.; Schubert, R.; Lindner, P.; Förster, S. *Langmuir* **2006**, *22*, 5843–7.

(96) Bellomo, E. G.; Wyrsta, M. D.; Pakstis, L.; Pochan, D. J.; Deming, T. J. *Nat. Mater.* **2004**, *3*, 244–8.

(97) Huang, Y.-C.; Yang, Y.-S.; Lai, T.-Y.; Jan, J.-S. *Polymer.* **2012**, *53*, 913–922.

(98) Du, J.; Armes, S. P. *Langmuir.* **2008**, 13710–13716.

(99) Yu, S.; Azzam, T.; Rouiller, I.; Eisenberg, A. *J. Am. Chem. Soc.* **2009**, *131*, 10557–66.

(100) Chécot, F.; Rodríguez-Hernández, J.; Gnanou, Y.; Lecommandoux, S. *Biomol. Eng.* **2007**, *24*, 81–5.

(101) Milhem, O. M.; Myles, C.; McKeown, N. B.; Attwood, D.; D'Emanuele, A. *Int. J. Pharm.* **2000**, *197*, 239–41.

(102) Holowka, E. P.; Pochan, D. J.; Deming, T. J. *J. Am. Chem. Soc.* **2005**, *127*, 12423–8.

(103) Koide, A.; Kishimura, A.; Osada, K.; Jang, W.-D.; Yamasaki, Y.; Kataoka, K. *J. Am. Chem. Soc.* **2006**, *128*, 5988–9.

(104) Cai, C.; Zhang, L.; Lin, J.; Wang, L. *J. Phys. Chem. B* **2008**, *112*, 12666–73.

(105) Liu, G.-Y.; Liu, X.-S.; Wang, S.-S.; Chen, C.-J.; J, J. *Langmuir.* **2012**, *28*, 557–62.

(106) Cerritelli, S.; Velluto, D.; Hubbell, J. *Biomacromolecules.* **2007**, *8*, 1966–72.

(107) Tong, X.; Wang, G.; Soldera, A.; Zhao, Y. *J. Phys. Chem. B* **2005**, *109*, 20281–7.

(108) Gaspard, J.; Silas, J.; Shantz, D. F.; Jan, J.-S. *Supramol. Chem.* **2010**, *22*, 178–185.

(109) Huang, C.; Chang, F. *Macromolecules.* **2008**, 7041–7052.

(110) Marsden, H. R.; Handgraaf, J.-W.; Nudelman, F.; Sommerdijk, N. J. M.; Kros, A. *J. Am. Chem. Soc.* **2010**, *132*, 2370–7.

(111) Peaker, F. W. *Analyst* **1960**, *85*, 235.

(112) Rech, P.; Grima-Pettenati, J.; Jauneau, A. *Plant J.* **2003**, *33*, 205–9.

(113) Marguet, M.; Edembe, L.; Lecommandoux, S. *Angew. Chem.* **2012**, *51*, 1173–6.

(114) Ferrando, M.; Spiess, W. E. L. *Food Sci. Technol. Int.* **2000**, *6*, 267–284.

(115) Oesterlin, C. *J Am Chem Soc.***1963**, 2149–2154.

(116) Yan, L. Z.; Dawson, P. E. *J. Am. Chem. Soc.* **2001**, *123*, 526–33.

(117) Canne, L. E.; Botti, P.; Simon, R. J.; Chen, Y.; Dennis, E. A.; Kent, S. B. H.; Francisco, S. S. *J Am Chem Soc.* **1999**, 8720–8727.

(118) Dawson, P. E.; Churchill, M. J.; Ghadiri, M. R.; Kent, S. B. H. *J Am Chem Soc.* **1997**, *7863*, 776–779.

(119) Deming, T. J. *Nature* **1997**, *390*, 386–9.

(120) Deming, T. J. *Adv. Drug Deliv. Rev.* **2002**, *54*, 1145–55.

(121) Conejos-Sánchez, I.; Duro-Castano, A.; Birke, A.; Barz, M.; Vicent, M. J. *Polym. Chem.* **2013**, *4*, 3182.

(122) Lin, Y.-L.; Jiang, G.; Birrell, L. K.; El-Sayed, M. E. H. *Biomaterials* **2010**, *31*, 7150–66.

(123) Sasaki, K.; Kogure, K.; Chaki, S.; Nakamura, Y.; Moriguchi, R.; Hamada, H.; Danev, R.; Nagayama, K.; Futaki, S.; Harashima, H. *Anal. Bioanal. Chem.* **2008**, *391*, 2717–27.

(124) Li, W.; Nicol, F.; Szoka, F. C. *Adv. Drug Deliv. Rev.* **2004**, *56*, 967–85.

(125) Pujals, S.; Fernández-Carneado, J.; López-Iglesias, C.; Kogan, M. J.; Giralt, E. *Biochim. Biophys. Acta.* **2006**, *1758*, 264–79.

(126) Lee, C. C.; Gillies, E. R.; Fox, M. E.; Guillaudeu, S. J.; Fréchet, J. M. J.; Dy, E. E.; Szoka, F. C. *Proc. Natl. Acad. Sci. U. S. A.* **2006**, *103*, 16649–54.

(127) Lundberg, P.; El-Andaloussi, S.; Sütlü, T.; Johansson, H.; Langel, U. *FASEB J.* **2007**, *21*, 2664–71.

(128) Drappier, C.; Oliveira, H.; Sandre, O.; Ibarboure, E.; Combet, S.; Garanger, E.; Lecommandoux, S. *Faraday Discuss.* **2013**, *166*, 83.

(129) Tahara, K.; Miyazaki, Y.; Kawashima, Y.; Kreuter, J.; Yamamoto, H. *Eur. J. Pharm. Biopharm.* **2011**, *77*, 84–8.

(130) Wang, R.; Zhang, Y.; Ma, G.; Su, Z. *Colloids Surf. B.* **2006**, *51*, 93–9.

(131) Zhang, J.; Wu, L.; Meng, F.; Wang, Z.; Deng, C.; Liu, H.; Zhong, Z. *Langmuir* **2012**, *28*, 2056–65.

(132) Upadhyay, K. K.; Mishra, A. K.; Chuttani, K.; Kaul, A.; Schatz, C.; Le Meins, J.-F.; Misra, A.; Lecommandoux, S. *Nanomedicine* **2012**, *8*, 71–80.

(133) Lee, J. S.; Groothuis, T.; Cusan, C.; Mink, D.; Feijen, J. *Biomaterials* **2011**.

(134) Ahmed, F.; Pakunlu, R. I.; Brannan, A.; Bates, F.; Minko, T.; Discher, D. E. *J. Control. Release* **2006**, *116*, 150–8.

(135) Saylor, D. M.; Kim, C.-S.; Patwardhan, D. V; Warren, J. *Acta Biomater.* **2007**, *3*, 851–64.

(136) Grassi, M.; Coceani, N.; Magarotto, L. *J. Colloid Interface Sci.* **2000**, *228*, 141–150.

(137) Berchane, N. S.; Carson, K. H.; Rice-Ficht, C.; Andrews, M. J. *Int. J. Pharm.* **2007**, *337*, 118–26.

(138) Siepmann, J.; Faisant, N.; Akiki, J.; Richard, J.; Benoit, J. P. *J. Control. Release* **2004**, *96*, 123–34.

(139) Mura, S.; Nicolas, J.; Couvreur, P. *Nat. Mater.* **2013**, *12*, 991–1003.

(140) Ganta, S.; Deshpande, D.; Korde, A.; Amiji, M. *Mol. Membr. Biol.* **2010**, *27*, 260–73.

(141) Luzio, J. P.; Poupon, V.; Lindsay, M. R.; Mullock, B. M.; Piper, R. C.; Pryor, P. R. *Mol. Membr. Biol.* **2003**, *20*, 141–54.

(142) Binauld, S.; Stenzel, M. H. *Chem. Commun.*. **2013**, *49*, 2082–102.

(143) Qin, S.; Geng, Y.; Discher, D. E.; Yang, S. *Adv. Mater.* **2006**, *18*, 2905–2909.

(144) Malemud, C. J. *Nature* **2006**, 1696–1701.

(145) Verma, R. P.; Hansch, C. *Bioorg. Med. Chem.* **2007**, *15*, 2223–68.

(146) Fonseca, K. B.; Bidarra, S. J.; Oliveira, M. J.; Granja, P. L.; Barrias, C. C. *Acta Biomater.* **2011**, *7*, 1674–82.

(147) Chau, Y.; Tan, F. E.; Langer, R. *Bioconjug. Chem.* **2004**, *15*, 931–41.

(148) Chau, Y.; Luo, Y.; Cheung, A. C. Y.; Nagai, Y.; Zhang, S.; Kobler, J. B.; Zeitels, S. M.; Langer, R. *Biomaterials* **2008**, *29*, 1713–9.

(149) Zhang, L.; He, Y.; Ma, G.; Song, C.; Sun, H. *Nanomedicine* **2011**, 1–10.

(150) Torchilin, V. *Adv. Drug Deliv. Rev.* **2011**, *63*, 131–5.

(151) Maeda, H.; Wu, J.; Sawa, T.; Matsumura, Y.; Hori, K. *J. Control. Release* **2000**, *65*, 271–84.

(152) Lammers, T.; Kiessling, F.; Hennink, W. E.; Storm, G. *J. Control. Release* **2011**.

(153) Shi, B. I. N.; Fang, C.; Pei, Y. *J Phys Sci* **2006**, *95*.

(154) Hommej, C. P.; Let, B. A. S. S.; Lard, M. A. R.; Spenlehauer, G. *J Phys Sci.* **2000**, *84*, 493–498.

(155) Jenkin, B. C. R.; Ph, D.; Rowley, D.*J Exp Med.* **1961**, *5*, 363–374.

(156) Houga, C.; Le Meins, J.-F.; Borsali, R.; Taton, D.; Gnanou, Y. *Chem. Commun.* **2007**, 3063–5.

(157) You, L.; Schlaad, H. *J. Am. Chem. Soc.* **2006**, *128*, 13336–7.

(158) Romberg, B.; Metselaar, J. M.; Baranyi, L.; Snel, C. J.; Bünger, R.; Hennink, W. E.; Szebeni, J.; Storm, G. *Int. J. Pharm.* **2007**, *331*, 186–9.

(159) Discher, D. E.; Eisenberg, A. *Science.* **2002**, *297*, 967–73.

(160) Lutz, J.-F.; Börner, H. G. *Prog. Polym. Sci.* **2008**, *33*, 1–39.

(161) Klok, H.-A. *Macromolecules* **2009**, *42*, 7990–8000.

(162) Fuks, G.; Mayap Talom, R.; Gauffre, F. *Chem. Soc. Rev.* **2011**, *40*, 2475–93.

(163) Becker, M. L.; Liu, J.; Wooley, K. L. *Biomacromolecules* **2005**, *6*, 220–8.

(164) Ten Cate, M. G. J.; Börner, H. G. *Macromol. Chem. Phys.* **2007**, *208*, 1437–1446.

(165) Hentschel, J.; Bleek, K.; Ernst, O.; Bo, H. G. *Macromolecules* **2008**, 1073–1075.

(166) Rabotyagova, O. S.; Cebe, P.; Kaplan, D. L. *Macromol. Biosci.* **2010**, *10*, 49–59.

(167) Singha, N. K.; Gibson, M. I.; Koiry, B. P.; Danial, M.; Klok, H.-A. *Biomacromolecules* **2011**, *12*, 2908–13.

(168) Danial, M.; Root, M. J.; Klok, H.-A. *Biomacromolecules* **2012**, *13*, 1438–47.

(169) Meszynska, A.; Badi, N.; Börner, H. G.; Lutz, J.-F. *Chem. Commun.* **2012**, *48*, 3887–9.

(170) Shu, J. Y.; Panganiban, B.; Xu, T. *Annu. Rev. Phys. Chem.* **2013**, *64*, 631–57.

(171) Sawada, T.; Mihara, H.; Serizawa, T. *Chem. Rec.* **2013**, *13*, 172–86.

(172) Löwik, D. W. P. M.; Leunissen, E. H. P.; van den Heuvel, M.; Hansen, M. B.; van Hest, J. C. M. *Chem. Soc. Rev.* **2010**, *39*, 3394–412.

(173) Turk, B. E.; Huang, L. L.; Piro, E. T.; Cantley, L. C. *Nat. Biotechnol.* **2001**, *19*, 661–7.

(174) Fèvre, M.; Pinaud, J.; Gnanou, Y.; Vignolle, J.; Taton, D. *Chem. Soc. Rev.* **2013**, *42*, 2142–72.

(175) Kiesewetter, M. K.; Shin, E. J.; Hedrick, J. L.; Waymouth, R. M. *Macromolecules* **2010**, *43*, 2093–2107.

(176) Dove, A. P. *ACS Macro Lett.* **2012**, *1*, 1409–1412.

(177) Kamber, N. E.; Jeong, W.; Waymouth, R. M.; Pratt, R. C.; Lohmeijer, B. G. G.; Hedrick, J. L. *Chem. Rev.* **2007**, *107*, 5813–40.

(178) Lowe, A. B. *Polym. Chem.* **2010**, *1*, 17.

(179) Hoyle, C. E.; Bowman, C. N. *Angew. Chem.* **2010**, *49*, 1540–73.

(180) Koo, S.; Stamenovi;, M. *J. Polym.* **2010**, *48*, 1699–1713.

(181) Kit, W.; Chau, Y. *J Am Chem Soc.* **2010,** 7, 132.

(182) Sanson, C.; Le Meins, J.-F.; Schatz, C.; Soum, a.; Lecommandoux, S. *Soft Matter* **2010**, *6*, 1722.

(183) Klok, H. -a.; Lecommandoux, S. *Adv. Mater.* **2001**, *13*, 1217.

(184) Kim, S.; Kim, J.-H.; Jeon, O.; Kwon, I. C.; Park, K. *Eur. J. Pharm. Biopharm.* **2009**, *71*, 420–30.

(185) Agut, W.; Brûlet, A.; Schatz, C.; Taton, D.; Lecommandoux, S. *Langmuir* **2010**, *26*, 10546–54.

(186) Eldar-Boock, A.; Miller, K.; Sanchis, J.; Lupu, R.; Vicent, M. J.; Satchi-Fainaro, R. *Biomaterials* **2011**, *32*, 3862–74.

(187) Marguet, M.; Sandre, O.; Lecommandoux, S. *Langmuir* **2012**, *28*, 2035–43.

(188) Mishra, B.; Patel, B. B.; Tiwari, S. *Nanomedicine* **2010**, *6*, 9–24.

(189) Nisbet, D. R.; Williams, R. J. *Biointerphases* **2012**, *7*, 2.

(190) Onaca, O.; Enea, R.; Hughes, D. W.; Meier, W. *Macromol. Biosci.* **2009**, *9*, 129–39.

(191) Kim, D.; Lee, E. S.; Oh, K. T.; Gao, Z. G.; Bae, Y. H. *Small* **2008**, *4*, 2043–50.

(192) Nishiyama, N.; Bae, Y.; Miyata, K.; Fukushima, S.; Kataoka, K. *Drug Discov. Today Technol.* **2005**, *2*, 21–26.